

1 **The climate and vegetation of Europe, North Africa and the**
2 **Middle East during the Last Glacial Maximum**
3 **(21,000 years BP) based on pollen data**

4
5
6 Basil A.S. Davis¹, Marc Fasel², Jed O. Kaplan³, Emmanuele Russo⁴, Ariane Burke⁵

7 ¹Institute of Earth Surface Dynamics, University of Lausanne, Lausanne, 1015, Switzerland

8 ²enviroSPACE lab, Institute for Environmental Sciences, University of Geneva, Geneva,
9 1211, Switzerland

10 ³Department of Earth Sciences, The University of Hong Kong, Hong Kong, Peoples Republic
11 of China

12 ⁴Department of Environmental Systems Science, ETH Zurich, Zurich, 8092, Switzerland

13 ⁵Laboratoire d'Ecomorphologie et de Paleoanthropologie, Departement d'Anthropologie,
14 Universite de Montreal, Montreal, Quebec, H3C 3J7, Canada

15
16 *Correspondence to:* Basil A. S. Davis (basil.davis@unil.ch)

17
18 **Abstract.** Pollen data represents one of the most widely available and spatially-resolved
19 sources of information about the past land cover and climate of the Last Glacial Maximum
20 (21,000 years BP). Previous pollen data compilations for Europe, the Mediterranean and the
21 Middle East however have been limited by small numbers of sites and poor dating control.
22 Here we present a new compilation of pollen data from the region that improves on both the
23 number of sites (63) and the quality of the chronological control. Data has been sourced from
24 both public data archives and published (digitized) diagrams. Analysis is presented based on
25 a standardized pollen taxonomy and sum, with maps shown for the major pollen taxa, biomes
26 and total arboreal pollen, as well as quantitative reconstructions of forest cover and winter,
27 summer and annual temperatures and precipitation. The reconstructions are based on the
28 modern analogue technique (MAT) adapted using PFT scores, and with a modern pollen
29 dataset taken from the latest Eurasian Modern Pollen Database (~8000 samples). A site-by-
30 site comparison of MAT and Inverse Modelling methods shows little or no significant
31 difference between the methods for the LGM, indicating that no-modern-analogue and low
32 CO₂ conditions during the LGM do not appear to have had a major effect on MAT transfer
33 function performance. Previous pollen-based climate reconstructions using modern pollen
34 datasets show a much colder and drier climate for the LGM than both Inverse Modelling and
35 climate model simulations, but our new results suggest much greater agreement. Differences
36 between our latest MAT reconstruction and those in earlier studies can be largely attributed
37 to bias in the small modern dataset previously used, and differences in the method itself
38 (Brewer et al. 2008, Salonen et al. 2019). We also find that quantitative forest cover
39 reconstructions show more forest than that previously suggested by biome reconstructions,
40 but less forest than that suggested by simple percentage arboreal pollen, although
41 uncertainties remain large. Overall, we find that LGM climatic cooling/drying was
42 significantly greater in winter than in summer, but with large site to site variance that
43 emphasizes the importance of topography and other local factors in controlling the climate
44 and vegetation of the LGM.

45 **1 Introduction**

46

47 During the Last Glacial Maximum (LGM) ~21,000 years BP (Mix et al., 2001), the climate,
48 vegetation and landscape of Europe and its surrounding regions were very different than
49 today. Scandinavia and a large part of the British Isles were covered by a single ice sheet,
50 with separate ice sheets covering the Alps and Pyrenees, while many smaller and lower
51 mountainous areas were also glaciated (Ehlers et al. 2011). As a result of this global build-up
52 of ice on land, sea levels were around 120 meters lower than today, resulting in the retreat of
53 Atlantic and Mediterranean coastlines and the emergence on land of the English Channel and
54 North Sea basin. Falling sea levels also led to the disconnection of the Black Sea from the
55 Mediterranean, and a subsequent drop in Black Sea water levels as evaporation exceeded
56 inflow (Arslanov et al. 2007). On land, permafrost and periglacial processes occurred
57 immediately to the south of the Scandinavian ice sheet, while the massive discharge of glacial
58 clays and sands provided material to be redeposited by the wind as belts of loess across
59 northern France, Benelux, Germany and central Europe (Lehmkuhl et al. 2021). Under these
60 cooler and drier climatic conditions, forests are thought to have retreated to the relative
61 shelter of Southern Europe and the Mediterranean, while relatively unproductive steppe and
62 tundra dominated the region north of the Alps (Grichuk 1992).

63

64 This traditional view of the LGM has been established for many years, but many details
65 concerning the climate and vegetation of the LGM remain debated. Much of this debate
66 concerns information derived from the pollen record, which represents one of the most
67 widely available and spatially-resolved sources of information concerning LGM vegetation
68 and climate, and the primary terrestrial proxy used to evaluate climate models in the
69 Palaeoclimate Modelling Intercomparison Project (PMIP) (Bartlein et al., 2011; Braconnot et
70 al., 2019; Harrison et al., 2014).

71

72 For example, climate model simulations continue to indicate a climate that is less cold and
73 more humid than pollen-based reconstructions (Jost et al., 2005). These results are similar to
74 reconstructions based on glaciological modelling (Allen et al., 2008b). On the other hand, the
75 pollen-based reconstructions that show the greatest disagreement with climate models have
76 themselves been criticized for not considering the possible effect of low atmospheric CO₂ on
77 the physiological relationship between plants and climate (Ramstein et al., 2007). Methods
78 that use modern pollen samples are based on the assumption that the relationship between
79 vegetation and climate remains the same through time, and that this is independent of change
80 in CO₂ concentration. Studies have shown however that plant growth processes and plant
81 resilience are sensitive to CO₂ concentration, and particularly water-use efficiency which
82 would make plants more drought sensitive in low CO₂ environments (Cowling & Sykes
83 1999). Atmospheric CO₂ during the LGM was around 190 ppm, some 100 ppm lower than
84 the pre-industrial period, and 200 ppm lower than the levels experienced in the last 50 years.
85 Concerns about the effects of lower CO₂ during the LGM has directly led to the development
86 of pollen-climate reconstruction methods that can take account of CO₂ effects, either through
87 use of a process-based vegetation model run in inverse mode (Guiot et al. 2000, Guiot et al.
88 2009), or through the use of a correction algorithm (Prentice et al. 2017; Cleator et al., 2020).
89 Pollen-climate reconstructions based on inverse modelling that account for these low CO₂
90 effects show less cooling and drying and consequently greater agreement with climate
91 models (Ramstein et al., 2007; Wu et al., 2007; Izumi & Bartlein., 2016; Wu et al. 2019).

92

93 Further data-model discrepancies have also been highlighted concerning LGM vegetation
94 cover. Earlier pollen synthesis studies, especially those that applied the biomisation method

95 (Elenga et al., 2000) give the impression that non-glaciated areas of LGM Europe were
96 dominated by treeless steppe, while vegetation models driven by climate model simulations
97 indicate large areas of forest and woodlands (Binney et al., 2017; Kaplan et al., 2016;
98 Velasquez et al., 2021). The apparent data-model discrepancy associated with steppe has led
99 to the suggestion that early humans, which are not included in vegetation models, could have
100 reduced the forest cover with only a relatively moderate use of fire because of the cold
101 climate and slow speed of vegetation recovery (Kaplan et al., 2016). This debate is important
102 because of studies that have shown the sensitivity of the climate system to vegetation
103 boundary conditions during the LGM (Ludwig et al., 2017; Velasquez et al., 2021). This
104 suggests that accurate knowledge of the vegetation cover during the LGM is a necessary
105 prerequisite to understanding the role of other influences on the climate system at this time.
106

107 More recent pollen and macrofossil studies from eastern Central Europe have shown that at
108 least in this region there existed areas of open boreal forest and woodland with some
109 temperate broadleaf species (Kuneš et al., 2008; Willis and Van Andel, 2004). The evidence
110 of forest, and particularly elements of temperate broadleaf forest, north of the Alps has come
111 to represent a challenge to the traditional view that forest species only survived the LGM in
112 sheltered refugia far to the south of the Fenoscandian ice sheet and close to the moderating
113 influence of the Mediterranean Sea. The presence of micro-refugia north of the Alps is
114 important because it would represent a very different baseline for understanding the later rate
115 and route of plant migrations under the rapid warming that occurred during the Late Glacial
116 to Holocene transition (Douda et al., 2014; Giesecke, 2016; Krebs et al., 2019; Nolan et al.,
117 2018), as well as understanding patterns of present-day genetic diversity (Normand et al.,
118 2011; Svenning et al., 2008). Modelling studies have shown difficulty in supporting the very
119 high rates of postglacial expansion that would be necessary for southern refugia (Feurdean et
120 al., 2013, Nogués-Bravo et al. 2018).
121

122 Much of this debate has been informed by an increasing number of LGM pollen studies from
123 an ever-broader geographical area, and especially from an increasing number of studies from
124 north of the Alps. Nevertheless, the synthesis of these studies into a single narrative is made
125 difficult by several factors, for instance: different taxonomic definitions, pollen percentages
126 calculated from non-standardized pollen sums, and quantitative analyses such as climate
127 reconstructions that are based on different training sets and methodologies. This has led to
128 some modelling studies ignoring the pollen record completely, on the basis that data from the
129 LGM is too scarce (Janská et al., 2017). Where standardized methods have been applied to
130 multiple LGM pollen records, poor dating control has resulted in the inclusion of many
131 records that may not actually be from the selected LGM time window. This is particularly
132 important because the 21 ± 2.0 ka time slice commonly used to represent the LGM period in
133 PMIP data-model comparisons and other synthesis studies (MARGO members, 2009;
134 Bartlein et al., 2011) occurs immediately after the glacial maxima in the Alps around 26-23
135 ka (Heiri et al., 2014; Spötl et al., 2021) and Heinrich stadial HS-2 (24.3-26.5), whilst also
136 being closely followed by Heinrich stadial HS-1 (15.6-18.0 ka) (Sanchez-Goñi & Harrison,
137 2010). These closely associated time periods can therefore be expected to represent both a
138 different vegetation and climate than the LGM itself.
139

140 For example, of the 18 European pollen records used in the PMIP benchmarking dataset
141 (Bartlein et al., 2011), 10 fall into the worst class ('poor') in the COHMAP chronological
142 quality classification scheme if relative dating such as pollen correlation is excluded. More
143 recent synthesis studies have also relied heavily on records from the European Pollen
144 Database (EPD) which currently has 116 records with samples of LGM age (as of June

145 2022). Many of these records however are based on chronologies that are considered reliable
146 for the Holocene (Giesecke et al., 2014), but have large uncertainties for the LGM as a result
147 of 1) excessive extrapolation back in time from Holocene age dates, 2) the use of pollen
148 correlation or other relative dating despite poorly defined regional biostratigraphy, or 3) the
149 inappropriate use of radiocarbon dates contaminated with old carbon. We found that 104 of
150 these 116 EPD records (Neotoma, 2021) fall into the worst class ('poor') in the COHMAP
151 chronological quality classification.

152

153 Here we address these problems using a new synthesis of LGM pollen records from
154 throughout Europe, the Mediterranean and the Middle East (EurMedMidEst) based on
155 rigorous quality control criteria. Records were compiled from an extensive review of public
156 databases and archives, and the scientific literature. Pollen records were selected according to
157 the robustness of their chronological control around the PMIP LGM time-window (21 ± 2
158 ka), and combined into a single dataset based on a harmonized taxonomy and standardized
159 pollen sum. The dataset was then analysed so that standardised maps could be produced to
160 show the distribution of the major pollen taxa, biomes and total arboreal pollen at the LGM.
161 In addition, quantitative reconstructions of forest cover as well as winter, summer and annual
162 temperatures and precipitation were undertaken using a modified version of the standard
163 Modern Analogue Technique (MAT) (Guiot et al. 1989), utilizing the latest Eurasian Modern
164 Pollen Database v2 dataset. These climate reconstructions are compared and evaluated
165 against previous LGM pollen-climate reconstructions, as well as reconstructions based on
166 other proxies. The dataset and results are fully documented and the complete data files are
167 provided in the supplementary information.

168

169 **2 Methods**

170

171 **2.1 Pollen Data**

172

173 LGM fossil pollen data from Europe and bordering regions including North Africa and the
174 Middle East were selected and collated into a single standardized project database. This data
175 was sourced from the EPD/Neotoma database (Williams et al., 2021), the Pangaea data
176 archive, publications in scientific journals, and from the original authors. We selected LGM
177 pollen sites/data according to strict quality control criteria. Where possible, primary raw
178 pollen counts were used where this was available. Where the original electronic data was not
179 available, the data was digitized from the published diagram. Overall we have included 63
180 records in our study, of which 35 were digitized and 28 consisted of the original pollen
181 counts (Table 1).

182

183 The distribution of the 63 sites reflects the distribution of suitable archives, with fewer
184 records available from climatically or environmentally challenging regions (Fig. 1). High
185 rates of erosion and a drier and colder climate during the LGM reduced the number of
186 suitable anoxic sediment sinks for pollen preservation, especially in Central Europe between
187 the Scandinavian and Alpine ice sheets. Nevertheless, our dataset includes sites from this
188 region, as well as North Africa and eastern Central Europe through to Iran, although most
189 sites are located in an arc across eastern Spain, the Alps, and Italy. Lakes sites are the most
190 numerous archive and tend to be located in the more sheltered and topographically favourable
191 regions of Southern Europe and the Mediterranean. Peat is the next most important archive,
192 followed by alluvial and colluvial sediments, as well as cave sites, the later also often being
193 known for their archaeological significance. Sites located at the ice margins that appear to be
194 under the ice reflect uncertainties in the location of the ice margin both in time and space

195 during the LGM, as well as the fact that the selected time window for this study (21 ± 2 ka) is
196 later than the maximum ice advance in some regions (Hughes and Gibbard, 2015). For
197 completeness, we also include 7 marine records which have the advantage of more
198 continuous deposition and often better dating over the LGM period, but which are prone to
199 taphonomic biases compared to terrestrial records. These biases are discussed later in this
200 section.

201

202 LGM pollen records were selected according to a number of quality control criteria, but
203 primary amongst these was the existence of sufficient independent chronological control
204 points to accurately identify samples that would fall within the 21 ± 2 ka BP time-slice of
205 interest. We have used all of the samples within this time frame where the samples have been
206 available in electronic form, else we have used the sample closest to the target time (21 ka
207 BP). For records taken from the EPD we have used the latest Bayesian age-depth models
208 where these were available (Giesecke et al., 2014), otherwise we have used the dates and
209 chronology proposed by the original authors. We classified chronologies according to the
210 COHMAP chronological quality scheme for the LGM period (Anderson et al., 1988; Yu and
211 Harrison, 1995), which classifies record quality from 1-6 depending on whether a date falls
212 within 2000 14C years (or less) of the time being assessed, or whether bracketing dates fall
213 within 6000 and 8000 14C years (or less) about the time being assessed (Table A1).

214 Chronologies based on dates that fall outside of these limits fall into COHMAP class 7, and
215 are regarded as ‘poorly dated’ with respect to the LGM. Importantly, we have only included
216 radiometric and other absolute dates (such as varves) in this assessment, and have excluded
217 dates based on correlation with regional pollen records. These pollen-based stratigraphic
218 dates have been widely used in previous LGM studies, but do not include estimates of
219 uncertainty and are generally regarded as unreliable at this time given the sparsity of well
220 dated pollen sites and samples on which to base any correlation (Giesecke et al., 2014).

221

222 All records that were classified as poorly dated (COHMAP class 7) were subsequently
223 excluded from our analysis. This has meant that many of the pollen records used in previous
224 studies were excluded, including 16 of the 26 LGM records used by PMIP and associated
225 studies in Europe (Bartlein et al., 2011; Elenga et al., 2000; Tarasov et al. 2000, Jost et al.,
226 2005; Peyron et al., 1998; Wu et al., 2007; Cleator et al., 2020). We also excluded 104 of the
227 116 records in the EPD with samples that fall within our LGM time window. Many of these
228 EPD pollen records have been used in more recent studies, although the exact record (EPD
229 Entity number) is often not stated. We estimate that we have excluded 16 of the 17 European
230 sites used by Binney et al. (2017) (this study only included sites above latitude 40N), 5 of the
231 6 European sites used by Allen et al. (2010), 28 of the 33 sites used by Cao et al. (2019) and
232 27 of the 71 sites used by Kaplan et al. (2016).

233

234 Other quality control criteria were also used in the selection of LGM pollen records.
235 Published pollen diagrams that only included a small part of the terrestrial pollen assemblage,
236 or only presented summary taxa, were excluded. Records were also excluded where the
237 dating information was incomplete, for instance where radiocarbon dating uncertainties were
238 not published or where it was not possible to determine if the date shown was in calibrated or
239 uncalibrated radiocarbon years.

240

241 The modern pollen data for the climate and tree cover reconstructions were sourced from the
242 latest version 2 of the Eurasian Modern Pollen Database (Davis et al., 2020), which is
243 managed as part of the EPD. The EMPD2 includes 8133 modern pollen samples from across
244 the Palearctic biogeographic region from Europe to the far East of Asia. The taxa from both

245 the fossil and modern pollen data were consolidated into 120 of the most commonly-
246 occurring terrestrial taxa types. This taxa list was designed to be compatible with the
247 biomisation scheme used in our study (Peyron et al., 1998; Tarasov et al., 2000) and that used
248 in the Holocene mapping study of Brewer et al. (2017). The count of *Larix* was amplified by
249 a factor of 10 due to its low pollen representation (Edwards et al. 2000, Bigelow et al. 2003,
250 Tarasov et al. 1998, 2000, 2013, Binney et al., 2017).

251

252 **2.2 Biomisation**

253

254 We converted pollen assemblages to biomes based on the European biomisation scheme of
255 Peyron et al (1998), which in turn is based on Prentice et al. (1996). The method is described
256 in detail in Collins et al. (2012). We expanded the number of taxa included in the biomisation
257 procedure proposed by Peyron et al (1998) to include taxa from the Northern Eurasian
258 biomisation procedure of Tarasov et al. (1998). The inclusion of additional Northern Eurasian
259 taxa reflects recent evidence that modern analogues of LGM vegetation occur in parts of
260 Siberia (Magyari et al., 2014a). The biomisation procedure (Prentice et al. 1996) assigns each
261 taxa to a plant functional type (PFT) and calculates a score for each of these PFT's based on
262 the sum of the square root of the percentage of each of the taxa included in that PFT. To
263 reduce the influence of long-distance transport, taxa below 0.5% are removed at the start of
264 the procedure. Each biome is then assigned one or more PFT's and a score for each biome is
265 calculated as the sum of the associated PFT scores. The biome with the highest score is then
266 viewed as the dominant biome. Where the highest score is the same for more than one biome,
267 the dominant biome is decided based on a hierarchy of unique PFT's. Peyron et al. (1998)
268 also included a procedure for distinguishing warm and cold steppe biomes based on re-
269 assigning certain steppe PFT's according to the presence or otherwise of PFT's indicative of
270 cold or warm conditions. Following the Biome6000 project (Elenga et al., 2000) and Allen et
271 al. (2010), we did not apply this additional procedure and present only the merged steppe
272 biome. In summary, the biomisation procedure categorised 39 arboreal pollen taxa and 39
273 non-arboreal taxa into 22 plant functional types (PFT's), which were then combined into 12
274 biomes.

275

276 **2.3 Quantitative climate reconstruction**

277

278 We reconstructed climate from pollen data based on a modified Modern Analogue Technique
279 (MAT) (Guiot et al. 1989) that used PFT scores to match fossil samples with modern pollen
280 samples (as used by Davis et al., 2003). "Other methods using PFT scores and artificial
281 neural network techniques have been developed to reconstruct the climate of Europe during
282 the LGM from pollen data (Peyron et al. (1998) and Jost et al (2005). PFT scores have been
283 used in previous large-scale European pollen-based climate reconstructions for the Holocene
284 (Davis et al., 2003; Mauri et al., 2014, 2015), where performance was found to be better than
285 the conventional approach based on individual taxa (eg Marsicek et al., 2018). A particular
286 advantage of the PFT approach for the LGM is that it can help overcome problems associated
287 with vegetation (pollen) assemblages that may have no modern analogue (Davis et al. 2003).
288 This can be a problem during the LGM when the climate and environment could be expected
289 to be very different from today, and when many taxa formed unusual vegetation assemblages
290 as a result of their forced retreat to sheltered refugia locations. The problem of modern
291 analogues is also addressed in our reconstruction by using the latest EMPD2 modern pollen
292 dataset. The EMPD2 provides a large number of potential modern analogues for many
293 different LGM vegetation types and climates found today across the Palearctic region. PFT
294 scores were calculated according to the methods outlined already in the Biomisation section,

295 then normalized so that each sample was proportional to every other sample (Juggins and
296 Birks, 2012).

297
298 The MAT method was applied using the Rioja program for R (Juggins, 2020). The modern
299 pollen data was taken from the latest version 2 of the EMPD (as detailed earlier). The
300 EMPD2 includes 8133 samples, which is considerably larger than the modern datasets used
301 in previous LGM pollen-based reconstructions. For instance, Peyron et al. (1998) used a
302 modern pollen dataset of 683 samples, which was updated by Jost et al (2005) to include an
303 additional 185 samples. These datasets were also mainly taken from the steppes of Kazakstan
304 and Mongolia, while the EMPD2 covers a much wider area, spanning most of the Eurasian
305 Palearctic region (Davis et al., 2020). The size and distribution of the modern training set in
306 climate and vegetation space is important because in order for the method to work
307 effectively, it is necessary to have samples representative of the likely vegetation and climate
308 space that could be occupied by the fossil assemblage (Turner et al. 2021, Chevalier et al.,
309 2020; Salonen et al. 2012, Juggins, 2013).

310
311 A known problem with MAT is the role of spatial auto-correlation in providing
312 unrealistically low estimates of uncertainty (Chevalier et al., 2020; Telford and Birks, 2009).
313 This results from the fact that closely analogous modern pollen samples can also be located
314 closely in physical space, and therefore in climate space. To reduce this problem it is possible
315 to exclude closely located samples from the analogue matching process using a filter based
316 on a set distance (h-block filter) (Telford and Birks, 2009). While this approach can help,
317 there are also three main problems associated with it. The first is error substitution, since
318 removing samples also reduces the number of potential analogues, creating a different source
319 of error that is not easy to categorise. Secondly, multiple samples taken from the same
320 location are actually a strength of pollen training sets, since they are more likely to capture
321 the full range of the assemblage diversity associated with a given climate. Thirdly, current
322 methods that limit spatial range such as the h-block filter only do so on the horizontal axis,
323 and do not consider the fact that samples can also be found at different elevations. In hilly or
324 mountainous regions samples can therefore be excluded because they are closely located in
325 horizontal space, but in fact they actually occupy very different climates and vegetation
326 associations, contradicting the logical premise of the h-block filter. It was therefore decided
327 not to apply this filter.

328
329 Uncertainties for the pollen-climate reconstructions were calculated using a standard method
330 for MAT (Juggins 2020) based on the spread of the climates associated with the best modern
331 pollen analogues used for each fossil sample. The closer the climates of the best modern
332 pollen analogues (6 in the case of this study) then the smaller are the calculated uncertainties
333 assigned to the reconstructed climate of the fossil pollen sample.

334
335 Climate reconstructions are presented as anomalies. These have been calculated with respect
336 to modern climate (1970-2000 average) at each core site location using WorldClim 2 (Fick
337 and Hijmans, 2017) (Table A2), which was also used to assign the modern climate for the
338 modern pollen samples in the transfer function (Davis et al., 2020).

339 **2.4 Marine pollen records**

340
341 We have included marine pollen records in our analysis for reasons explained below, but it is
342 important that these records should be viewed with caution, particularly when used for biome
343 and quantitative MAT reconstructions, and when compared with terrestrial records from
344

345 different archives. Biomisation methods have been applied to individual marine pollen
346 records (Combourieu Nebout et al., 2009), as well as multi-site synthesis studies such as the
347 ACER project (ACER project members et al., 2017). However, marine records were
348 specifically excluded from the Biome6000 project (Elenga et al., 2000). Similarly,
349 quantitative climate methods have been applied to individual marine pollen records
350 (Combourieu Nebout et al., 2009; Fletcher et al., 2010), as well as multi-site synthesis studies
351 (Sánchez Goñi et al., 2005; Brewer et al., 2008; Salonen et al., 2021). However, marine
352 records have also been specifically excluded from other major pollen-climate studies
353 (Cheddadi et al., 1996; Davis et al., 2003; Marsicek et al., 2018), as well as quantitative forest
354 cover reconstructions (Zanon et al. 2018).

355
356 Discussion on the advantages and problems associated with marine records can be found
357 elsewhere (Chevalier et al., 2020; Daniau et al., 2019), but are reviewed briefly here where
358 relevant to the methodologies applied in this study. Marine sedimentary records provide
359 continuous and well dated pollen records for the LGM that are often lacking from many
360 terrestrial regions, especially in arid areas with few alternative anaerobic sediment sinks.
361 Conversely however, pollen source areas for marine sites may be many hundreds of
362 kilometers from the coring site and may be liable to change through time in response to
363 changes in distance to the coastline, rates of river discharge and ocean and atmospheric
364 dynamics. This can theoretically give rise to changes in the vegetation shown in the pollen
365 assemblage recorded at the marine site without any actual change in climate or other
366 environmental pressure. The large and indeterminable source area of marine records also
367 mean that it is difficult to apply quantitative MAT reconstruction methods, not least because
368 the mean climate or forest cover of the source area is almost impossible to determine. In
369 addition, the fossil pollen record and the modern pollen dataset to which it is being compared
370 are composed largely of terrestrial lakes and bog sites with much smaller and more
371 homogeneous source areas. This creates a series of problems, the more obvious of which is
372 the calculation of anomalies, since we cannot assume that the modern climate at the (marine)
373 coring site location is representative of the (terrestrial) source area. In this study we have
374 taken the closest point on land as the modern climate for the calculation of anomalies, but
375 provide the absolute values for all sites so that these can be recalculated if necessary (Table
376 A2). The next problem is that the large source area may capture a combination of different
377 vegetation types that is not going to be represented in a modern pollen dataset based on
378 samples from terrestrial sites with much smaller source areas, for instance a mixture of
379 coastal and mountain vegetation, or even vegetation from different continents (Magri and
380 Parra, 2002). However, in our analysis we did not find any sample from a marine record (or
381 terrestrial record) that did not have a reasonable modern analogue in our training set (chord
382 distance <0.3)(Huntley, 1990), even though we did not adjust the pollen assemblage for the
383 over-representation of *Pinus* (and other Pinaceae) in the marine pollen samples.

384
385 Typically, the Pinaceae component is excluded from the terrestrial pollen sum when
386 calculating percentages for marine pollen samples, and in some cases has been excluded
387 entirely from the samples used in marine pollen-climate reconstructions (Combourieu Nebout
388 et al., 2009). The problem with excluding *Pinus* is two-fold, the first is that *Pinus* often
389 represents the main forest forming tree in the Koeppen Csb climate zone on the Atlantic coast
390 where many marine sites are located (García-Amorena et al., 2007), as well as representing
391 the most abundant tree taxa in Europe during the LGM (Figure A10).

392
393 The effect of excluding Pinaceae on the biomisation algorithm and MAT climate
394 reconstruction process has not been widely investigated. We therefore decided to evaluate

395 this problem for 1) biomisation, and 2) pollen-climate reconstruction. In table S3 we show
396 the biomisation results for 8213 modern pollen samples taken from the EMPD2 modern
397 pollen database. Using this as the control, we then artificially varied the amount of Pinaceae
398 (*Pinus*, *Abies* and *Picea*) in the assemblage of each pollen sample and compiled the results
399 (Table S3). This shows quite clearly that removing all of the Pinaceae has a much more
400 profound effect on the biomisation process than artificially inflating the amount of Pinaceae
401 (as might be expected in a marine sample where Pinaceae can be over-represented). Even
402 when Pinaceae was artificially inflated by as much as 400% of the original value, the biomes
403 were changed in only 2348 samples, compared to 5860 samples if all the Pinaceae was
404 removed entirely. In terms of the effects on individual biomes, removing the Pinaceae
405 considerably increased the amount of CLDE, STEP and TUND, whilst greatly reducing the
406 amount of XERO, almost eliminating the amount of TAIG, and completely eliminating the
407 COCO biome. In contrast, the effect of inflating the amount of Pinaceae tended to be more
408 evenly distributed between the biomes, with the biggest increase seen in TUND and biggest
409 decrease in STEP. This suggests that even if the over-representation of Pinaceae was quite
410 extreme in marine pollen samples, the effect on biome classification (and by definition, the
411 underlying PFT scores) is less than removing Pinaceae completely from the pollen
412 assemblage.

413
414 In a second test, we compared the reconstruction of LGM climate from marine pollen
415 samples when Pinaceae was included, and excluded. The results are shown in table S4 and
416 indicate reconstructed temperatures are generally 1-2C cooler, and precipitation slightly
417 higher when Pinaceae is excluded. The differences between the two methods however are
418 small, and generally less than half of the uncertainties, suggesting that differences are
419 statistically indistinguishable when considered in the context of the overall uncertainties.

420
421 In summary we find that including Pinaceae in the biomisation process is less likely to lead to
422 miss-assignment of the biome than excluding Pinaceae, except in extreme cases of over-
423 representation. Percentages of Pinaceae in the LGM marine samples range on average
424 between 23-88%, suggesting that while Pinaceae was high at some sites, it does not appear to
425 completely overwhelm the assemblage as might be expected if over-representation was to be
426 a significant problem. We also find that including Pinaceae in the pollen assemblage of the
427 LGM marine pollen samples gives pollen-climate reconstructions that are statistically
428 indistinguishable from those obtained by excluding Pinaceae from the assemblage. Including
429 Pinaceae in marine samples also provides compatibility with terrestrial samples, particularly
430 when calculating and plotting pollen taxa percentages. For these reasons we have included
431 Pinaceae in the analysis of all marine pollen samples in this study, although it is important to
432 recognize that Pinaceae in such samples can be subject to over-representation and that the
433 results presented here from marine sites should consequently be viewed with caution.

434 435 **2.5 Quantitative tree cover reconstruction**

436
437 It has long been recognized that the proportional representation of individual pollen taxa in a
438 pollen assemblage does not necessarily reflect the proportion of land area covered by that
439 taxa in the pollen source area surrounding the sample site (Davis 1963, Gaillard et al. 2010,
440 Zanon et al. 2018). These differences can be caused by variations in pollen productivity,
441 differential transport, deposition and preservation of pollen grains, and even the ease or
442 otherwise of the identification of pollen grains themselves. This can make the interpretation
443 of pollen taxa percentages difficult, even for relatively simple questions such as the
444 proportion of forest to non-forest in the landscape.

445

446 There have been two main methods developed to account for this quantification problem, one
447 using a physical modelling technique (PMT) based on estimates of pollen production for
448 individual taxa (Gaillard et al., 2010), and the other using a MAT very similar to that used in
449 pollen-climate reconstructions (Williams and Jackson, 2003). Both approaches have been
450 widely applied during the Holocene in Europe (Zanon et al., 2018), but we know of no
451 previous study that has applied either of these approaches to the LGM. The LGM presents a
452 number of challenges, not least the problem of potential missing vegetation analogues, as
453 well as low atmospheric CO₂, which has been shown to influence pollen productivity (Leroy
454 and Arpe, 2007).

455

456 Here we use the MAT to provide quantitative estimates of forest cover, following the
457 approach of Zanon et al. (2018) who applied this method to the Holocene pollen record of
458 Europe. We apply MAT in exactly the same way as for the climate reconstructions described
459 earlier, including the use of PFT scores to match fossil and modern pollen samples. Instead of
460 modern climate values, we assigned an estimate of modern forest cover to each of our
461 modern pollen sites. To do this we use a high resolution (~100m) remote sensing dataset
462 derived from satellite observations (Hansen et al., 2013). Zanon et al. (2018) have shown that
463 the MAT calibrated in this way gives comparable results to the PMT approach in Europe, at
464 least for the Holocene. One of the main differences however is that the PMT is designed to
465 provide estimates of the proportions of different taxa, whereas the MAT (as applied here) is
466 designed to provide estimates of the proportion of forest cover. Where the PMT can only
467 reconstruct the proportion of forest forming trees, irrespective of their size, the MAT
468 (following Zanon et al. 2018) is calibrated specifically to reconstruct forest composed of trees
469 over 5m tall. This follows the FAO definition of forest as “land spanning more than 0.5
470 hectares with trees higher than 5 meters and a canopy cover of more than 10 percent, or trees
471 able to reach these thresholds in situ” (FAO Terms and definitions 2020
472 <http://www.fao.org/3/I8661EN/i8661en.pdf>).

473

474 **2.6 Maps**

475

476 We present our results in the form of maps that include the main physiographic features of
477 the LGM in the study area. The maps are based on the WGS84 projection. Coastlines reflect
478 LGM sea level at 120m below present, while ice sheets are based on Ehlers et al. (2011).
479 Modern national country boundaries are also included for reference.

480

481 A5

482 **3. Results**

483

484 **3.1 Vegetation & Biomes**

485

486 Results of the biomisation analysis shows that steppe (STEP) was the most common biome at
487 the LGM across the study area, occurring at 36 out of 63 sites, indicating that the landscape
488 was largely dominated by cool temperate grasslands across much of western Central Europe,
489 central and eastern Mediterranean, as well as North Africa and the Middle East (Fig. 2).
490 However, at the same time we also find that there were a significant number of sites where
491 we find that woody and forest biomes occur, more particularly in southern and eastern Iberia,
492 northern Italy and central eastern Europe. The most dominant of these forest and woody
493 biomes are taiga (TAIG) in the north, and cool-mixed forest (COMX) and xerophytic
494 woodlands (XERO) in the south.

495
496 As would be expected, the dominance of STEP biomes is generally reflected in low arboreal
497 pollen percentages across the same areas/sites (Fig. 3 & 4). Exceptions to this rule can be
498 found at marine sites such as [MD99-2331 site #3] and [MD01-2430 site #58] where STEP is
499 reconstructed despite arboreal pollen percentages of 71 and 80 percent respectively. This
500 apparent contradiction illustrates some of the idiosyncrasies of the biomisation method,
501 especially when applying the method to marine pollen samples. In this case it is important to
502 remember that the AP% is calculated from the sum of the percentages of each relevant taxa,
503 but the score for each biome is the sum of the square root of the percentages of each of its
504 constituent taxa. This results in biomes with taxa with large percentage values scoring
505 proportionally smaller, and biomes with taxa with small percentage values scoring
506 proportionally larger. For example, a single taxa at 50% has a square root of 7.07, but the
507 sum of the square roots of 10 taxa each at 5% is 22.36 even though the sum of the
508 percentages is the same 50%. This effect can be particularly pronounced in marine pollen
509 samples because they are usually dominated by a single taxa (*Pinus*) that forms a high
510 percentage of the total assemblage. Since there are often more non-arboreal taxa than
511 arboreal taxa in a pollen assemblage, the non-arboreal taxa can dominate in the biomisation
512 process even if collectively their percentage of the assemblage is a lot less than the arboreal
513 taxa, resulting in a non-arboreal biome such as STEP having the highest biome score.

514
515 Of the main arboreal biomes, Taiga (TAIG) is the dominant biome at 3 sites at the eastern
516 end of the Alpine ice sheet, as well as at a site just to the north in northern Germany and a
517 site in Slovakia, while Cool Conifer Forest (COCO) is found at 1 site close to the
518 Scandinavian ice sheet in Lithuania. Cool Mixed Forest (COMX) is found much more widely
519 at 8 sites south of the Alps from south-west Iberia to Romania, with Xerophytic Scrub
520 (XERO) occurring at 8 sites with a similar distribution but not as far east or west. Cold
521 Mixed Forest (CLMX) occurs at just two sites in Georgia and the Alboran Sea at the far east
522 and west of the study area, while Warm Mixed Forest (WAMX) is the dominant biome at just
523 1 site in Southern Spain. We do not record Temperate Deciduous Forest (TEDE), Tundra
524 (TUND) or Desert (DESE) as the dominant biome at any site at the LGM, although they do
525 occur as sub-dominant biomes.

526
527 An alternative picture of LGM tree-cover is provided by the MAT reconstructions (Fig. 4).
528 MAT performance statistics for tree cover are shown in table 2, based on an evaluation using
529 the modern training set. This shows a relatively large root mean square error (RMSE) of
530 21.03. and an R2 of 0.52 that is not as good as for the MAT climate analysis, but overall the
531 results are comparable with previous MAT tree cover studies (Zanon et al., 2018). In general,
532 the MAT values (site average 34%) show forest-cover around 16% less than that suggested
533 from AP% (site average 50%) (Fig. A1), although sites with very low AP% also show higher
534 values based on MAT. These differences are consistent with comparisons between MAT and
535 AP% in Zanon et al (2018), although it should be noted that uncertainties related to the MAT
536 reconstructions are large ($\pm 23\%$). Zanon et al (2018) found that the differences between
537 MAT and AP% were greatest over Northern Europe and in Arctic and sub-Arctic climate
538 regions that are likely to be comparable to many areas of Europe during the LGM. These
539 regions today are associated with tree-forming taxa such as Birch that fail to grow to a height
540 of 5m or more, developing only as shrubs or krummholz forms.

541
542 Pollen taxa percentages are shown in supplementary figure A2, and distribution maps of the
543 33 most common taxa are shown in the supplementary figures A3-A8. Of the 21 arboreal
544 taxa, *Pinus* generally has the highest values and is the most widespread, being present at all

545 63 sites. Other acicular arboreal taxa include *Juniperus*, which also has a wide distribution
546 across EurMedMidEst although at lower values. The rest of the acicular arboreal taxa have
547 more regional distributions. *Picea* is found mainly to the north of the study region, away from
548 the Mediterranean, whilst *Abies* is generally found more to the south. *Larix* occurs only in the
549 central European area including the northern edge of the Po plain just south of the Alps,
550 whilst *Cedrus* is found mainly across south and west Europe in locations much further north
551 than its Holocene and modern distribution which is confined mainly to Morocco and Lebanon
552 (Collins et al., 2012). Temperate broadleaf arboreal taxa which also include cold-tolerant
553 species such as *Betula* and *Salix* are relatively widely spread across the EurMedMidEst
554 during the LGM, while less drought tolerant taxa such as *Alnus*, *Carpinus* and *Corylus* are
555 found more to the south-west through to the north-east. Other temperate broadleaf arboreal
556 taxa such as *Quercus* (deciduous) and *Ulmus* have a much more southern distribution, with
557 *Fraxinus*, *Olea*, and *Quercus* (evergreen) being more prevalent in the south-west. In contrast,
558 *Fagus* occurs more to centre and the east, while *Tilia* is found even in more northern
559 locations of central Europe. The remaining arboreal taxa are more shrubby and drought
560 adapted, with *Ephedra* and particularly *Ephedra fragilis* having a southern distribution,
561 whilst the more cold adapted *Hippophae* being found even in the north of central Europe
562 (similar to *Tilia*).

563
564 The main non-arboreal taxa generally indicate cool, dry and environmentally disturbed
565 conditions across much of the EurMedMidEst. The most widely distributed taxon is Poaceae,
566 which like *Pinus*, is found in all records. Other non-arboreal taxa with a widespread
567 distribution include Rubiaceae, Apiaceae and Asteraceae (Asteroideae), while *Plantago*,
568 Cayophyllaceae, Brassicaceae and Asteraceae (Cichorioideae) have a more southern and
569 western distribution. *Thalictrum* can be found mostly at sites in the centre of the
570 EurMedMidEst, along with *Helianthemum* which also extends to sites in the south-west.
571 Other taxa such as *Chenopodiaceae* and *Artemisia* have a more southern distribution,
572 reflecting their preference for drier and less cold climates.

573

574 **3.2 Climate reconstruction evaluation**

575

576 Evaluation of transfer function performance based on the modern training set is presented in
577 table 2. This shows that root mean square error predicted (RMSEP) values were smallest for
578 summer temperatures (2.21C), and largest for winter temperature (3.35C), with mean annual
579 temperatures in between (2.28C). The weaker performance for winter temperatures largely
580 reflects the much greater range of winter temperatures in the training set. In turn, this
581 contributes to a better R2 performance for winter temperatures (0.91) than annual
582 temperatures (0.9) and summer temperatures (0.81). Overall R2 performance for precipitation
583 is weaker than for temperature, which is typical because of the higher spatial variability of
584 precipitation compared to temperature. Summer precipitation has the strongest R2
585 performance (0.75) compared to winter and annual precipitation (both 0.69), as well as
586 smaller RMSE values (52mm) than winter (78mm).

587

588 Given the widespread occurrence of steppe during the LGM, we also undertook a separate
589 evaluation of transfer function performance in this type of environment. For this we used a
590 subset of 1588 pollen samples from the EMPD2 that are classified with the steppe pollen-
591 biome (Davis et al. 2020). The results indicate (Table A5) little difference in performance
592 compared to the full dataset, with a small decrease in performance in annual and summer
593 seasons in both precipitation and temperature, and a slight increase in performance in winter.

594

595 The results overall indicate good transfer function performance especially for temperature,
596 and are comparable with those found in other continental scale pollen-climate studies
597 (Bartlein et al., 2011). It is important to remember though that comparisons between studies
598 can only be made with caution because results are often heavily dependent on the nature of
599 the modern pollen dataset used as the training set (Juggins, 2013), as well as the method used
600 (Salonen et al. 2019, Brewer et al. 2008, Peyron et al., 2013).

601

602

603 **3.3 Climate reconstruction**

604

605 Reconstructed LGM temperatures indicate an overall mean annual cooling of $-7.2 \pm 3.3\text{C}$,
606 with a greater cooling of around $-9.3 \pm 4.5\text{C}$ in winter and $-5.0 \pm 3.2\text{C}$ in summer (Fig. 5). All
607 sites apart from Lake Van [site #62] in eastern Turkey show cooler temperatures at the LGM
608 compared to modern (Fig. 6), and even at this site cooler conditions fall within the
609 uncertainties. With greater cooling in winter compared to summer, the difference in
610 temperature between winter and summer also increased (shown by positive anomalies) at
611 most (but not all) sites (Fig. 6). This increase in continentality was around $+4.2\text{C}$ on average
612 across all sites (Fig. 5).

613

614 We reconstruct an overall decline in mean annual precipitation of around $-91 \pm 270\text{mm}$ ($-$
615 13%) at the LGM. Most of this decline is in winter ($-38 \pm 90\text{mm}$) (-21%), while in summer a
616 small increase is shown ($10 \pm 57\text{mm}$) (6%), although uncertainties are large (Fig. 7).

617 Compared to temperature there is significant seasonal and spatial variability in positive and
618 negative precipitation anomalies (Fig. 8). Positive anomalies appear more predominant in
619 eastern and southern Spain and in central eastern Europe in both summer and winter, while
620 positive anomalies are found more generally in summer across sites in Southern Europe and
621 the Mediterranean. These more positive summer anomalies also reflect a relative shift from
622 winter to summer in the seasonality of precipitation in this region.

623

624 **4.0 Discussion**

625

626 Before we consider the results of our analysis it is important to provide some context in terms
627 of European LGM geography and environment, which was very different from today (Fig. 1).
628 Major ice sheets covered Scandinavia and much of the UK, the Alps, and the Pyrenees. Sea
629 level was 120m lower, resulting in much of the North Sea and English Channel becoming dry
630 land, and the European coastline extending over 100 km out into the Atlantic and
631 Mediterranean, especially around the Bay of Biscay and Adriatic. The Black Sea was no
632 longer connected to the Mediterranean, and was smaller with a water level around 100m
633 lower than today (Genov, 2016). These changes in sea or water level had two main
634 consequences, the first being that the marine sites were closer to land, and therefore closer to
635 (low lying) terrestrial vegetation and (pollen carrying) river discharge points than they are
636 today. The second consequence of lower seas levels is that terrestrial pollen sites were
637 located further from the moderating effect of the ocean than they are today, resulting in a
638 localised modification of the climate experienced by the site irrespective of regional or global
639 changes (Geiger, 1960).

640

641 The maps used in our analysis shows the maximum ice sheet at $21\text{k} \pm 2\text{k}$ (Ehlers et al., 2011).
642 The precise geographical location of the ice sheet is difficult to resolve at a fine spatial scale,
643 however, which explains why some sites close to the ice margin appear to be actually located
644 under the ice (for example sites Kersdorf-Briesen site #46 & Mickunai site #54). The

645 resolution of the map also shows the occurrence of permanent ice not only to the north and
646 over the Alps, but also on many subsidiary areas of high ground across central and southern
647 Europe, including areas such as the Pyrenees, Massif Central, Vosges and Carpathian
648 Mountains. While global ice volume may have peaked ~21 ka individual ice sheets in Europe
649 and other areas are known to have reached their maximum extent at different times (Hughes
650 et al., 2016). The larger ice sheets are likely to have had a significant influence on regional
651 climate and environmental conditions across Europe, but the smaller ice sheets had similar if
652 more localized impacts as well. Surrounding each ice sheet would have been an unglaciated
653 area of active peri-glacial processes and newly created and unstable ground. This would
654 include outwash plains, impounded lakes and recently drained lake beds, seasonally and
655 sporadically flooded areas, moraines, kettle holes and other glaciological and peri-glacial
656 features. Soils in these areas would be non-existent or skeletal, and vegetation would find it
657 difficult to obtain nutrients and water for survival, irrespective of the prevailing climatic
658 conditions. Outside of these areas, permafrost is also likely to have been present, particularly
659 north of the Alps (Vandenberghe et al., 2014), which would also act as an impediment to
660 vegetation growth.

661
662 In terms of regional climate, the major ice sheets would have provided significant barriers to
663 westerly atmospheric circulation, or even north-south circulation in the case of the Alps and
664 Pyrenees. As well as representing a physical obstruction, the thermodynamic response of the
665 atmosphere to these high, cold obstructions would have been to encourage the formation of
666 areas of semi-permanent high pressure, similar to those found today for instance over the
667 Greenland ice sheet. In addition, the Laurentide ice sheet located over North America would
668 have generated downstream effects over Europe (COHMAP, 1988). These physical and
669 thermodynamic effects would have affected the direction of storm tracks, as well as more
670 local climatic effects commonly associated with ice sheets such as strong katabatic winds
671 (Kageyama, et al. 2021, Velasquez et al. 2021, Luetscher et al. 2015, Lefort et al. 2019)

672 673 **4.1 Vegetation Cover**

674
675 The nature and extent of forest cover during the LGM remains a matter of considerable
676 debate. Vegetation models driven by LGM climate model simulations generally indicate
677 extensive areas of boreal forest north of the Alps, and a mix of temperate and warm-
678 temperate woodland to the south across southern Europe and much of the Mediterranean.
679 Treeless areas such as steppe are mainly confined to those areas where it is also found today,
680 namely inland Iberia, Ukraine, southern Russia and Turkey, while tundra is found to the north
681 close to the Scandinavian Ice Sheet (Allen et al., 2010; Cao et al., 2019; Prentice et al., 2011;
682 Velasquez et al., 2021).

683
684 Evaluation of these vegetation-model simulations against data has been largely based on
685 comparison with compilations of pollen-biome reconstructions (Prentice et al., 2011; Allen et
686 al., 2010; Cao et al., 2019; Velasquez et al., 2021). Early studies were based on only a limited
687 number of sites from southern Europe, and showed steppe at all sites in contradiction with
688 model simulations (Elenga et al. 2000). More recent pollen compilations have included more
689 sites especially to the north that have revealed a more mixed picture of vegetation cover, with
690 forest biomes at some sites both south and north of the Alps that appear more consistent with
691 model simulations (Binney et al., 2017; Cao et al., 2019). However, many of these pollen
692 sites used in these studies were assigned an LGM age based on poor or incorrect dating
693 control, and likely date to MIS3, the Late-Glacial or even the Holocene. Nevertheless, based
694 on our compilation of more securely dated LGM pollen sites, we also show a wider

695 distribution of forest biomes particularly in Iberia, northern Italy and Central Europe,
696 although with greater areas of steppe than suggested by the models over the remaining
697 regions.

698
699 However, the interpretation of biome reconstructions requires care since the forest cover and
700 vegetation composition may not be as clear as the dominant biome suggests. For instance, we
701 find that steppe is still reconstructed as the dominant biome at some sites despite arboreal
702 pollen forming 70-80% of the pollen assemblage. In addition, it is important to remember
703 that pollen-biomes are based only on the proportion of taxa that can form forest and
704 woodland, while these taxa may in fact exist only as shrubs or stunted krummholz forms in
705 the challenging climate and environment of the LGM. Alternatively, similar conditions may
706 favour low-lying non-arboreal taxa forms with poor pollen dispersion or even insect
707 pollinated taxa forms that may be poorly represented in the pollen assemblage, giving greater
708 prominence to arboreal taxa whose pollen may be the result of long-distance transport
709 particularly *Pinus*. However there also appear to be plenty of samples with low or even very
710 low (<20%) arboreal percentages, so not all sites in open areas may be affected by long-
711 distance transport of *Pinus* in the same way.

712
713 Quantitative MAT based reconstructions of forest cover can overcome some of these
714 problems, where they can be detected, based on the composition of the pollen assemblage
715 when compared with the modern land-cover. Chord-distance measurements of the match
716 between fossil and modern pollen assemblages indicate good LGM analogues exist in our
717 large Eurasian modern pollen dataset. The results of the MAT forest cover reconstruction
718 indicates that forest cover was low but not entirely devoid of woodland in most areas, similar
719 to the modern boreal forests of Siberia and consistent with a steppe-tundra-woodland mosaic
720 proposed by many authors (e.g. Birks and Willis, 2008; Willis and Van Andel, 2004). This is
721 confirmed in an analysis of the most commonly found modern analogue ecoregions for LGM
722 pollen samples at each site (Table A6). Uncertainties are large, but for comparison the MAT
723 site-average of 33% forest cover is slightly less than the average today over the Boreal region
724 of Europe (43%) and slightly more than the average today over Mediterranean region (27%)
725 (Zanon et al. 2018).

726
727 By calculating the percentage of each of the taxa in each LGM pollen sample using a
728 standardized pollen sum, we are able to make direct comparisons between different LGM
729 pollen records and their taxa percentages (Figure A2, A3). The results show a preponderance
730 of boreal forest taxa to the north of the Alps, consistent with biome results mentioned earlier.
731 *Pinus* is the most common forest forming taxa in this boreal zone, together with *Picea*, and
732 including *Larix* to the east and *Abies* to the west. The occurrence of *Betula* and *Juniperus*
733 also suggests shrubby elements consistent with arctic shrub-tundra, although high Poaceae
734 and other herbaceous taxa such as *Artemisia* and *Chenopodiaceae* indicate more steppe than
735 tundra. Other deciduous taxa found north of the Alps include cold tolerant generalists such as
736 *Corylus* and *Alnus*, as well as low percentages of relatively thermophilous taxa in the east,
737 such as *Carpinus* and *Tilia*.

738
739 These results are consistent with charcoal (Magyari et al., 2014a; Willis and Van Andel,
740 2004), malacological (Juříčková et al., 2014), biomarkers (Zech et al., 2010) and genetic
741 evidence (Stivrins et al., 2016; Willis and Van Andel, 2004) that the main forest region north
742 of the Alps was in the eastern region of Central Europe around the Carpathian basin. This
743 was also an area where cold and moisture sensitive deciduous taxa were also able to survive
744 (Magyari et al., 2014), although evidence of temperate taxa found in the pollen record has yet

745 to be supported by charcoal and macrofossil records (Feurdean et al., 2014). Our pollen
746 evidence indicates an open taiga or cool mixed forest that extended in central and eastern
747 Europe to areas close to the Scandinavian and Alpine ice caps, as proposed by Willis and Van
748 Andel (2004) and Huntley and Allen (2003), although whether this represents isolated
749 pockets of forest or an extended open steppe-forest is difficult to determine (Kuneš et al.,
750 2008). Even steppe or tundra areas in western Europe show a low but significant presence of
751 the pollen of tree taxa at sites close to the ice sheets that are unlikely to be solely the result of
752 long distance transport or reworking (Kelly et al., 2010). The presence of woodland in these
753 areas is also supported by mammalian remains, for instance at Kents Cavern in SW England
754 (Stewart and Lister, 2001).

755
756 Overall however, our results clearly show a much greater predominance of thermophilous
757 and moisture sensitive deciduous taxa south of the Alps, particularly in Iberia and Northern
758 Italy, where temperate broadleaf forests survived in sheltered refugia (Kaltenrieder et al.,
759 2009). Most of these appear to be in hilly areas with the ability to generate orographic rainfall
760 (Monegato et al., 2015), on south facing slopes to make the most of the sun's radiant energy
761 and located above the valley floor to escape frost and flooding. We might also expect these
762 areas to be sheltered from cold northerly winds, and benefit from relatively mild and moisture
763 laden winds coming from the Mediterranean Sea. For instance, the presence of woodland and
764 low glacier altitudes along the southern slopes of the Alps around the Po Valley and Trentino
765 region is consistent with strong orographic rains generated by southerly and easterly winds
766 that today can be generated by low pressure located south of the Alps in the Gulf of Genoa,
767 and consistent with a southerly storm track around the Alps (Kehrwald et al., 2010; Luetscher
768 et al., 2015). Generally, as might be expected, areas of forest reconstruct similar or increased
769 precipitation compared to today, and areas of steppe indicate decreased precipitation (see next
770 section).

771
772 Independent evidence of LGM vegetation is provided by archaeozoological data. This data
773 supports the palynological evidence for the existence of forest and woodland refugia across
774 the ice-free areas of Europe at latitudes north of the Alps. For instance, large vertebrates in
775 these areas show patterns of extirpation and extinction in response to shifts in climate and
776 vegetation cover that is different for different species, indicating a variety of environments
777 and niches (Lister and Stuart, 2008; Stewart and Lister, 2001). As with the pollen record, the
778 presence of temperate adapted large vertebrate taxa within the glacial landscape of Western
779 Europe also suggests the existence of temperate “micro-refugia” (Stewart and Lister, 2001) ,
780 consistent with suggestions that temperate arboreal taxa were not entirely extirpated from the
781 region during the LGM (Magri, 2010). Further east, mammal assemblages indicate
782 generalized loss of forest components in the East European Plain (Demay et al. 2021,
783 Puzachenko et al., 2021) which is consistent with our data indicating low forest cover in this
784 region. In other areas, evidence of the prevailing land cover at the LGM comes from studies
785 of small vertebrate communities, which have a closer affinity to the prevailing environment
786 than large vertebrates (López-García and Blain, 2020) that have the propensity to migrate
787 large distances, often on a seasonal basis. These studies of small vertebrate assemblages also
788 support the existence of temperate “micro-refugia” in France (Royer et al., 2016) and the
789 existence of woodland components in many regions across Southern Europe including parts
790 of Iberia (Bañuls-Cardona et al., 2014) Italy (Berto et al., 2019) and the Balkan Peninsula
791 (Mauch Lenardić et al., 2018).

792
793 Other paleobotanical evidence also supports our land cover reconstruction. Schafer et al.
794 (2016) suggest leaf wax patterns from palaeosols in Spain may indicate the presence of

795 drought intolerant deciduous trees and more humid conditions during the LGM. Significantly,
796 none of the pollen sites indicate that temperate broadleaf forests were dominant, and
797 broadleaf temperate taxa always appear part of a mixed woodland together with cold or
798 aridity adapted evergreen and needleleaf taxa, including typical Mediterranean taxa. This type
799 of mixed vegetation probably extended to the Balkans where the hilly terrain and proximity
800 to the Mediterranean would appear to have provided favourable climatic conditions, although
801 we still lack LGM sites from this region. At sites in central and southern Italy and east
802 through Greece and Turkey to the Middle East (and including North Africa), the vegetation
803 appears drier with a greater prevalence of steppe. Only a site in Georgia at the edge of the
804 Caucasian mountains indicates the presence of significant amounts of forest (mainly *Pinus*), a
805 result that was also found by Tarasov et al. (2000), and probably linked to favourable
806 orographic precipitation and proximity to the Black Sea.

807
808 Comparison with LGM land cover from vegetation modelling studies driven by climate
809 model simulations indicate a much wider presence of forest than that shown by the pollen
810 data (Kaplan et al., 2016). Data-model agreement appears to be closest over eastern-central
811 Europe where pollen indicates the presence of open boreal forest, and over south-west
812 Europe with the presence of cool mixed temperate forest, including broadleaf deciduous and
813 thermophilous elements (Prentice et al., 2011; Allen et al., 2010; Cao et al., 2019; Velasquez
814 et al., 2021). Nevertheless, agreement still appears to be weak over western-central Europe
815 and Southern and Eastern Europe through to the Middle East, where pollen data continues to
816 indicate widespread steppe. One proposed explanation for this data-model discrepancy has
817 been the role of fire (including man-made fire) in maintaining forest openness, a factor
818 influencing forest cover that is not included in most vegetation models (Kaplan et al., 2016).
819 In the Carpathian basin Magyari et al. (2014a) noted that charcoal increased as forest cover
820 declined, suggesting that wildfires played a role in decreasing forest cover during the LGM.
821 Other studies have noted low levels of charcoal and therefore fires during the LGM, although
822 these tend to be from steppe areas with low biomass and fuel availability (Connor et al.,
823 2013; Kaltenrieder et al., 2009). Recent LGM vegetation simulations that include fire indicate
824 much lower values of forest cover than those without fire over western central Europe, while
825 forest remains in central eastern Europe (Velasquez et al., 2021). This appears closer to the
826 data, but the values are perhaps too low compared with our MAT reconstructions here
827 (Figure 4).

828 829 **4.2 Climate**

830 831 **4.2.1 Comparison with previous pollen-based reconstructions**

832
833 The climate of the LGM is generally considered to have been cooler and drier than today, but
834 data-model comparisons continue to highlight important discrepancies, not only in the degree
835 of cooling and drying but also in their seasonal and spatial distribution. Data-model
836 comparisons over Europe have mainly used pollen-based climate reconstructions, especially
837 the Paleoclimate Modelling Intercomparison Project (PMIP/CMIP) (Kageyama et al., 2021,
838 Bartlein et al., 2011; Harrison et al., 2015; Kageyama et al., 2006; [Braucher et al 2007](#) ;
839 [Braucher et al 2012](#), [Cleator et al 2020](#)). The most commonly used reconstructions have
840 been based on two main methods, a neural-network methodology (ANN) of Peyron et al.
841 (1998) and Jost et al. (2005), and an Inverse Modelling approach (INV) applied by Wu et al.
842 (2007). The ANN method uses modern pollen samples and does not include any correction
843 for CO₂ effects, being similar in these respects with the MAT method used in this study. In
844 contrast the INV method does not use modern pollen samples, but instead uses a process-

845 based vegetation model run in inverse mode (Guiot et al. 2000). Ordinarily, a vegetation
846 model will use climate as an input to generate a vegetation as an output, but in inverse mode
847 the model is reconfigured so that the input climate (and CO₂) can be varied iteratively until
848 the closest match is found between the vegetation simulated by the model (represented by
849 PFT scores) and the fossil pollen assemblage (also represented by PFT scores). . One of the
850 advantages of the INV method is that CO₂ can also be varied as an input, and therefore the
851 effect of changes in CO₂ on the vegetation, and therefore reconstructed climate, can be
852 investigated. Comparison of these ANN and INV reconstructions have shown important
853 differences, with the INV reconstruction generally not as cold and somewhat drier than ANN
854 (Wu et al. 2007). These differences between pollen-climate methods have often been
855 attributed to CO₂ effects (Wu et al. 2007) but this is not clear since there may be other
856 factors, such as the size and location of the training set used in the ANN reconstruction.

857
858 We make a comparison with these earlier reconstructions based on 10 sites/records in our
859 dataset which we identified as also being included in these earlier studies (Fig. 9). While we
860 were able to identify the site and data source, as well as the time window, we were unable to
861 establish if the the data represented a single sample or the mean of multiple samples within a
862 time-window or the exact depth of those samples, or the actual sediment core in the case of
863 multiple cores from the same site. While these aspects are unknown, it seems likely that the
864 pollen data we used in our analysis was very similar if not identical in most cases, and
865 reconstructed biomes for these sites from our pollen dataset are identical to the biomes
866 reconstructed using the earlier pollen dataset (Elenga et al., 2000).

867
868 We compare our MAT with the ANN and INV reconstructions in figure 9. On average across
869 all 10 records, the MAT and INV methods give almost identical results for both anomalies of
870 mean annual temperature (MAT -6.6C, INV -7.2C) and precipitation (MAT 158mm, INV
871 165mm). Uncertainties are also similar for both methods. In contrast, the ANN method gives
872 much cooler mean annual temperature anomalies (ANN -13.9C) and drier precipitation
873 anomalies (ANN -474mm). On a site by site basis the MAT and INV methods show closer
874 agreement for temperatures than precipitation, although precipitation has proportionally
875 larger uncertainties. The reconstructions based on these two methods are close enough that
876 the uncertainties overlap at all sites for both temperature and precipitation, except the
877 precipitation reconstruction at Lac de Bouchet (site #25). The reason for this is not clear, but
878 there could easily be minor differences with the pollen data analysed by Wu et al. (2007) in
879 their INV reconstruction since the pollen record (Reille and de Beaulieu, 1988) includes
880 multiple cores each with many different samples covering the LGM period.

881
882 This comparison shows that our MAT reconstructions are very similar to the INV method,
883 but not as cold or dry as the ANN method. This has two main implications. The first is that
884 our reconstructions indicate greater agreement with the results of climate model simulations
885 since climate models indicate temperatures closer to the INV reconstructions (Latombe et al.,
886 2018) than the ANN reconstructions (Jost et al., 2005; Kageyama et al., 2006). The difference
887 between our MAT and earlier ANN reconstructions is likely the result of the modern pollen
888 datasets used, since the ANN reconstruction was based on a considerably smaller number of
889 samples taken mainly from the cold dry steppes of Kazakstan and Mongolia.

890
891 The second implication is that the MAT method may not be significantly impacted by the
892 effects of lower CO₂ (Cowling and Sykes, 1999; Prentice and Harrison, 2009; Williams et
893 al., 2000) or indeed insolation changes during the LGM, since the MAT results are similar to
894 those based on the INV method which specifically takes account of these non-climatic factors

895 (Wu et al., 2007). This would suggest that MAT could also work well for pollen-based
896 climate reconstructions on longer glacial-interglacial timescales where insolation and CO₂
897 vary significantly from their modern values. This is consistent with the findings of Pini et al.
898 (2021) who applied a correction algorithm developed by Prentice et al. (2017) and Cleator et
899 al. (2020) to a MAT reconstruction of mean annual precipitation at Lake Fimon in Northern
900 Italy. This shows a very small correction of 0mm to 30mm for samples across the LGM time-
901 window, which indicates that CO₂ is not a very significant factor in influencing this type of
902 reconstruction, at least compared to the overall uncertainties (+/- 200mm) of the
903 reconstruction itself. The uncertainties associated with the correction algorithm are not
904 discussed, but given that inputs include estimates of both LGM temperature and cloud cover,
905 it seems likely that these could be significant. Importantly, both Pini et al (2021) and Cleator
906 et al (2020) specifically exclude the necessity of applying a correction algorithm to
907 temperature reconstructions, since they consider only hydrological variables to be affected by
908 changes in atmospheric CO₂.

909
910

911 **4.2.2 Comparison with climate reconstructions based on other proxies**

912
913

913 **4.2.2.1 Temperature**

914

915 Proxies that are not based on plants should remain unaffected by the CO₂ problem during the
916 LGM, and provide an alternative basis for evaluating pollen-based reconstructions. Samartin
917 et al. (2016) reconstructed LGM summer temperatures based on chironomid remains from
918 Lago della Costa (site #34) in Northern Italy. They also undertook pollen analysis on the
919 same samples down the core, allowing us to make a sample-by-sample comparison between
920 the chironomid temperature record and our MAT reconstruction (Fig. 10). Our pollen-climate
921 reconstruction is for JJA mean temperature, while the chironomid reconstruction is for July
922 mean temperature, with the anomalies based on the modern equivalent JJA and July mean
923 temperatures respectively. The average anomaly values for all 8 samples reconstructed by the
924 pollen-climate MAT are $-10.2 \pm 3.5^{\circ}\text{C}$, and for the chironomids $-9.5 \pm 3.0^{\circ}\text{C}$. This indicates
925 that pollen and chironomid average summer temperature reconstructions are very similar on
926 average, taking into account the overlapping uncertainties, while also showing a strong
927 similarity on a sample-by-sample basis throughout the time-series.

928

929 Other reconstructions based on other proxies provide a basis for more general regional
930 comparisons (Figure A9, A5). We reconstruct both summer and winter temperatures and
931 show that cooling in winter was greater than in summer at most sites, associated with an
932 increase in continentality (increased temperature difference between summer and winter). A
933 similar seasonal pattern of temperature change has also been shown in other studies that
934 reconstruct both summer and winter LGM temperatures, including Prud'homme et al. (2016)
935 using d18O analysis of earthworm calcite granules at Nussloch near the French-German
936 border, Bañuls-Cardona et al. (2014) using faunal remains of small mammals at 4 locations in
937 western Spain, and Ferguson et al. (2011) who examined seasonal temperature change using
938 d18O and Mg/Ca analysis of limpet shells at Gibraltar in southern Spain. The increase in
939 continentality at Nussloch (Prud'homme et al., 2016) was reconstructed at between 11.6 to
940 15.6 °C, comparable at the lower end with nearby pollen sites [La Grotte Walou site #28]
941 $10.4 \pm 5.8^{\circ}\text{C}$ and [Bergsee site #29] $7.9 \pm 5.7^{\circ}\text{C}$. The faunal sites in western Spain studied
942 by Bañuls-Cardona et al. (2014) gave much reduced increases in continentality, but
943 nevertheless similar to nearby pollen sites. For instance at Valdavara 5.1°C [MD99-2331 site
944 #3] $5.2 \pm 3.1^{\circ}\text{C}$, El Miron 1.2°C [Tourbiere de l'Estalles site #19] $5.1 \pm 6.2^{\circ}\text{C}$, El Portalon

945 0.9C [Torrecilla de Valmadrid site #16] 2.8 ± 1.8 °C and Cueva de Maltrvieso 6.1C [SU81-18
946 site #2] 4.8 ± 3.4 °C. Further south at Gibraltar the limpet-based study of Ferguson et al.
947 (2011) also shows a relatively small increase of 2 °C. The nearest pollen site [Gorham Cave
948 site #5] however shows a larger increase of 4.7 ± 2.3 °C, although differences could be
949 expected given the different temporal resolution of annual laminae on mollusk shells
950 compared to pollen assemblages that reflecting much slower changes in trees and other long-
951 lived flora.

952
953 Summer temperatures were warm enough during the LGM over the Alpine areas that Swiss
954 lakes were largely ice free in summer, while glacier ELA's around the time of the LGM
955 suggest summers were -6.5 to -7.7 °C cooler compared to the LIA (Heiri et al., 2014). This
956 cooling was similar to that found at Nussloch some 200km north of the Swiss border by
957 Prud'homme et al. (2016), who reconstructed anomalies of -6 to -8 ± 4 °C from d18O
958 analysis of earthworm calcite granules (representing warm season May-September
959 temperatures). Slightly less cooling was found close by at the nearby site of Achenheim
960 where analysis of Mollusc assemblages gave summer (August) cooling estimates of -3.5 to -
961 6.5 °C based on MAT (Rousseau, 1991), and -5.5 to -9.5 °C based on the Mutual Climatic
962 Range method (Moine et al., 2002). These reconstructions appear somewhat cooler than
963 nearby pollen sites [La Grotte Walou site #28] -1.4 ± 3.6 °C and [Bergsee site #29] -2.7 ± 5.1
964 °C, although comparable with the pollen site [Pilsensee site #32] -7.3 ± 5.0 °C 200 km further
965 east. Similar differences also occur at the site of Les Echets on the western edge of the Alps
966 where a diatom based reconstruction of summer (July) temperatures (Ampel et al., 2010)
967 indicated a greater cooling (-10.5 to -11.5 °C) than our pollen reconstruction [Les Echets G
968 site #27] (-4 ± 2.7 °C). However, the authors caution that the results were based on poor
969 analogues and rare taxa, as well as a small training set of only 90 lakes in Switzerland.

970
971 South of the Alps, other proxies show the opposite relationship with the pollen
972 reconstructions. For instance, at Lago della Costa in the Po valley, a summer (July)
973 temperature chironomid reconstruction by Samartin et al. (2016) is around 1-2 °C less cool
974 than the pollen reconstruction (JJA) for the same site [Lago della Costa site #34] $-11.4 \pm$
975 2.7 °C, although both reconstructions fall within their respective uncertainty ranges (Figure 8).
976 In the Pindus Mountains in Greece, Hughes et al. (2006) estimated LGM summer
977 temperature anomalies of -7 °C based on glacier modelling, which is comparable with that
978 reconstructed at the nearest pollen site [Ioannina site #51] -7.7 ± 2.8 °C. In Spain the analysis
979 of small mammal remains by Bañuls-Cardona et al. (2014) shows similarly less cooling in
980 summer or even warmer than present positive anomalies compared to the nearest pollen sites,
981 such as Valdavara 1.4 °C [MD99-2331 site #3] -2.3 ± 2.8 °C, El Miron -2.3 °C [Tourbiere de
982 l'Estarres site #19] -5.7 ± 5.4 °C, El Portalon 0.8 °C [Torrecilla de Valmadrid site #16] $-2.6 \pm$
983 1.1 °C and Cueva de Maltrvieso -1.1C [SU81-18 site #2] -10.4 ± 2.8 °C. Further south at
984 Gibraltar, the limpet-based study of Ferguson et al. (2012) suggests an anomaly of around -7
985 °C, which is a greater cooling than the pollen reconstruction from this location [Gorham Cave
986 site #5] -1.3 ± 2.2 °C, although comparable with other pollen sites slightly further east.

987
988 Winter temperature reconstructions from non-pollen proxies show a similar pattern in relation
989 to pollen reconstructions as for summer temperatures. North of the Alps at Achenheim,
990 Prud'homme et al. (2016) use d18O on earthworm remains to reconstruct particularly cold
991 winter anomalies of -17.6 to -23.6 °C compared to nearby pollen sites [La Grotte Walou site
992 #28] -11.8 ± 8.0 °C and [Bergsee site #29] -10.6 ± 6.3 °C. South of the Alps in Spain, the
993 analysis by Bañuls-Cardona et al (2014) based on the remains of small mammals shows less
994 cooling in winter compared to the nearest pollen sites, in particular Valdavara -3.7 °C

995 [MD99-2331 site #3] -7.5 ± 3.4 °C , El Miron -3.5 °C [Tourbiere de l'Estarrès site #19] -10.8
996 ± 7.0 °C, El Portalon -0.1 °C [Torrecilla de Valmadrid #16] -5.4 ± 2.5 °C and Cueva de
997 Maltrvieso -7.2 °C [SU81-18 site #2] -15.2 ± 4.0 °C. And again, in southern Spain at Gibraltar,
998 analysis of limpet shells by Ferguson et al (2011) suggests winter cooling of around -9 °C
999 while the pollen reconstruction suggests [Gorham Cave site #5] -6.0 ± 2.5 °C, although sites
1000 further east indicate cooler conditions.

1001
1002 A number of additional proxies have also been used to reconstruct LGM mean annual
1003 temperature. Heyman et al. (2013) applied glacier mass balance modelling at sites located in
1004 the smaller mountain regions north of the Alps. These are generally slightly cooler than our
1005 pollen-based reconstructions at sites close to the Vosges Mountains -12.7 ± 2.0 °C and Black
1006 Forest -11.4 ± 2.3 °C [Bergsee site #29] -8.2 ± 3.3 °C, Bavarian Forest -10.7 ± 2.2 [Pilsensee
1007 site #32] -9.2 ± 1.2 °C and Giant Mountains -8.5 ± 1.8 [Kersdorf-Briesen site #46] -7.3 ± 0.3
1008 °C. These values obtained by Heyman et al. (2013) are warmer than Pud'homme et al. (2016)
1009 who estimated annual mean temperature anomalies of -15.1 to -19.1 °C based on $\delta 18\text{O}$ of
1010 earthworm calcite at the Nussloch site just north of the Vosge and Black Forest. The annual
1011 temperatures reconstructed by Heyman et al. (2013) are also around 2°C warmer than Allen et
1012 al. (2008) who applied a similar, although simpler method to over 29 different mountainous
1013 regions across Europe that had been glaciated during the LGM. Since glacier mass balance is
1014 a function of both snowfall and temperature, these estimated temperatures vary according to
1015 estimated changes in precipitation. For instance, mean annual temperature estimates by Allen
1016 et al. (2008a) are much cooler than reconstructed by pollen, with an average anomaly of -13.2
1017 °C for the 29 sites assuming a 40% reduction in precipitation, but this is reduced to -11.8 °C
1018 assuming the same precipitation as modern. *These average anomalies across all sites*
1019 *calculated by Allen et al (2008a) compare with an average temperature anomaly of -7.2 °C*
1020 *across all 63 of our pollen sites.* The glacier mass balance modelling by Allen et al. (2008a)
1021 assumes a seasonal distribution of precipitation that is similar to the present day, and does not
1022 consider increases in winter precipitation or mean annual precipitation above present day
1023 levels. Both of these are suggested by the pollen data in some regions, and both could explain
1024 glacier extent found during the LGM based on less extreme temperature anomalies more
1025 comparable with the pollen data. Mean annual temperatures have also been reconstructed
1026 from the Paris basin area in Eastern France by Bekaert et al. (2023) using the Noble gas
1027 proxy. The authors suggest an LGM temperature anomaly of -9.1 ± 0.9 °C although this is
1028 actually dated to 25.6 ± 0.5 k, which is earlier than our 21 ± 2.0 k time window that we adopt
1029 here. The sample closest to 21k is at 21.9 ± 0.5 k and suggests slightly warmer temperatures at
1030 -7.77 °C, which compares well with our pollen reconstructions nearby at [Bergsee site #29] -
1031 8.2 ± 3.3 °C and [La Grotte Walou site #28] -6.6 ± 3.1 °C.

1032
1033 To the east of the Alps in the Panonian basin, mean annual temperature anomaly estimates
1034 have been made from noble gas measurements on groundwater ranging from -2 to -4 °C
1035 (Stute and Deak, 1990) up to -9 °C (Varsányi et al., 2011). These are similar to estimates
1036 ranging from -2 to -9 °C from oxygen isotope ratios from mammoth tooth enamel (Kovács et
1037 al., 2012) and are comparable with nearby pollen sites [Feher Lake site #50] -8.2 ± 3.3 °C and
1038 [Kokad site #52] -4.5 ± 2.3 °C. On a broader scale, Sanchi et al (2014) estimated LGM
1039 cooling in the Danube and Dneiper basins based on Lipid biomarkers in a core from the
1040 Black Sea and came up with similar mean annual temperature anomalies between -6 to -10
1041 °C, which again are comparable with pollen sites from the region that range from
1042 [Nagymohos site #48] -10.5 ± 4.1 °C to [Straldzha site #57] -4.3 ± 5.8 °C.
1043

1044 Further south and west, García-Amorena et al. (2007) reported mean annual temperature
1045 anomalies of -2.0 to -11.3 °C at LGM sites along the Portuguese coast, based on an indicator
1046 species method using plant macrofossils. This is similar to the closest marine pollen sites off
1047 the coast, which recorded values of [MD95-2039 site #1] -10.5 ± 4.6 °C and [MD99-2331 site
1048 #3] -5.3 ± 2.9 °C. Meanwhile, in the far east of the study area, Zaarur et al. (2016) estimated a
1049 mean annual temperature anomaly of around -3 °C based on clumped isotope analysis of
1050 *Melanopsis* shells from LGM sediments in the Sea of Galilee. This limited cooling appears
1051 similar to the nearest pollen site [Lake Zeribar site #63] where we reconstruct a cooling of -
1052 2.2 ± 4.6 °C.

1053
1054 Reconstructions of LGM sea surface temperatures (SST's) provide yet another source of
1055 comparison with our terrestrial pollen-based reconstructions, although many of the physical
1056 processes controlling surface sea temperatures such as upwelling, surface mixing, surface
1057 currents, stratification and thermal inertia through the seasonal cycle, represent quite different
1058 processes to those controlling surface temperatures over land, particularly at the sub-regional
1059 scale. Nevertheless, the Atlantic coastal waters of Iberia and the waters throughout the
1060 Mediterranean Sea include many SST sites that lie in relative proximity to our terrestrial
1061 pollen-sites, allowing us to make a comparison at the largest scale. Within this area the
1062 MARGO database (MARGO Members, 2009) includes 13 Alkenone, 2 Mg/Ca and 41
1063 Foraminifera based SST records of mean annual temperature, with the Foraminifera records
1064 also providing an additional 41 winter (JFM) and summer (JAS) SST estimates. We compare
1065 the SST records with the 36 closest terrestrial pollen records which fall within a box of -11 to
1066 35 degrees longitude and 32 to 43 degrees latitude containing all of the SST records. A
1067 simple site average indicates a mean annual SST anomaly of -5.5 ± 1.0 °C which is relatively
1068 close to the value of -7.2 ± 3.4 °C obtained from the terrestrial pollen sites [sites #1-4, 5, 7-
1069 24, 25, 26, 30, 35-38, 41, 47, 51, 53, 56-59]. Interestingly the inter-site variance (standard
1070 deviation of the reconstructed temperatures across all sites) is almost identical for the two
1071 datasets, 2.57 °C for the SST sites and 2.63 °C for the pollen sites, despite representing very
1072 different environments, proxies and uncertainties. However, when we look at the seasonal
1073 temperature anomalies, we find very different results. Site averaged winter SST anomalies
1074 are -3.7 ± 1.1 °C compared to -9.3 ± 4.2 °C for winter temperatures from terrestrial pollen
1075 sites, while in summer the values are reversed, -7.0 ± 0.8 °C compared to -5.38 ± 3.3 °C
1076 respectively. This suggests that SST's experienced greater cooling in summer compared to
1077 winter, which is the opposite to that generally found in terrestrial seasonal temperature
1078 reconstructions throughout the region, although this is consistent with model simulations
1079 (Mikolajewicz, 2011).

1080 1081 **4.2.2.2 Precipitation**

1082
1083 Few proxies apart from pollen provide quantitative reconstructions of precipitation during the
1084 LGM. Glacier mass balance modelling includes assumptions about precipitation in order to
1085 derive temperatures (Allen et al., 2008a), but neither is independent of the other. Hughes et
1086 al. (2006) estimate from glacier modelling that mean annual precipitation during the LGM at
1087 sites in the Pindus mountains in Greece was around 2300 ± 200 mm, which they consider to
1088 be similar to the present day (>2000mm). A small change in precipitation compared to
1089 modern values is also indicated by the nearest pollen site, which is around 47 km to the south
1090 [Ioannina #51], and indicates a mean annual precipitation anomaly of -152 ± 294 mm,
1091 representing just 15% of the modern value. A larger reduction in mean annual precipitation of
1092 -45% (maximum) is reconstructed by García-Amorena et al. (2007) based on plant
1093 macrofossil remains from sites on the Portuguese coast. In comparison, the closest pollen

1094 sites record values which are a little lower, ranging from [MD95-2039 site #1] -22% to
1095 [MD99-2331 site #3] -34%. Further north in south-west Germany, Prud'homme et al. (2018)
1096 reconstructed mean annual precipitation from the delta 13C of earthworm calcite granules at
1097 Fussloch. They estimate a field site average of 333 (159-574) mm/yr at the LGM, which
1098 represents an anomaly of -503 mm/yr (-60%) relative to the modern precipitation of 836
1099 mm/yr. This is comparable with the closest pollen site [Bergsee #29] with an anomaly of -
1100 540 mm/yr.

1101
1102 As with glaciers, lake levels reflect changes in moisture balance that includes the effects of
1103 both temperature (via evapotranspiration) and precipitation, rather than just precipitation.
1104 They also represent semi-quantitative data at best, with changes often described relative to
1105 the modern or other baseline. There are few lake level records available north of the Alps, but
1106 to the south, many records indicate high lake levels in areas such as Spain (Lacey et al., 2016;
1107 Moreno et al., 2012; Vegas et al., 2010), Italy (Belis et al., 1999; Giraudi, 2017), Greece and
1108 Turkey (Harrison et al., 1996; Reimer et al., 2009) and the Middle East (Kolodny et al., 2005;
1109 Lev et al., 2019). These lake records are also supported by evidence of higher river levels in
1110 Morocco (El Amrani et al., 2008). The cause of the higher lake levels has been the subject of
1111 some debate, since many pollen records (and especially early biome reconstructions) show
1112 steppe vegetation that would suggest aridity that appears incompatible with higher lake
1113 levels. Prentice et al. (1992) proposed that the co-existence of steppe vegetation and high lake
1114 levels could be possible if precipitation increased outside of the summer growing season,
1115 while summers themselves were drier and cooler with decreased evaporation. However, the
1116 results of our analysis tend to indicate the opposite in regions with higher lake levels, with
1117 increased summer rainfall and decreased winter rainfall. In addition, the increase in summer
1118 precipitation was enough to compensate for the decrease in winter rainfall, leading to an
1119 overall increase in mean annual precipitation at many pollen sites in Spain and Greece for
1120 instance. This together with depressed temperatures and consequently decreased evaporation
1121 could explain the higher lake levels, whilst also limiting the growth of trees as a result of
1122 cooler temperatures and prolonged aridity outside of the summer season. Davis & Stevenson
1123 (2007) also note a differential hydrological response between summer and winter rainfall in
1124 the Mediterranean during the Holocene that may also provide an explanation. In this case
1125 sporadic summer storms may result in high rates of runoff that may fill run-off fed lakes, but
1126 low rates of soil moisture recharge that fails to benefit vegetation in the same way winter
1127 rainfall does.

1128
1129 Overall, we reconstruct only a small reduction in precipitation during the LGM of around
1130 91mm (13%) averaged over all sites, which is less than the ~200mm reduction based on the
1131 sites in the pollen-climate compilation used by PMIP (Bartlein et al., 2011). Since our
1132 precipitation reconstruction on average matches that of the INV reconstruction by Wu et al
1133 (2007), we can attribute much of the difference to the greater aridity shown in the ANN
1134 reconstruction by Peyron et al and Jost et al (2005) (see figure 9). As with temperature, this is
1135 probably a reflection of the modern training set used in the ANN reconstruction which is
1136 much smaller than our training set and is largely taken from the arid steppes of Kazakhstan
1137 and Mongolia. However, it is also important to recognize the significant spatial variability in
1138 precipitation, which means that a simple average of different sets of sites from different
1139 regions may not accurately reflect the change in LGM precipitation at the European scale.
1140 Nevertheless, one of the most consistent signals in our dataset is for an increase in summer
1141 precipitation over many areas of Southern Europe and the Mediterranean. This is also found
1142 in climate models, where it has been attributed to an increase in convection-driven
1143 precipitation, although the amount of precipitation generated by this mechanism varies

1144 significantly between models (Beghin et al., 2016). It may seem counter-intuitive to see an
1145 increase in reconstructed precipitation in the same regions where we also find a
1146 preponderance of steppe or xerophytic biomes and taxa, including *Artemisia* and
1147 *Chenopodiaceae*. This is attributable to the fact that climate can change quite markedly with
1148 necessarily invoking a major change in vegetation, and especially the pollen biome. For
1149 instance, a semi-arid climate ranges from 250-500mm rainfall a year, so we could expect a
1150 semi-arid vegetation to be dominant even if the rainfall increases 250mm (100%).

1151

1152 A more consistent response in models is for an increase in winter precipitation across
1153 Southern Europe and the Mediterranean related to a stronger and more southerly displaced jet
1154 stream, with winter precipitation also accounting for much of the change in mean annual
1155 precipitation (Beghin et al., 2016). Our reconstruction of winter precipitation however shows
1156 less support for this scenario with a more general decrease in winter precipitation apart from
1157 southern and eastern Iberia, and with summer precipitation generally more important in those
1158 sites that show an overall increase in mean annual precipitation. This may not necessarily
1159 contradict the models in terms of the strength and position of the winter jet stream, but may
1160 instead indicate that models over-estimate the amount of moisture being carried westward
1161 from the cold North Atlantic along the storm track, especially across the far northern
1162 Mediterranean. The increase in winter precipitation across southern and eastern Iberia is
1163 however entirely consistent with a strengthened and more southerly jet stream, which also
1164 brings increased winter precipitation to the region today as a result of blocking over northern
1165 Europe/Atlantic and a negative NAO (Vicente-Serrano et al., 2011).

1166

1167 Other areas that show an increase in winter precipitation include pollen sites around the
1168 eastern end of the Alps. This is consistent with a recent study by Spötl et al (2021) who
1169 argued, on the basis of cryogenic carbonates preserved in a cave in Austria, that heavy winter
1170 (and autumn) precipitation was a significant factor in driving LGM glaciation in the region.
1171 The seasonally specific nature of this precipitation is also supported by the same pollen sites,
1172 which do not show any increase in summer precipitation at this time.

1173

1174 **5.0 Conclusions**

1175

1176 We have reconstructed the climate and vegetation cover across Europe, North Africa and the
1177 Middle East at the time of the LGM based on 63 pollen records. These records were selected
1178 using strict quality control criteria, with particular attention paid to dating control, which led
1179 to the exclusion of many records that have been used in previous studies. This fully
1180 documented dataset represents the most chronologically precise and spatially resolved view
1181 of LGM climate and vegetation during the PMIP benchmarking time window at 21 ± 2 ka.
1182 Nevertheless, it is important to recognize that there are still significant spatial gaps in pollen
1183 sites especially north of the Alps, the Balkans, Turkey and the Middle East, and we continue
1184 to have only a partial understanding of the LGM over these areas.

1185

1186 One of the key questions concerning the vegetation landscape of the LGM in Europe has
1187 been the extent to which forest rather than steppe covered the continent, and to what extent
1188 temperate elements could be found north of the classical refugia areas of Southern Europe
1189 and the Mediterranean. Our results show that although steppe and tundra was extensive at the
1190 time of the LGM, areas of open forest also occurred in many regions, particularly (but not
1191 exclusively) in Iberia, northern Italy and Central Europe. These forest or woodland stands are
1192 likely to have been located in environmentally favourable areas, with good soils, elevated
1193 rainfall and shelter from cold, desiccating winds. In those areas where woodland existed,

1194 boreal taxa generally dominated north and east of the Alps, while temperate and
1195 thermophilous (mainly drought adapted) taxa were generally confined to areas south of the
1196 Alps and around the Mediterranean. The temperate deciduous forests that compose the
1197 climax community in many areas of Europe today were displaced to the south and reduced to
1198 a partnership role with boreal elements. Overall our new reconstruction indicates greater
1199 agreement with model land cover simulations, but models still appear to over-estimate the
1200 amount of forest and woodland over areas such as France and the Benelux, Greece, Turkey
1201 and the Far East.

1202
1203 Another key question about the LGM concerns the ability of climate models to simulate the
1204 climate of this period and whether pollen-based climate reconstructions which show
1205 disagreement with models have been biased by the effects of low CO₂ on plant physiology.
1206 We find that our new pollen-climate reconstruction shows much closer agreement with
1207 climate models than previous reconstructions that did not take account of low CO₂ effects.
1208 We also find close agreement with previous reconstructions that did take account of CO₂
1209 effects. Since our MAT method itself does not specifically take account of low CO₂ effects,
1210 this would suggest that this problem is not a significant hindrance to MAT performance at the
1211 time of the LGM, at least not compared to other uncertainties. Instead, we suggest that the
1212 main factor in the performance of pollen-climate transfer functions that use modern analogue
1213 methods is the provision of a large enough modern pollen dataset with suitable LGM
1214 analogues.

1215
1216 This conclusion is supported by comparison with climate reconstructions based on other
1217 proxies. We found little difference between our MAT reconstruction and a Chironomid-based
1218 summer temperature record based on a downcore sample by sample comparison, as well as
1219 comparisons with records from a variety of other proxies at a regional scale. However, it is
1220 notable that some studies using glacier mass balance modelling methods indicate LGM
1221 temperatures that are much cooler than our pollen-based reconstruction. The reasons behind
1222 this are not clear, but our pollen-based results indicate higher than present precipitation in
1223 some areas that could potentially explain low elevation glacier ELA's without the need for
1224 such cold temperatures.

1225
1226 We also find that although our pollen-based reconstruction and those of SST's generally
1227 agree in terms of mean annual temperatures, SST's indicate greater cooling in summer
1228 compared to winter, while terrestrial records indicate greater cooling in winter compared to
1229 summer. These seasonal differences are also reproduced in climate models, and probably
1230 reflect the different processes driving seasonal temperature change in the terrestrial and
1231 marine domain.

1232
1233 Our reconstructions of precipitation show large spatial and seasonal variability, but generally
1234 indicate less overall aridity than previously suggested from smaller scale studies which
1235 sampled less of the spatial domain. We find that in some regions of Southern Europe
1236 precipitation may actually have been greater than present, especially in summer, but also in
1237 winter in southern and eastern Iberia and around the southern slopes of the Alps. This may
1238 have important implications in understanding the development of LGM glaciation, which
1239 may be less a function of temperature than previously supposed. This could also help better
1240 explain the observed asynchronous nature of glaciation even within relatively small regions
1241 such as Europe, as a result of more localized controls on ice sheet development such as
1242 precipitation.

1243

1244 We hope that this new continental-scale dataset of climate and vegetation reconstructions will
1245 provide an improved baseline for data-model comparisons and other studies that will allow us
1246 to better understand the complex LGM environment.

1247
1248

1249 **Code/Data availability**

1250

1251 All of the data shown in the figures together with the fossil and modern pollen datasets will
1252 be made available on pangaea.de once the review process has been completed and these
1253 datasets are therefore no longer subject to change.

1254

1255 **Author contribution**

1256

1257 BASD designed the study, undertook the analysis and wrote the manuscript. MF and ER
1258 designed and prepared the maps. JOK and AB reviewed the manuscript and provided
1259 additional input.

1260

1261 **Competing interests**

1262

1263 The authors declare that they have no conflict of interest.

1264

1265 **Acknowledgements**

1266

1267 This work was supported by a grant from the Fonds de Recherche du Québec Société et
1268 Culture (2019-SE3-254686) to AB. Data were obtained from the European Pollen Database
1269 (EPD), based within the Neotoma Paleoecology Database (<http://www.neotomadb.org>). The
1270 work of data contributors, data stewards, and the Neotoma and EPD community is gratefully
1271 acknowledged. We dedicate this paper in memory of Eric Grimm, whose tireless work for the
1272 EPD and Neotoma helped make this study possible.

1273

1274

1275

1276 **References**

1277

1278 ACER project members, Goñi, M. F. S., Desprat, S., Daniau, A. L., Bassinot, F. C., Polanco-
1279 Martínez, J. M., Harrison, S. P., Allen, J. R. M., Scott Anderson, R., Behling, H., Bonnefille,
1280 R., Burjachs, F., Carrión, J. S., Cheddadi, R., Clark, J. S., Combourieu-Nebout, N., Mustaphi,
1281 C. J. C., Debusk, G. H., Dupont, L. M., Finch, J. M., Fletcher, W. J., Giardini, M., González,
1282 C., Gosling, W. D., Grigg, L. D., Grimm, E. C., Hayashi, R., Helmens, K., Heusser, L. E.,
1283 Hill, T., Hope, G., Huntley, B., Igarashi, Y., Irino, T., Jacobs, B., Jiménez-Moreno, G.,
1284 Kawai, S., Peter Kershaw, A., Kumon, F., Lawson, I. T., Ledru, M. P., Lézine, A. M., Mei
1285 Liew, P., Magri, D., Marchant, R., Margari, V., Mayle, F. E., Merna Mckenzie, G., Moss, P.,
1286 Müller, S., Müller, U. C., Naughton, F., Newnham, R. M., Oba, T., Pérez-Obiol, R., Pini, R.,
1287 Ravazzi, C., Roucoux, K. H., Rucina, S. M., Scott, L., Takahara, H., Tzedakis, P. C., Urrego,
1288 D. H., Van Geel, B., Guido Valencia, B., Vandergoes, M. J., Vincens, A., Whitlock, C. L.,
1289 Willard, D. A. and Yamamoto, M.: The ACER pollen and charcoal database: A global
1290 resource to document vegetation and fire response to abrupt climate changes during the last
1291 glacial period, *Earth Syst. Sci. Data*, 9(2), 679–695, doi:10.5194/essd-9-679-2017, 2017.

1292

1293 Allen, J. R. M., Hickler, T., Singarayer, J. S., Sykes, M. T., Valdes, P. J. and Huntley, B.:
1294 Last glacial vegetation of northern Eurasia, *Quat. Sci. Rev.*, 29(19–20), 2604–2618,
1295 doi:10.1016/j.quascirev.2010.05.031, 2010.

1296

1297 Allen, R., Siegert, M. J. and Payne, A. J.: Reconstructing glacier-based climates of LGM
1298 Europe and Russia – Part 2 : A dataset of LGM precipitation / temperature relations derived
1299 from degree-day modelling of palaeo glaciers, , 249–263, 2008a.

1300

1301 Allen, R., Siegert, M. J. and Payne, A. J.: Reconstructing glacier-based climates of LGM
1302 Europe and Russia – Part 3 : Comparison with previous climate reconstructions, , (1999),
1303 265–280, 2008b.

1304

1305 Ampel, L., Bigler, C., Wohlfarth, B., Risberg, J., Lotter, A. F. and Veres, D.: Modest summer
1306 temperature variability during DO cycles in western Europe, *Quat. Sci. Rev.*, 29(11–12),
1307 1322–1327, doi:10.1016/j.quascirev.2010.03.002, 2010.

1308

1309 El Amrani, M., Macaire, J. J., Zarki, H., Bréhéret, J. G. and Fontugne, M.: Contrasted
1310 morphosedimentary activity of the lower Kert River (northeastern Morocco) during the Late
1311 Pleistocene and the Holocene. Possible impact of bioclimatic variations and human action,
1312 *Comptes Rendus - Geosci.*, 340(8), 533–542, doi:10.1016/j.crte.2008.05.004, 2008.

1313

1314 Anderson, P. M., Barnosky, C. W., Bartlein, P. J., Behling, P. J., Brubaker, L., Cushing, E. J.,
1315 Dodson, J., Dworetsky, B., Guetter, P. J., Harrison, S. P., Huntley, B., Kutzbach, J. E.,
1316 Markgraf, V., Marvel, R., McGlone, M. S., Mix, A., Moar, N. T., Morley, J., Perrott, R. A.,
1317 Peterson, G. M., Prell, W. L., Prentice, I. C., Ritchie, J. C., Roberts, N., Ruddiman, W. F.,
1318 Salinger, M. J., Spaulding, W. G., Street-Perrott, F. A., Thompson, R. S., Wang, P. K., Webb,
1319 T., Winkler, M. G. and Wright, H. E.: Climatic changes of the last 18,000 years:
1320 Observations and model simulations, *Science* (80-), 241(4869), 1043–1052,
1321 doi:10.1126/science.241.4869.1043, 1988.

1322

1323 Arpe, K., Leroy, S. A. G. and Mikolajewicz, U.: A comparison of climate simulations for the
1324 last glacial maximum with three different versions of the ECHAM model and implications
1325 for summer-green tree refugia, *Clim. Past*, 91–114, doi:10.5194/cp-7-91-2011, 2011.
1326

1327 Arslanov, K. A., Dolukhanov, P. M. and Gei, N. A.: Climate, Black Sea levels and human
1328 settlements in Caucasus Littoral 50,000-9000 BP, *Quat. Int.*, 167–168, 121–127,
1329 doi:10.1016/j.quaint.2007.02.013, 2007.
1330

1331 Bañuls-Cardona, S., López-García, J. M., Blain, H. A., Lozano-Fernández, I. and Cuenca-
1332 Bescós, G.: The end of the Last Glacial Maximum in the Iberian Peninsula characterized by
1333 the small-mammal assemblages, *J. Iber. Geol.*, 40(1), 19–27,
1334 doi:10.5209/rev_JIGE.2014.v40.n1.44085, 2014.
1335

1336 Bartlein, P. J., Harrison, S. P., Brewer, S., Connor, S., Davis, B. A. S., Gajewski, K., Guiot,
1337 J., Harrison-Prentice, T. I., Henderson, A., Peyron, O., Prentice, I. C., Scholze, M., Seppä, H.,
1338 Shuman, B., Sugita, S., Thompson, R. S., Viau, A. E., Williams, J. and Wu, H.: Pollen-based
1339 continental climate reconstructions at 6 and 21 ka: A global synthesis, *Clim. Dyn.*, 37(3),
1340 775–802, doi:10.1007/s00382-010-0904-1, 2011.
1341

1342 de Beaulieu, J.-L. and Reille, M.: Pollen analysis of a long upper Pleistocene continental
1343 sequence in a Velay maar (Massif Central, France), *Palaeogeogr. Palaeoclimatol. Palaeoecol.*,
1344 80(1), 35–48, 1990.

1345 Beghin, P., Charbit, S., Kageyama, M., Combourieu-Nebout, N., Hatté, C., Dumas, C. and
1346 Peterschmitt, J. Y.: What drives LGM precipitation over the western Mediterranean? A study
1347 focused on the Iberian Peninsula and northern Morocco, *Clim. Dyn.*, 46(7–8), 2611–2631,
1348 doi:10.1007/s00382-015-2720-0, 2016.
1349

1350 Bekaert, D. V., Blard, P.-H., Raoult, Y., Pik, R., Kipfer, R., Seltzer, A. M., Legrain, E., and
1351 Marty, B.: Last glacial maximum cooling of 9 °C in continental Europe from a 40 kyr-long
1352 noble gas paleothermometry record, *Quaternary Sci. Rev.*, 310,
1353 108123, <https://doi.org/10.1016/j.quascirev.2023.108123>, 2023
1354

1355 Belis, C. A., Lami, A., Guilizzoni, P., Ariztegui, D. and Geiger, W.: The late Pleistocene
1356 ostracod record of the crater lake sediments from Lago di Albano (Central Italy): Changes in
1357 trophic status, water level and climate, *J. Paleolimnol.*, 21(2), 151–169,
1358 doi:10.1023/A:1008095805748, 1999.
1359

1360 Berto, C., López-García, J. M. and Luzi, E.: Changes in the Late Pleistocene small-mammal
1361 distribution in the Italian Peninsula, *Quat. Sci. Rev.*, 225,
1362 doi:10.1016/j.quascirev.2019.106019, 2019.
1363

1364 Bigelow, N.H., Brubaker, L.B., Edwards, M.E., Harrison, S.P., Prentice, I.C., Anderson,
1365 P.M., Andreev, A.A., Bartlein, P.J., Christiansen, T.R., Cramer, W., Kaplan, J.O., Lozhkin,
1366 A.V., Matveyeva, N.V., Murray, D.F., McGuire, A.D., Razzhivin, V.Y., Ritchie, J.C., Smith,
1367 B., Walker, D.A., Gajewski, K., Wolf, V., Holmqvist, B.H., Igarashi, Y., Kremenetskii, K.,
1368 Paus, A., Pisaric, M.F.J., Volkova, V.S.: Climate change and arctic ecosystems: 1. Vegetation
1369 changes north of 55 N between the last glacial maximum, mid-Holocene, and present. *J.*
1370 *Geophys. Res.* 108 (D19), 8170. doi.org/10.1029/2002JD002558, 2013.
1371

1372 Binney, H., Edwards, M., Macias-Fauria, M., Lozhkin, A., Anderson, P., Kaplan, J. O.,
1373 Andreev, A., Bezrukova, E., Blyakharchuk, T., Jankovska, V., Khazina, I., Krivonogov, S.,
1374 Kremenetski, K., Nield, J., Novenko, E., Ryabogina, N., Solovieva, N., Willis, K. and
1375 Zernitskaya, V.: Vegetation of Eurasia from the last glacial maximum to present: Key
1376 biogeographic patterns, *Quat. Sci. Rev.*, 157, 80–97, doi:10.1016/j.quascirev.2016.11.022,
1377 2017.

1378

1379 Birks, H. J. B. and Willis, K. J.: Alpines, trees, and refugia in Europe, *Plant Ecol. Divers.*,
1380 1(2), 147–160, doi:10.1080/17550870802349146, 2008.

1381

1382 Bonatti, E.: Pollen sequence in the lake sediments. In: *Ianula: an account of the history and*
1383 *development of the Lago di Monterosi, Latium, Italy*, in *Trans. Am. phil. Soc.*, vol. 60, edited
1384 by G. E. Hutchinson, pp. 26–31., 1970.

1385

1386 Braconnot, P., Harrison, S.P., Kageyama, M., Bartlein, P.J., Masson-Delmotte, V., Abe-
1387 Ouchi, A., Otto-Bliesner, B., and Zhao, Y.: Evaluation of climate models using
1388 palaeoclimatic data, *Nat. Clim. Change*, 2, 417–424, doi:10.1038/nclimate1456, 2012.

1389

1390 Brewer, S., Guiot, J., Sánchez-Goñi, M. F. and Klotz, S.: The climate in Europe during the
1391 Eemian: a multi-method approach using pollen data, *Quat. Sci. Rev.*, 27(25–26), 2303–2315,
1392 doi:10.1016/j.quascirev.2008.08.029, 2008.

1393

1394 Brewer, S., Giesecke, T., Davis, B. A. S., Finsinger, W., Wolters, S., Binney, H., de
1395 Beaulieu, J. L., Fyfe, R., Gil-Romera, G., Kühl, N., Kuneš, P., Leydet, M. and Bradshaw, R.
1396 H.: Mapping Lateglacial and Holocene European pollen data: The maps, *J. Maps*, 13(2), 921–
1397 928, doi:10.1080/17445647.2016.1197613, 2017.

1398

1399 Camuera, J., Jiménez-Moreno, G., Ramos-Román, M. J., García-Alix, A., Toney, J. L.,
1400 Anderson, R. S., Jiménez-Espejo, F., Bright, J., Webster, C., Yanes, Y. and Carrión, J. S.:
1401 Vegetation and climate changes during the last two glacial-interglacial cycles in the western
1402 Mediterranean: A new long pollen record from Padul (southern Iberian Peninsula), *Quat. Sci.*
1403 *Rev.*, 205, 86–105, doi:10.1016/j.quascirev.2018.12.013, 2019.

1404

1405 Cao, X., Tian, F., Dallmeyer, A. and Herzschuh, U.: Northern Hemisphere biome changes
1406 (>30°N) since 40 cal ka BP and their driving factors inferred from model-data comparisons,
1407 *Quat. Sci. Rev.*, 220, 291–309, doi:10.1016/j.quascirev.2019.07.034, 2019.

1408

1409 Carrión, J. S.: Late quaternary pollen sequence from Carihuela Cave, southern Spain, *Rev.*
1410 *Palaeobot. Palynol.*, 71(1–4), doi:10.1016/0034-6667(92)90157-C, 1992.

1411

1412 Carrión, J. S.: Patterns and processes of Late Quaternary environmental change in a montane
1413 region of southwestern Europe, *Quat. Sci. Rev.*, 21, 2047–2066, 2002.

1414

1415 Carrión, J. S., Finlayson, C., Fernández, S., Finlayson, G., Allué, E., López-Sáez, J. A.,
1416 López-García, P., Gil-Romera, G., Bailey, G. and González-Sampériz, P.: A coastal reservoir
1417 of biodiversity for Upper Pleistocene human populations: palaeoecological investigations in
1418 Gorham’s Cave (Gibraltar) in the context of the Iberian Peninsula, *Quat. Sci. Rev.*, 27(23–
1419 24), 2118–2135, doi:10.1016/j.quascirev.2008.08.016, 2008.

1420

1421 Cheddadi, R., Yu, G., Guiot, J., Harrison, S. P. and Colin Prentice, I.: The climate of Europe
1422 6000 years ago, *Clim. Dyn.*, 13(1), 1–9, 1996.

1423
1424 Chevalier, M., Davis, B. A. S., Heiri, O., Seppä, H., Chase, B. M., Gajewski, K., Lacourse,
1425 T., Telford, R. J., Finsinger, W., Guiot, J., Kühl, N., Maezumi, S. Y., Tipton, J. R., Carter, V.
1426 A., Brussel, T., Phelps, L. N., Dawson, A., Zanon, M., Vallé, F., Nolan, C., Mauri, A., de
1427 Vernal, A., Izumi, K., Holmström, L., Marsicek, J., Goring, S., Sommer, P. S., Chaput, M.
1428 and Kupriyanov, D.: Pollen-based climate reconstruction techniques for late Quaternary
1429 studies, *Earth-Science Rev.*, 210, doi:10.1016/j.earscirev.2020.103384, 2020.

1430
1431 Cleator, S. F., Harrison, S. P., Nichols, N. K., Colin Prentice, I. and Roulstone, I.: A new
1432 multivariable benchmark for Last Glacial Maximum climate simulations, *Clim. Past*, 16(2),
1433 699–712, doi:10.5194/cp-16-699-2020, 2020.

1434
1435 COHMAP,: Climatic changes of the last 18,000 years: observations and model
1436 simulations. *Science*, 241, 1043-1052, 1988.

1437
1438 Collins, P. M., Davis, B. A. S. and Kaplan, J. O.: The mid-Holocene vegetation of the
1439 Mediterranean region and southern Europe, and comparison with the present day, *J.*
1440 *Biogeogr.*, 39(10), doi:10.1111/j.1365-2699.2012.02738.x, 2012.

1441
1442 Combourieu Nebout, N., Peyron, O., Dormoy, I., Desprat, S., Beaudouin, C., Kotthoff, U.
1443 and Marret, F.: Rapid climatic variability in the west Mediterranean during the last 25 000
1444 years from high resolution pollen data, *Clim. Past*, 5(3), 503–521, doi:10.5194/cp-5-503-
1445 2009, 2009.

1446
1447 Connor, S. E., Ross, S. A., Sobotkova, A., Herries, A. I. R., Mooney, S. D., Longford, C. and
1448 Iliev, I.: Environmental conditions in the SE Balkans since the Last Glacial Maximum and
1449 their influence on the spread of agriculture into Europe, *Quat. Sci. Rev.*, 68, 200–215,
1450 doi:10.1016/j.quascirev.2013.02.011, 2013.

1451
1452 Cowling, S. A. and Sykes, M. T.: Physiological significance of low atmospheric CO₂ for
1453 plant-climate interactions, *Quat. Res.*, 52(2), 237–242, doi:10.1006/qres.1999.2065, 1999.

1454
1455 Damblon, F.: L'enregistrement palynologique de la sequence pléistocène et holocène de la
1456 grotte Walou, in *La grotte Walou à Trooz (Belgique)*, edited by C. Draily, S. Pirson, and M.
1457 Toussaint, pp. 84–129, Service public de Wallonie (Etudes et Documents, Archéologie, 21).,
1458 2011.

1459
1460 Daniau, A.-L., Desprat, S., Aleman, J. C., Bremond, L., Davis, B., Fletcher, W., Marlon, J.
1461 R., Marquer, L., Montade, V., Morales-Molino, C., Naughton, F., Rius, D. and Urrego, D. H.:
1462 Terrestrial plant microfossils in palaeoenvironmental studies, pollen, microcharcoal and
1463 phytolith. Towards a comprehensive understanding of vegetation, fire and climate changes
1464 over the past one million years, *Rev. Micropaleontol.*, 63, doi:10.1016/j.revmic.2019.02.001,
1465 2019.

1466
1467 Davis, B. A. S. and Stevenson, A. C.: The 8.2 ka event and Early-Mid Holocene forests, fires
1468 and flooding in the Central Ebro Desert, NE Spain, *Quat. Sci. Rev.*, 26(13–14),
1469 doi:10.1016/j.quascirev.2007.04.007, 2007.

1470

- 1471 Davis, B. A. S., Brewer, S., Stevenson, A. C., Guiot, J., Allen, J., Almqvist-Jacobson, H.,
1472 Ammann, B., Andreev, A. A., Argant, J., Atanassova, J., Balwierz, Z., Barnosky, C. D.,
1473 Bartley, D. D., De Beaulieu, J. L., Beckett, S. C., Behre, K. E., Bennett, K. D., Berglund, B.
1474 E. B., Beug, H.-J., Bezusko, L., Binka, K., Birks, H. H., Birks, H. J. B., Björck, S.,
1475 Bliakhartchouk, T., Bogdel, I., Bonatti, E., Bottema, S., Bozilova, E. D. B., Bradshaw, R.,
1476 Brown, A. P., Brugiapaglia, E., Carrion, J., Chernavskaya, M., Clerc, J., Clet, M., Coüteaux,
1477 M., Craig, A. J., Cserny, T., Cwynar, L. C., Dambach, K., De Valk, E. J., Digerfeldt, G.,
1478 Diot, M. F., Eastwood, W., Elina, G., Filimonova, L., Filipovitch, L., Gaillard-Lemdhal, M.
1479 J., Gauthier, A., Göransson, H., Guenet, P., Gunova, V., Hall, V. A. H., Harmata, K., Hicks,
1480 S., Huckerby, E., Huntley, B., Huttunen, A., Hyvärinen, H., Ilves, E., Jacobson, G. L., Jahns,
1481 S., Jankovská, V., Jóhansen, J., Kabailiene, M., Kelly, M. G., Khomutova, V. I., Königsson,
1482 L. K., Kremenetski, C., Kremenetskii, K. V., Krisai, I., Krisai, R., Kvavadze, E., Lamb, H.,
1483 Lazarova, M. A., Litt, T., Lotter, A. F., Lowe, J. J., Magyar, E., Makohonienko, M.,
1484 Mamakowa, K., Mangerud, J., Mariscal, B., Markgraf, V., McKeever, Mitchell, F. J. G.,
1485 Munuera, M., Nicol-Pichard, S., Noryskiewicz, B., Odgaard, B. V., Panova, N. K.,
1486 Pantaleon-Cano, J., Paus, A. A., Pavel, T., Peglar, S. M., Penalba, M. C., Pennington, W.,
1487 Perez-Obiol, R., et al.: The temperature of Europe during the Holocene reconstructed from
1488 pollen data, *Quat. Sci. Rev.*, 22(15–17), doi:10.1016/S0277-3791(03)00173-2, 2003.
- 1489
1490 Davis, B. A. S., Chevalier, M., Sommer, P., Carter, V. A., Finsinger, W., Mauri, A., Phelps,
1491 L. N., Zanon, M., Abegglen, R., Åkesson, C. M., Alba-Sánchez, F., Scott Anderson, R.,
1492 Antipina, T. G., Atanassova, J. R., Beer, R., Belyanina, N. I., Blyakharchuk, T. A., Borisova,
1493 O. K., Bozilova, E., Bukreeva, G., Jane Bunting, M., Clò, E., Colombaroli, D., Combourieu-
1494 Nebout, N., Desprat, S., Di Rita, F., Djamali, M., Edwards, K. J., Fall, P. L., Feurdean, A.,
1495 Fletcher, W., Florenzano, A., Furlanetto, G., Gaceur, E., Galimov, A. T., Galka, M., García-
1496 Moreiras, I., Giesecke, T., Grindean, R., Guido, M. A., Gvozdeva, I. G., Herzsuh, U.,
1497 Hjelle, K. L., Ivanov, S., Jahns, S., Jankovska, V., Jiménez-Moreno, G., Karpínska-Kołaczek,
1498 M., Kitaba, I., Kołaczek, P., Lapteva, E. G., Latałowa, M., Lebreton, V., Leroy, S., Leydet,
1499 M., Lopatina, D. A., López-Sáez, J. A., Lotter, A. F., Magri, D., Marinova, E., Matthias, I.,
1500 Mavridou, A., Mercuri, A. M., Mesa-Fernández, J. M., Mikishin, Y. A., Milecka, K.,
1501 Montanari, C., Morales-Molino, C., Mrotzek, A., Sobrino, C. M., Naidina, O. D., Nakagawa,
1502 T., Nielsen, A. B., Novenko, E. Y., Panajiotidis, S., Panova, N. K., Papadopoulou, M.,
1503 Pardoe, H. S., Pędziszewska, A., Petrenko, T. I., Ramos-Román, M. J., Ravazzi, C., Rösch,
1504 M., Ryabogina, N., Ruiz, S. S., Sakari Salonen, J., Sapelko, T. V., Schofield, J. E., Seppä, H.,
1505 Shumilovskikh, L., Stivrins, N., Stojakowits, P., Svitavska, H. S., Święta-Musznicka, J.,
1506 Tantau, I., Tinner, W., Tobolski, K., Tonkov, S., Tsakiridou, M., et al.: The Eurasian Modern
1507 Pollen Database (EMPD), version 2, *Earth Syst. Sci. Data*, 12(4), 2423–2445,
1508 doi:10.5194/essd-12-2423-2020, 2020.
- 1509
1510 Davis M.B.: On the theory of pollen analysis. *American Journal of Sciences*, 26, 897–912,
1511 1963.
- 1512
1513 Demay, L., Julien, M.A., Anghelinu, M., Shydlovskiy, P.S., Koulakovska, L.V., P’ean, S.,
1514 Stupak, D.V., Vasyliov, P.M., Obřada, T., Wojtal, P., Belyaeva, V.I.: Study of human
1515 behaviors during the Late Pleniglacial in the East European Plain through their relation to the
1516 animal world. *Quat. Int.* <https://doi.org/10.1016/j.quaint.2020.10.047>, 2021.
- 1517
1518 Douda, J., Doudová, J., Drašnarová, A., Kuneš, P., Hadincová, V., Krak, K., Zákavský, P.
1519 and Mandák, B.: Migration patterns of subgenus *Alnus* in Europe since the last glacial
1520 maximum: A systematic review, *PLoS One*, 9(2), doi:10.1371/journal.pone.0088709, 2014.

1521
1522 Duprat-Oualid, F., Rius, D., Bégeot, C., Magny, M., Millet, L., Wulf, S. and Appelt, O.:
1523 Vegetation response to abrupt climate changes in Western Europe from 45 to 14.7k cal a BP:
1524 the Bergsee lacustrine record (Black Forest, Germany), *J. Quat. Sci.*, 32(7), 1008–1021,
1525 doi:10.1002/jqs.2972, 2017.

1526
1527 Dupre Ollivier, M.: *Palinología y paleoambiente- nuevos datos españoles referencias*,
1528 Universidad de Valencia., 1988.

1529
1530 Edwards, M. E., Anderson, P. M., Brubaker, L. B., Ager, T., Andreev, A. A., Bigelow, N. H.,
1531 Cwynar, L. C., Eisner, W. R., Harrison, S. P., Hu, F.-S., Jolly, D., Lozhkin, A. V.,
1532 MacDonald, G. M., Mock, C. J., Ritchie, J. C., Sher, A. V., Spear, R. W., Williams, J. & Yu,
1533 G.: Pollen-based biomes for Beringia 18,000, 6000 and 0 14C yr bp. *Journal of*
1534 *Biogeography*, 27, 521– 554, doi: [10.1046/j.1365-2699.2000.00426.x](https://doi.org/10.1046/j.1365-2699.2000.00426.x), 2000.

1535
1536 Ehlers, J., Gibbard, P. L. and Hughes, P. D.: *Quaternary Glaciations - Extent and Chronology*
1537 *A Closer Look*, edited by J. Ehlers, P. L. Gibbard, and P. D. Hughes, Elsevier., 2011.

1538
1539 Elenga, H., Peyron, O., Bonnefille, R., Jolly, D., Cheddadi, R., Guiot, J., Andrieu, V.,
1540 Bottema, S., Buchet, G., De Beaulieu, J. L., Hamilton, A. C., Maley, J., Marchant, R., Perez-
1541 Obiol, R., Reille, M., Riollot, G., Scott, L., Straka, H., Taylor, D., Van Campo, E., Vincens,
1542 A., Laarif, F. and Jonson, H.: Pollen-based biome reconstruction for southern Europe and
1543 Africa 18,000 yr BP, *J. Biogeogr.*, 27(3), 621–634, doi:10.1046/j.1365-2699.2000.00430.x,
1544 2000.

1545
1546 Ferguson, J. E., Henderson, G. M., Fa, D. A., Finlayson, J. C. and Charnley, N. R.: Increased
1547 seasonality in the Western Mediterranean during the last glacial from limpet shell
1548 geochemistry, *Earth Planet. Sci. Lett.*, 308(3–4), 325–333, doi:10.1016/j.epsl.2011.05.054,
1549 2011.

1550
1551 Feurdean A, Bhagwat SA, Willis KJ, Birks HJB, Lischke H, Hickler T.: Tree migration-rates:
1552 narrowing the gap between inferred post-glacial rates and projected rates. *PLoS ONE* 8:
1553 e71797, 2013.

1554
1555 Feurdean, A., Perşoiu, A., Tanţău, I., Stevens, T., Magyari, E. K., Onac, B. P., Marković, S.,
1556 Andrić, M., Connor, S., Fărcaş, S., Gałka, M., Gaudeny, T., Hoek, W., Kolaczek, P., Kuneš,
1557 P., Lamentowicz, M., Marinova, E., Michczyńska, D. J., Perşoiu, I., Plóciennik, M.,
1558 Słowiński, M., Stancikaite, M., Sumegi, P., Svensson, A., Tămaş, T., Timar, A., Tonkov, S.,
1559 Toth, M., Veski, S., Willis, K. J. and Zernitskaya, V.: Climate variability and associated
1560 vegetation response throughout Central and Eastern Europe (CEE) between 60 and 8ka, *Quat.*
1561 *Sci. Rev.*, 106, 206–224, doi:10.1016/j.quascirev.2014.06.003, 2014.

1562
1563 Fick, S. E. and Hijmans, R. J.: WorldClim 2: new 1-km spatial resolution climate surfaces for
1564 global land areas, *Int. J. Climatol.*, 37(12), 4302–4315, doi:10.1002/joc.5086, 2017.

1565
1566 Fletcher, W. J., Goni, M. F. S., Peyron, O. and Dormoy, I.: Abrupt climate changes of the last
1567 deglaciation detected in a Western Mediterranean forest record, *Clim. Past*, 6(2), 245–264,
1568 doi:10.5194/cp-6-245-2010, 2010.

1569

1570 Gaillard, M. J., Sugita, S., Mazier, F., Trondman, A. K., Broström, A., Hickler, T., Kaplan, J.
1571 O., Kjellström, E., Kokfelt, U., Kuneš, P., Lemmen, C., Miller, P., Olofsson, J., Poska, A.,
1572 Rundgren, M., Smith, B., Strandberg, G., Fyfe, R., Nielsen, A. B., Alenius, T., Balakauskas,
1573 L., Barnekow, L., Birks, H. J. B., Bjune, A., Björkman, L., Giesecke, T., Hjelle, K., Kalnina,
1574 L., Kangur, M., Van Der Knaap, W. O., Koff, T., Lageras, P., Latałowa, M., Leydet, M.,
1575 Lechterbeck, J., Lindbladh, M., Odgaard, B., Peglar, S., Segerström, U., Von Stedingk, H.
1576 and Seppä, H.: Holocene land-cover reconstructions for studies on land cover-climate
1577 feedbacks, *Clim. Past*, 6(4), 483–499, doi:10.5194/cp-6-483-2010, 2010.

1578

1579 García-Amorena, I., Gómez Manzanque, F., Rubiales, J. M., Granja, H. M., Soares de
1580 Carvalho, G. and Morla, C.: The Late Quaternary coastal forests of western Iberia: A study of
1581 their macroremains, *Palaeogeogr. Palaeoclimatol. Palaeoecol.*, 254(3–4), 448–461,
1582 doi:10.1016/j.palaeo.2007.07.003, 2007.

1583

1584 Genov, I.: The Black Sea level from the Last Glacial Maximum to the present time, *Geol.*
1585 *Balc.*, 45(1–3), 3–19, 2016.

1586

1587 Giesecke, T.: Did thermophilous trees spread into central Europe during the Late Glacial?,
1588 *New Phytol.*, 212(1), 15–18, doi:10.1111/nph.14149, 2016.

1589

1590 Giesecke, T., Davis, B., Brewer, S., Finsinger, W., Wolters, S., Blaauw, M., de Beaulieu, J.-
1591 L., Binney, H., Fyfe, R. M., Gaillard, M.-J., Gil-Romera, G., van der Knaap, W. O., Kuneš,
1592 P., Kühl, N., van Leeuwen, J. F. N., Leydet, M., Lotter, A. F., Ortu, E., Semmler, M. and
1593 Bradshaw, R. H. W.: Towards mapping the late Quaternary vegetation change of Europe,
1594 *Veg. Hist. Archaeobot.*, 23(1), doi:10.1007/s00334-012-0390-y, 2014.

1595

1596 Geiger, R.: *The climate near the ground*. Cambridge: Blue Hill Met. Observ. Harvard
1597 University 1960

1598

1599 Giraudi, C.: Lake levels and climate for the last 30,000 years in the fucino area (Abruzzo-
1600 Central Italy) - A review, *Palaeogeogr. Palaeoclimatol. Palaeoecol.*, 70(1–3), 249–260,
1601 doi:10.1016/0031-0182(89)90094-1, 1989.

1602

1603 Giraudi, C.: Climate evolution and forcing during the last 40 ka from the oscillations in
1604 Apennine glaciers and high mountain lakes, Italy, *J. Quat. Sci.*, 32(8), 1085–1098,
1605 doi:10.1002/jqs.2985, 2017.

1606

1607 Guido, M. A., Molinari, C., Moneta, V., Branch, N., Black, S., Simmonds, M., Stastney, P.
1608 and Montanari, C.: Climate and vegetation dynamics of the Northern Apennines (Italy)
1609 during the Late Pleistocene and Holocene, *Quat. Sci. Rev.*, 231,
1610 doi:10.1016/j.quascirev.2020.106206, 2020.

1611 Hansen, M. C., Potapov, P. V., Moore, R., Hancher, M., Turubanova, S. A., Tyukavina, A.,
1612 Thau, D., Stehman, S. V., Goetz, S. J., Loveland, T. R., Kommareddy, A., Egorov, A., Chini,
1613 L., Justice, C. O. and Townshend, J. R. G.: High-resolution global maps of 21st-century
1614 forest cover change, *Science (80-.)*, 342(6160), 850–853, doi:10.1126/science.1244693,
1615 2013.

1616

1617 Grichuk, V. P.: Main types of vegetation (ecosystems) for the maximum cooling of the last
1618 glaciation. B. Frenzel, B. Pecs, A.A. Velichko (Eds.), *Atlas of Palaeoclimates and*

1619 Palaeoenvironments of the Northern Hemisphere, NQUA/Hungarian Academy of
1620 Sciences, Budapest, pp. 123-124, doi: [10.2307/1551555](https://doi.org/10.2307/1551555), 1992.

1621

1622

1623 Guiot, J., Pons, A., Beaulieu, J. L. de, and Reille, M. A 140,000-year climatic reconstruction
1624 from two European pollen records. *Nature* 338, 309-313, doi:10.1038/338309a0, 1989.

1625

1626 Guiot, J., Torre, F., Jolly, D., Peyron, O., Boreux, J.J., Cheddadi, R.: Inverse vegetation
1627 modeling by Monte Carlo sampling to reconstruct palaeoclimates under changed precipitation
1628 seasonality and CO₂ conditions: application to glacial climate in Mediterranean region. *Ecol.*
1629 *Model.* 127, 119–140. doi: 10.1016/
1630 S0304-3800(99)00219-7, 2000.

1631

1632 Harrison, S. P., Yu, G. E. and Tarasov, P. E.: Late Quaternary Lake-Level Record from
1633 Northern Eurasia, *Quat. Res.*, 45(2), 138–159, doi:10.1006/qres.1996.0016, 1996.

1634

1635 Harrison, S. P., Bartlein, P. J., Brewer, S., Prentice, I. C., Boyd, M., Hessler, I., Holmgren,
1636 K., Izumi, K. and Willis, K.: Climate model benchmarking with glacial and mid-Holocene
1637 climates, *Clim. Dyn.*, 43(3–4), 671–688, doi:10.1007/s00382-013-1922-6, 2014.

1638

1639 Harrison, S. P., Bartlein, P. J., Izumi, K., Li, G., Annan, J., Hargreaves, J., Braconnot, P. and
1640 Kageyama, M.: Evaluation of CMIP5 palaeo-simulations to improve climate projections, *Nat.*
1641 *Clim. Chang.*, 5(8), 735–743, doi:10.1038/nclimate2649, 2015.

1642

1643 Heiri, O., Koinig, K. A., Spötl, C., Barrett, S., Brauer, A., Drescher-Schneider, R., Gaar, D.,
1644 Ivy-Ochs, S., Kerschner, H., Luetscher, M., Moran, A., Nicolussi, K., Preusser, F., Schmidt,
1645 R., Schoeneich, P., Schwörer, C., Sprafke, T., Terhorst, B. and Tinner, W.: Palaeoclimate
1646 records 60-8 ka in the Austrian and Swiss Alps and their forelands, *Quat. Sci. Rev.*, 106,
1647 186–205, doi:10.1016/j.quascirev.2014.05.021, 2014.

1648

1649 Heyman, B. M., Heyman, J., Fickert, T., Harbor, J. M. and Forest, B.: Paleo-climate of the
1650 central European uplands during the last glacial maximum based on glacier mass-balance
1651 modeling Bavarian Forest Republic, *Quat. Res.*, 79(1), 49–54,
1652 doi:10.1016/j.yqres.2012.09.005, 2013.

1653

1654 Hughes, A. L. C., Gyllencreutz, R., Lohne, Ø. S., Mangerud, J. and Svendsen, J. I.: The last
1655 Eurasian ice sheets - a chronological database and time-slice reconstruction, *DATED-1,*
1656 *Boreas*, 45(1), 1–45, doi:10.1111/bor.12142, 2016.

1657

1658 Hughes, P. D. and Gibbard, P. L.: A stratigraphical basis for the Last Glacial Maximum
1659 (LGM), *Quat. Int.*, 383(June 2014), 174–185, doi:10.1016/j.quaint.2014.06.006, 2015.

1660

1661 Hughes, P. D., Woodward, J. C. and Gibbard, P. L.: Late Pleistocene glaciers and climate in
1662 the Mediterranean, *Glob. Planet. Change*, 50(1–2), 83–98,
1663 doi:10.1016/j.gloplacha.2005.07.005, 2006.

1664 Huntley, B.: Dissimilarity mapping between fossil and contemporary pollen spectra in
1665 Europe for the past 13,000 years, *Quat. Res.*, 33(3), 360–376, doi:10.1016/0033-
1666 5894(90)90062-P, 1990.

1667

1668 Huntley B.: Dissimilarity mapping between fossil and contemporary pollen spectra in Europe
1669 for the past 13,000 years. *Quaternary Research* 33:360–376, 1990.

1670

1671 Huntley, B. and Allen, J. R. M.: Glacial environments III. Palaeovegetation patterns in late
1672 glacial Europe, in *Neanderthals and modern humans in the European landscape during the*
1673 *last glaciation*, edited by T. H. Van Andel and H. C. Davies, pp. 79–102, McDonald Institute
1674 for Archaeological Research, Cambridge., 2003.

1675

1676 Huntley, B. and Birks, H. J. B.: *An Atlas of Past and Present Pollen Maps for Europe: 0–*
1677 *13,000 B.P. years ago*, Cambridge University Press, Cambridge., 1983.

1678

1679 Izumi, K. and Bartlein, P., North American paleoclimate reconstructions for the Last Glacial
1680 Maximum using an inverse modeling through iterative forward modeling approach applied to
1681 pollen data, <https://doi.org/10.1002/2016GL070152>, 2016

1682

1683 Jalut, G., Andrieu, V., Delibrias, G., Fontaugne, M. and Pages, P.: Palaeoenvironment of the
1684 valley of Ossau (Western French Pyrenees) during the last 27 000 year, *Pollen et Spores*,
1685 30(3–4), 357–393, 1988.

1686

1687 Jalut, G., Marti, J. M., Fontugne, M., Delibrias, G., Vilaplana, J. M. and Julia, R.: Glacial to
1688 interglacial vegetation changes in the northern and southern Pyrénées: Deglaciation,
1689 vegetation cover and chronology, *Quat. Sci. Rev.*, 11(4), 449–480, doi:10.1016/0277-
1690 3791(92)90027-6, 1992.

1691

1692 Jankovska, V.: Vegetation cover in West Carpathians during the Last Glacial period -
1693 analogy of present day siberian forest-tundra nad taiga, *Palynol. Stratigr. geoecology*,
1694 (SEPTEMBER 2008), 282–289, 2008.

1695

1696 Janská, V., Jiménez-Alfaro, B., Chytrý, M., Divišek, J., Anenkhonov, O., Korolyuk, A.,
1697 Lashchinskyi, N. and Culek, M.: Palaeodistribution modelling of European vegetation types
1698 at the Last Glacial Maximum using modern analogues from Siberia: Prospects and
1699 limitations, *Quat. Sci. Rev.*, 159, 103–115, doi:10.1016/j.quascirev.2017.01.011, 2017.

1700

1701 Jost, A., Lunt, D., Abe-Ouchi, A., Abe-Ouchi, A., Peyron, O., Valdes, P. J. and Ramstein, G.:
1702 High-resolution simulations of the last glacial maximum climate over Europe: A solution to
1703 discrepancies with continental palaeoclimatic reconstructions?, *Clim. Dyn.*, 24(6), 577–590,
1704 doi:10.1007/s00382-005-0009-4, 2005.

1705

1706 Juggins, S.: Quantitative reconstructions in palaeolimnology : new paradigm or sick
1707 science ?, *Quat. Sci. Rev.*, 64, 20–32, doi:10.1016/j.quascirev.2012.12.014, 2013.

1708

1709 Juggins, S.: *Rioja: Analysis of Quaternary Science Data*, [online] Available from:
1710 <https://cran.r-project.org/package=rioja>, 2020.

1711
1712 Juggins, S. and Birks, H. J. B.: Quantitative Environmental Reconstructions from Biological
1713 Data, in *Developments in Paleoenvironmental Research 5*, edited by H. J. B. Birks, pp. 431–
1714 494, Springer ScienceCBusiness Media B.V., 2012.

1715
1716 Juříčková, L., Horáčková, J. and Ložek, V.: Direct evidence of central European forest
1717 refugia during the last glacial period based on mollusc fossils, *Quat. Res. (United States)*,
1718 82(1), 222–228, doi:10.1016/j.yqres.2014.01.015, 2014.

1719
1720 Kageyama, M., Laine, A., Abe-Ouchi, A., Braconnot, P., Cortijo, E., Crucifix, M., de Vernal,
1721 A., Guiot, J., Hewitt, C. D., Kitoh, A., Kucera, M., Marti, O., Ohgaito, R., Otto-Bliesner, B.,
1722 Peltier, W. R., Rosell-Melé, A., Vettoretti, G., Weber, S. L. and Yu, Y.: Last Glacial
1723 Maximum temperatures over the North Atlantic, Europe and western Siberia: a comparison
1724 between PMIP models, MARGO sea-surface temperatures and pollen-based reconstructions,
1725 *Quat. Sci. Rev.*, 25(17–18), 2082–2102, doi:10.1016/j.quascirev.2006.02.010, 2006.

1726
1727 Kageyama, M., Harrison, S. P., Kapsch, M. L., Lofverstrom, M., Lora, J. M., Mikolajewicz,
1728 U., ... & Zhu, J. The PMIP4 Last Glacial Maximum experiments: preliminary results and
1729 comparison with the PMIP3 simulations. *Climate of the Past*, 17(3), 1065-1089, 2021.

1730
1731 Kaltenrieder, P., Belis, C. A., Hofstetter, S., Ammann, B., Ravazzi, C. and Tinner, W.:
1732 Environmental and climatic conditions at a potential Glacial refugial site of tree species near
1733 the Southern Alpine glaciers. New insights from multiproxy sedimentary studies at Lago
1734 della Costa (Euganean Hills, Northeastern Italy), *Quat. Sci. Rev.*, 28(25–26), 2647–2662,
1735 doi:10.1016/j.quascirev.2009.05.025, 2009.

1736
1737 Kaplan, J. O., Pfeiffer, M., Kolen, J. C. A. and Davis, B. A. S.: Large scale anthropogenic
1738 reduction of forest cover in last glacial maximum Europe, *PLoS One*, 11(11),
1739 doi:10.1371/journal.pone.0166726, 2016.

1740
1741 Kehrwald, N. M., McCoy, W. D., Thibeault, J., Burns, S. J. and Oches, E. A.: Paleoclimatic
1742 implications of the spatial patterns of modern and LGM European land-snail shell $\delta^{18}\text{O}$,
1743 *Quat. Res.*, 74(1), 166–176, doi:10.1016/j.yqres.2010.03.001, 2010.

1744
1745 Kelly, A., Charman, D. J. and Newnham, R. M.: A last glacial maximum pollen record from
1746 bodmin moor showing a possible cryptic Northern refugium in Southwest England, *J. Quat.*
1747 *Sci.*, 25(3), 296–308, doi:10.1002/jqs.1309, 2010.

1748
1749 Kolodny, Y., Stein, M. and Machlus, M.: Sea-rain-lake relation in the Last Glacial East
1750 Mediterranean revealed by $\delta^{18}\text{O}$ - $\delta^{13}\text{C}$ in Lake Lisan aragonites, *Geochim. Cosmochim.*
1751 *Acta*, 69(16), 4045–4060, doi:10.1016/j.gca.2004.11.022, 2005.

1752
1753 Kovács, J., Moravcová, M., Újvári, G. and Pintér, A. G.: Reconstructing the
1754 paleoenvironment of East Central Europe in the Late Pleistocene using the oxygen and
1755 carbon isotopic signal of tooth in large mammal remains, *Quat. Int.*, 276–277, 145–154,
1756 doi:10.1016/j.quaint.2012.04.009, 2012.

1757
1758 Krebs, P., Pezzatti, G. B., Beffa, G., Tinner, W. and Conedera, M.: Revising the sweet
1759 chestnut (*Castanea sativa* Mill.) refugia history of the last glacial period with extended pollen

1760 and macrofossil evidence, *Quat. Sci. Rev.*, 206, 111–128,
1761 doi:10.1016/j.quascirev.2019.01.002, 2019.

1762

1763 Kuneš, P., Pelánková, B., Chytrý, M., Jankovská, V., Pokorný, P. and Petr, L.: Interpretation
1764 of the last-glacial vegetation of eastern-central Europe using modern analogues from southern
1765 Siberia, *J. Biogeogr.*, 35(12), 2223–2236, doi:10.1111/j.1365-2699.2008.01974.x, 2008.

1766

1767 Küster, H.: Postglaziale Vegetationsgeschichte Südbayerns. Geobotanische Studien zur
1768 Prähistorischen Landschaftskunde, Akademie Verlag, Berlin., 1995.

1769

1770 Lacey, J. H., Leng, M. J., Höbig, N., Reed, J. M., Valero-Garcés, B. and Reicherter, K.:
1771 Western Mediterranean climate and environment since Marine Isotope Stage 3: a 50,000-year
1772 record from Lake Banyoles, Spain, *J. Paleolimnol.*, 55(2), 113–128, doi:10.1007/s10933-015-
1773 9868-9, 2016.

1774

1775 Latombe, G., Burke, A., Vrac, M., Levvasseur, G. and Dumas, C.: Comparison of spatial
1776 downscaling methods of general circulation model results to study climate variability during
1777 the Last Glacial Maximum, , 2563–2579, 2018.

1778

1779 Lefort J.P., Monnier J.L., Danukalova G.: Transport of Late Pleistocene loess particles by
1780 katabatic winds during the lowstands of the English Channel. *Journal of the Geological*
1781 *Society* 176: 1169–1181, doi: [10.1144/jgs2019-07](https://doi.org/10.1144/jgs2019-07), 2019.

1782

1783 Lehmkuhl, F., Nett, J.J., Pöfner, S., Schulte, P., Sprafke, T., Jary, Z., Antoine, P., Wacha, L.,
1784 Wolf, D., Zerboni, A., Hošek, J., Marković, S.B., Obrecht, I., Sümege, P., Veres, D.,
1785 Zeeden, C., Boemke, B., Schaubert, V., Viehweger, J., Hambach, U.: Loess landscapes of
1786 Europe e mapping, geomorphology, and zonal differentiation. *Earth Sci. Rev.* 215, 103496.
1787 <https://doi.org/10.1016/j.earscirev.2020.103496>, 2021.

1788

1789 Leroy, S. A. G. and Arpe, K.: Glacial refugia for summer-green trees in Europe and south-
1790 west Asia as proposed by ECHAM3 time-slice atmospheric model simulations, *J. Biogeogr.*,
1791 34(12), 2115–2128, doi:10.1111/j.1365-2699.2007.01754.x, 2007.

1792

1793 Lev, L., Stein, M., Ito, E., Fruchter, N., Ben-Avraham, Z. and Almogi-Labin, A.:
1794 Sedimentary, geochemical and hydrological history of Lake Kinneret during the past 28,000
1795 years, *Quat. Sci. Rev.*, 209, 114–128, doi:10.1016/j.quascirev.2019.02.015, 2019.

1796

1797 Lister, A. M. and Stuart, A. J.: The impact of climate change on large mammal distribution
1798 and extinction: Evidence from the last glacial/interglacial transition, *Comptes Rendus -*
1799 *Geosci.*, 340(9–10), 615–620, doi:10.1016/j.crte.2008.04.001, 2008.

1800

1801 López-García, J. M. and Blain, H. A.: Quaternary small vertebrates: State of the art and new
1802 insights, *Quat. Sci. Rev.*, 233, doi:10.1016/j.quascirev.2020.106242, 2020.

1803

1804 Ludwig, P., Pinto, J. G., Raible, C. C. and Shao, Y.: Impacts of surface boundary conditions
1805 on regional climate model simulations of European climate during the Last Glacial
1806 Maximum, *Geophys. Res. Lett.*, 44(10), 5086–5095, doi:10.1002/2017GL073622, 2017.

1807

1808

1809 Luetscher, M., Boch, R., Sodemann, H., Spötl, C., Cheng, H., Edwards, R. L., Frisia, S., Hof,
1810 F. and Müller, W.: North Atlantic storm track changes during the Last Glacial Maximum
1811 recorded by Alpine speleothems, *Nat. Commun.*, 6, 27–32, doi:10.1038/ncomms7344, 2015.
1812

1813 Magri, D.: Persistence of tree taxa in Europe and Quaternary climate changes, *Quat. Int.*,
1814 219(1–2), 145–151, doi:10.1016/j.quaint.2009.10.032, 2010.
1815

1816 Magri, D. and Parra, I.: Late Quaternary western Mediterranean pollen records and African
1817 winds, *Earth Planet. Sci. Lett.*, 200(3–4), 401–408, doi:10.1016/S0012-821X(02)00619-2,
1818 2002.
1819

1820 Magri, D. and Sadori, L.: Late Pleistocene and Holocene pollen stratigraphy at Lago di Vico,
1821 central Italy, *Veg. Hist. Archaeobot.*, 8(4), 247–260, doi:10.1007/BF01291777, 1999.
1822

1823 Magyari, E., Jakab, G., Rudner, E. and Sümegei, P.: Palynological and plant macrofossil data
1824 on Late Pleistocene short-term climatic oscillations in NE-Hungary, *Acta Palaeobot. Suppl.*,
1825 2(January), 491–502, 1999.
1826

1827 Magyari, E. K., Kuneš, P., Jakab, G., Sümegei, P., Pelánková, B., Schäbitz, F., Braun, M. and
1828 Chytrý, M.: Late Pleniglacial vegetation in eastern-central Europe: Are there modern
1829 analogues in Siberia?, *Quat. Sci. Rev.*, 95, 60–79, doi:10.1016/j.quascirev.2014.04.020,
1830 2014a.
1831

1832 Magyari, E. K., Veres, D., Wennrich, V., Wagner, B., Braun, M., Jakab, G., Karátson, D.,
1833 Pál, Z., Ferenczy, G., St-Onge, G., Rethemeyer, J., Francois, J. P., von Reumont, F. and
1834 Schäbitz, F.: Vegetation and environmental responses to climate forcing during the Last
1835 Glacial Maximum and deglaciation in the East Carpathians: Attenuated response to
1836 maximum cooling and increased biomass burning, *Quat. Sci. Rev.*, 106, 278–298,
1837 doi:10.1016/j.quascirev.2014.09.015, 2014b.
1838

1839 Magyari, E. K., Pál, I., Vincze, I., Veres, D., Jakab, G., Braun, M., Szalai, Z., Szabó, Z. and
1840 Korponai, J.: Warm Younger Dryas summers and early late glacial spread of temperate
1841 deciduous trees in the Pannonian Basin during the last glacial termination (20-9 kyr cal BP),
1842 *Quat. Sci. Rev.*, 225, doi:10.1016/j.quascirev.2019.105980, 2019.
1843

1844 Margari, V., Gibbard, P. L., Bryant, C. L. and Tzedakis, P. C.: Character of vegetational and
1845 environmental changes in southern Europe during the last glacial period; evidence from
1846 Lesvos Island, Greece, *Quat. Sci. Rev.*, 28(13–14), 1317–1339,
1847 doi:10.1016/j.quascirev.2009.01.008, 2009.
1848

1849 Marsicek, J., Shuman, B. N., Bartlein, P. J., Shafer, S. L. and Brewer, S.: Reconciling
1850 divergent trends and millennial variations in Holocene temperatures, *Nature*, 554(7690), 92–
1851 96, doi:10.1038/nature25464, 2018.
1852

1853 Mauch Lenardić, J., Oros Sršen, A. and Radović, S.: Quaternary fauna of the Eastern Adriatic
1854 (Croatia) with the special review on the Late Pleistocene sites, *Quat. Int.*, 494, 130–151,
1855 doi:10.1016/j.quaint.2017.11.028, 2018.
1856

1857 Mauri, A., Davis, B. A. S., Collins, P. M. and Kaplan, J. O.: The influence of atmospheric
1858 circulation on the mid-Holocene climate of Europe: A data-model comparison, *Clim. Past*,
1859 10(5), 1925–1938, doi:10.5194/cp-10-1925-2014, 2014.
1860

1861 Mauri, A., Davis, B. A. S., Collins, P. M. and Kaplan, J. O.: The climate of Europe during the
1862 Holocene: A gridded pollen-based reconstruction and its multi-proxy evaluation, *Quat. Sci.*
1863 *Rev.*, 112, doi:10.1016/j.quascirev.2015.01.013, 2015.
1864

1865 MARGE Project Members.: Constraints on the magnitude and patterns of ocean cooling at
1866 the Last Glacial Maximum, , (January), 1–6, doi:10.1038/ngeo411, 2009.
1867

1868 Mikolajewicz, U.: Modeling mediterranean ocean climate of the last glacial maximum, *Clim.*
1869 *Past*, 7(1), 161–180, doi:10.5194/cp-7-161-2011, 2011.
1870

1871 Miola, A., Bondesan, A., Corain, L., Favaretto, S., Mozzi, P., Piovan, S. and Sostizzo, I.:
1872 Wetlands in the Venetian Po Plain (northeastern Italy) during the Last Glacial Maximum:
1873 Interplay between vegetation, hydrology and sedimentary environment, *Rev. Palaeobot.*
1874 *Palynol.*, 141(1–2), 53–81, doi:10.1016/j.revpalbo.2006.03.016, 2006.
1875

1876 Mix, A. C., Bard, E. and Schneider, R.: Environmental processes of the ice age: Land,
1877 oceans, glaciers (EPILOG), *Quat. Sci. Rev.*, 20(4), 627–657, doi:10.1016/S0277-
1878 3791(00)00145-1, 2001.
1879

1879 Moine, O., Rousseau, D. D., Jolly, D. and Vianey-Liaud, M.: Paleoclimatic reconstruction
1880 using mutual climatic range on terrestrial mollusks, *Quat. Res.*, 57(1), 162–172,
1881 doi:10.1006/qres.2001.2286, 2002.
1882

1883 Monegato, G., Ravazzi, C., Donegana, M., Pini, R., Calderoni, G. and Wick, L.: Evidence of
1884 a two-fold glacial advance during the last glacial maximum in the Tagliamento end moraine
1885 system (eastern Alps), *Quat. Res.*, 68(2), 284–302, doi:10.1016/j.yqres.2007.07.002, 2007.
1886

1887 Monegato, G., Ravazzi, C., Culiberg, M., Pini, R., Bavec, M., Calderoni, G., Jež, J. and
1888 Perego, R.: Sedimentary evolution and persistence of open forests between the south-eastern
1889 Alpine fringe and the Northern Dinarides during the Last Glacial Maximum, *Palaeogeogr.*
1890 *Palaeoclimatol. Palaeoecol.*, 436, 23–40, doi:10.1016/j.palaeo.2015.06.025, 2015.
1891

1892 Moreno, A., González-Sampériz, P., Morellón, M., Valero-Garcés, B. L. and Fletcher, W. J.:
1893 Northern Iberian abrupt climate change dynamics during the last glacial cycle: A view from
1894 lacustrine sediments, *Quat. Sci. Rev.*, 36, 139–153, doi:10.1016/j.quascirev.2010.06.031,
1895 2012.
1896

1897 Nogues-Bravo D, Rodríguez-Sánchez F, Orsini L, de Boer E, Jansson R, Morlon, H.,
1898 Fordham, D.A., Jackson, S.T.: Cracking the code of biodiversity responses to past climate
1899 change. *Trends Ecol. Evol.* 33:765–76, 2018.
1900

1901

1902 Nolan, C., Overpeck, J. T., Allen, J. R. M., Anderson, P. M., Betancourt, J. L., Binney, H. A.,
1903 Brewer, S., Bush, M. B., Chase, B. M., Cheddadi, R., Djamali, M., Dodson, J., Edwards, M.
1904 E., Gosling, W. D., Haberle, S., Hotchkiss, S. C., Huntley, B., Ivory, S. J., Kershaw, A. P.,
1905 Kim, S. H., Latorre, C., Leydet, M., Lézine, A. M., Liu, K. B., Liu, Y., Lozhkin, A. V.,
1906 McGlone, M. S., Marchant, R. A., Momohara, A., Moreno, P. I., Müller, S., Otto-Bliesner, B.

1907 L., Shen, C., Stevenson, J., Takahara, H., Tarasov, P. E., Tipton, J., Vincens, A., Weng, C.,
1908 Xu, Q., Zheng, Z. and Jackson, S. T.: Past and future global transformation of terrestrial
1909 ecosystems under climate change, *Science* (80-.), 361(6405), 920–923,
1910 doi:10.1126/science.aan5360, 2018.

1911
1912 Normand, S., Treier, U. A. and Odgaard, B. V.: Tree refugia and slow forest development in
1913 response to post - LGM warming in North - Eastern European Russia, , 2(4), 2–5, 2011.

1914
1915 Paganelli, A.: Evolution of vegetation and climate in the Veneto-Po Plain during the Late-
1916 Glacial and Early Holocene using pollen-strat-igraphical data, *Alp. Mediterr. Quat.*, 9(2),
1917 581–589, 1996.

1918
1919 Peyron, O., Guiot, J., Cheddadi, R., Tarasov, P., Reille, M., De Beaulieu, J. L., Bottema, S.
1920 and Andrieu, V.: Climatic Reconstruction in Europe for 18,000 YR B.P. from Pollen Data,
1921 *Quat. Res.*, 49(2), 183–196, doi:10.1006/qres.1997.1961, 1998a.

1922
1923 Peyron, O., Magny, M., Goring, S., Joannin, S., de Beaulieu, J.-L., Brugiapaglia, E., Sadori,
1924 L., Garfi, G., Kouli, K., Ioakim, C., Combourieu-Nebout, N., Contrasting patterns of climatic
1925 changes during the Holocene across the Italian Peninsula reconstructed from pollen data.
1926 *Clim. Past* 9 (3), 1233–1252. Doi:10.5194/cp-9-1233-2013, 2013.

1927
1928 Pons, A. and Reille, M.: The Holocene- and upper Pleistocene pollen record from Padul
1929 (Granada, Spain): A new study, *Palaeogeogr. Palaeoclimatol. Palaeoecol.*, 66(3–4),
1930 doi:10.1016/0031-0182(88)90202-7, 1988.

1931
1932 Potì, A., Kehl, M., Broich, M., Carrión Marco, Y., Hutterer, R., Jentke, T., Linstädter, J.,
1933 López-Sáez, J. A., Mikdad, A., Morales, J., Pérez-Díaz, S., Portillo, M., Schmid, C., Vidal-
1934 Matutano, P. and Weniger, G. C.: Human occupation and environmental change in the
1935 western Maghreb during the Last Glacial Maximum (LGM) and the Late Glacial. New
1936 evidence from the Iberomaurusian site Ifri El Baroud (northeast Morocco), *Quat. Sci. Rev.*,
1937 220, 87–110, doi:10.1016/j.quascirev.2019.07.013, 2019.

1938
1939 Prentice, I. C., Cleator, S. F., Huang, Y. H., Harrison, S. P., and Roulstone, I.: Reconstructing
1940 ice-age palaeoclimates: Quantifying low-CO₂ effects on plants, *Global Planet. Change*, 149,
1941 166–176, <https://doi.org/10.1016/j.gloplacha.2016.12.012>, 2017.

1942
1943 Prentice, I. C. and Harrison, S. P.: Ecosystem effects of CO₂ concentration: Evidence from
1944 past climates, *Clim. Past*, 5(3), 297–307, doi:10.5194/cp-5-297-2009, 2009.

1945
1946 Prentice, I. C., Guiot, J. and Harrison, S. P.: Mediterranean vegetation, lake levels and
1947 palaeoclimate at the Last Glacial Maximum, *Nature*, 360(6405), 658–660,
1948 doi:10.1038/360658a0, 1992.

1949
1950 Prentice, I. C., Guiot, J., Huntley, B., Jolly, D. and Cheddadi, R.: Reconstructing biomes
1951 from palaeoecological data: A general method and its application to European pollen data at
1952 0 and 6 ka, *Clim. Dyn.*, 12(3), 185–194, doi:10.1007/BF00211617, 1996.

1953
1954 Prentice, I. C., Harrison, S. P. and Bartlein, P. J.: Global vegetation and terrestrial carbon
1955 cycle changes after the last ice age, *New Phytol.*, 189(4), 988–998, doi:10.1111/j.1469-
1956 8137.2010.03620.x, 2011.

1957
1958 Prud'homme, C., Lécuyer, C., Antoine, P., Moine, O., Hatté, C., Fourel, F., Martineau, F. and
1959 Rousseau, D. D.: Palaeotemperature reconstruction during the Last Glacial from $\delta^{18}\text{O}$ of
1960 earthworm calcite granules from Nussloch loess sequence, Germany, *Earth Planet. Sci. Lett.*,
1961 442, 13–20, doi:10.1016/j.epsl.2016.02.045, 2016.
1962
1963 Prud'homme, C., Lécuyer, C., Antoine, P., Hatté, C., Moine, O., Fourel, F., Amiot, R.,
1964 Martineau, F. and Rousseau, D. D.: $\delta^{13}\text{C}$ signal of earthworm calcite granules: A new proxy
1965 for palaeoprecipitation reconstructions during the Last Glacial in western Europe, *Quat. Sci.*
1966 *Rev.*, 179, 158–166, doi:10.1016/j.quascirev.2017.11.017, 2018.
1967
1968 Puzachenko, A. Y., Markova, A. K. and Pawłowska, K.: Evolution of Central European
1969 regional mammal assemblages between the late Middle Pleistocene and the Holocene (MIS7–
1970 MIS1), *Quat. Int.*, (November), doi:10.1016/j.quaint.2021.11.009, 2021.
1971
1972 Ramstein, G., Kageyama, M., Guiot, J. and Wu, H.: How cold was Europe at the Last Glacial
1973 Maximum ? A synthesis of the progress achieved since the first PMIP model-data
1974 comparison, , 331–339, 2007.
1975
1976 Reille, M. and Andrieu, V.: The late Pleistocene and Holocene in the Lourdes Basin, Western
1977 Pyrénées, France: new pollen analytical and chronological data, *Veg. Hist. Archaeobot.*, 4(1),
1978 1–21, doi:10.1007/BF00198611, 1995.
1979
1980 Reille, M. and de Beaulieu, J. L.: History of the Würm and Holocene vegetation in western
1981 velay (Massif Central, France): A comparison of pollen analysis from three corings at Lac du
1982 Bouchet, *Rev. Palaeobot. Palynol.*, 54(3–4), 233–248, doi:10.1016/0034-6667(88)90016-4,
1983 1988.
1984
1985 Reimer, A., Landmann, G. and Kempe, S.: Lake Van, Eastern Anatolia, hydrochemistry and
1986 history, *Aquat. Geochemistry*, 15(1–2), 195–222, doi:10.1007/s10498-008-9049-9, 2009.
1987
1988 Rousseau, D. D.: Climatic transfer function from quaternary molluscs in European loess
1989 deposits, *Quat. Res.*, 36(2), 195–209, doi:10.1016/0033-5894(91)90025-Z, 1991.
1990
1991 Royer, A., Montuire, S., Legendre, S., Discamps, E., Jeannet, M. and Lécuyer, C.:
1992 Investigating the influence of climate changes on rodent communities at a regional-scale
1993 (MIS 1-3, Southwestern France), *PLoS One*, 11(1), 1–25, doi:10.1371/journal.pone.0145600,
1994 2016.
1995
1996 Ruiz-Zapata, M. B., Vegas, J., Garcia-Cortes, A., Gil Garcia, M. J., Torres, T., Ortiz, J. E.
1997 and Perez-Gonzalez, A.: Vegetation evolution during the Last Maximum Glacial Period in
1998 FU-1 sequence (Fuentillejo Lacustrin Maar, Campo de Calatrava, Ciudad Real), *Polen*, 18,
1999 37–49, 2008.
2000
2001 Salonen, J., Sanchez Goñi, M.F., Renssen, H. and Pliikk, A.: Contrasting northern and
2002 southern European winter climate trends during the Last Interglacial. *Geology* 49.
2003 10.1130/G49007.1. 2021
2004
2005 Salonen, J.S., Korpela, M., Williams, J.W., Luoto, M., Machine-learning based
2006 reconstructions of primary and secondary climate variables from North American and

2007 European fossil pollen data. *Sci. Rep.* 9, 1–13. doi: 10.1038/s41598-019-
2008 52293-4, 2019.

2009

2010 Salonen, J.S., Ilvonen, L., Seppä, H., Holmström, L., Telford, R.J., Gaidamavicius, A.,
2011 Stancikaite, M., Subetto, D. Comparing different calibration methods (WA/WA-PLS
2012 regression and Bayesian modelling) and different-sized calibration sets in pollen-based
2013 quantitative climate reconstruction. *The Holocene* 22, 413–424, 2012.

2014

2015 Samartin, S., Heiri, O., Kaltenrieder, P., Köhl, N. and Tinner, W.: Reconstruction of full
2016 glacial environments and summer temperatures from Lago della Costa, a refugial site in
2017 Northern Italy, *Quat. Sci. Rev.*, 143, 107–119, doi:10.1016/j.quascirev.2016.04.005, 2016.

2018

2019 Sánchez Goñi, M.F., Loutre, M.F., Crucifix, M., Peyron, O., Santos, L., Duprat, J., Malaizé,
2020 B., Turon, J.-L., and Peyrouquet, J.-P.: Increasing vegetation and climate gradient in western
2021 Europe over the Last Glacial inception (122–110 ka): Data–model comparison. *Earth and
2022 Planetary Science Letters*, 231, 111–130, doi: 10.1016/j.epsl.2004.12.010, 2005.

2023

2024 Sanchez Goñi, M.F., Harrison, S.P.: Millennial-scale climate variability and vegetation
2025 changes during the Last Glacial: concepts and terminology. *Quaternary Science
2026 Reviews* 29, 2823–2827, doi: [10.1016/j.quascirev.2009.11.014](https://doi.org/10.1016/j.quascirev.2009.11.014), 2010.

2027

2028 Sanchi, L., Ménot, G. and Bard, E.: Insights into continental temperatures in the northwestern
2029 Black Sea area during the Last Glacial period using branched tetraether lipids, *Quat. Sci.
2030 Rev.*, 84, 98–108, doi:10.1016/j.quascirev.2013.11.013, 2014.

2031

2032 Satkūnas, J. and Grigienė, A.: Eemian-Weichselian palaeoenvironmental record from the
2033 Mickūnai glacial depression (Eastern Lithuania), *Geologija*, 54(2), 35–51,
2034 doi:10.6001/geologija.v54i2.2482, 2012.

2035 Schäfer, I. K., Bliedtner, M., Wolf, D., Faust, D. and Zech, R.: Evidence for humid
2036 conditions during the last glacial from leaf wax patterns in the loess–paleosol sequence El
2037 Paraíso, Central Spain, *Quat. Int.*, 407, 64–73, doi:10.1016/j.quaint.2016.01.061, 2016.

2038

2039 Scourse, J. D.: Late Pleistocene stratigraphy and palaeobotany of the Isles of Scilly, *Philos.
2040 Trans. - R. Soc. London, B*, 334(1271), 405–448, doi:10.1098/rstb.1991.0125, 1991.

2041

2042 Spötl, C., Koltai, G., Jarosch, A. H. and Cheng, H.: Increased autumn and winter
2043 precipitation during the Last Glacial Maximum in the European Alps, *Nat. Commun.*, 12(1),
2044 doi:10.1038/s41467-021-22090-7, 2021.

2045

2046 Stewart, J. R. and Lister, A. M.: Cryptic northern refugia and the origins of the modern biota,
2047 *Trends Ecol. Evol.*, 16(11), 608–613, doi:10.1016/S0169-5347(01)02338-2, 2001.

2048

2049 Stivrins, N., Soininen, J., Amon, L., Fontana, S. L., Gryguc, G., Heikkilä, M., Heiri, O.,
2050 Kisieliene, D., Reitalu, T., Stančikaitė, M., Veski, S. and Seppä, H.: Biotic turnover rates
2051 during the Pleistocene-Holocene transition, *Quat. Sci. Rev.*, 151, 100–110,
2052 doi:10.1016/j.quascirev.2016.09.008, 2016.

2053

2054 Strahl, J.: Zur Pollenstratigraphie des Weichselspätglazials von Berlin-Brandenburg [On the
2055 palynostratigraphy of the Late Weichselian in Berlin-Brandenburg], *Brand.
2056 Geowissenschaftliche Beiträge*, 12, 87–112, 2005.

2057
2058 Stute, M. and Deak, J.: Environmental isotope study (14C, 13C, 18O, D, noble gases) on
2059 deep groundwater circulation systems in Hungary with reference to paleoclimate,
2060 Radiocarbon, 31(3), 902–918, doi:10.1017/s0033822200012522, 1990.
2061
2062 Svenning, J., Normand, S. and Kageyama, M.: Glacial refugia of temperate trees in Europe :
2063 insights from species distribution modelling, , (Svenning 2003), 1117–1127,
2064 doi:10.1111/j.1365-2745.2008.01422.x, 2008.
2065
2066 Tarasov, P. E., Webb, T., Andreev, A. A., Afanas'eva, N. B., Berezina, N. A., Bezusko, L.
2067 G., Blyakharchuk, T. A., Bolikhovskaya, N. S., Cheddadi, R., Chernavskaya, M. M.,
2068 Chernova, G. M., Dorofeyuk, N. I., Dirksen, V. G., Elina, G. A., Filimonova, L. V., Glebov,
2069 F. Z., Guiot, J., Gunova, V. S., Harrison, S. P., Jolly, D., Khomutova, V. I., Kvavadze, E. V.,
2070 Osipova, I. M., Panova, N. K., Prentice, I. C., Saarse, L., Sevastyanov, D. V., Volkova, V. S.
2071 and Zernitskaya, V. P.: Present-day and mid-Holocene biomes reconstructed from pollen and
2072 plant macrofossil data from the former Soviet Union and Mongolia, *J. Biogeogr.*, 25(6),
2073 1029–1053, doi:10.1046/j.1365-2699.1998.00236.x, 1998.
2074
2075 Tarasov, P. E., Volkova, V. S., Webb, T., Guiot, J., Andreev, A. A., Bezusko, L. G.,
2076 Bezusko, T. V., Bykova, G. V., Dorofeyuk, N. I., Kvavadze, E. V., Osipova, I. M., Panova,
2077 N. K. and Sevastyanov, D. V.: Last glacial maximum biomes reconstructed from pollen and
2078 plant macrofossil data from northern Eurasia, *J. Biogeogr.*, 27(3), 609–620,
2079 doi:10.1046/j.1365-2699.2000.00429.x, 2000.
2080
2081 Tarasov, P.E., Andreev, A.A., Anderson, P.M., Lozhkin, A.V., Haltia-Hovi, E., Nowaczyk,
2082 N.R., Wennrich, V., Brigham-Grette, J., Melles, M.: A pollen-based biome reconstruction
2083 over the last 3.562 million years in the Far East Russian Arctic e new insights on climate-
2084 vegetation relationships at the regional scale. *Clim. Past* 9, 2759-2775, doi: 10.5194/cp-9-
2085 2759-2013, 2013.
2086
2087 Telford, R. J. and Birks, H. J. B.: Evaluation of transfer functions in spatially structured
2088 environments, *Quat. Sci. Rev.*, 28(13–14), 1309–1316, doi:10.1016/j.quascirev.2008.12.020,
2089 2009.
2090
2091 Turner, M. G., Wei, D., Prentice, I. C., & Harrison, S. P. The impact of methodological
2092 decisions on climate reconstructions using WA-PLS. *Quaternary Research*, 99, 341-356,
2093 2021.
2094
2095 Valero-Garcés, B. L., González-Sampériz, P., Navas, A., Machin, J., Delgado-Huertas, A.,
2096 Pena-Monné, J. L., Sancho-Marcén, C., Stevenson, T. and Davis, B.: Paleohydrological
2097 fluctuations and steppe vegetation during the last glacial maximum in the central Ebro valley
2098 (NE Spain), *Quat. Int.*, 122(1 SPEC. ISS.), doi:10.1016/j.quaint.2004.01.030, 2004.
2099
2100 Valsecchi, V., Sanchez Goñi, M. F. and Londeix, L.: Vegetation dynamics in the
2101 Northeastern Mediterranean region during the past 23 000 yr: Insights from a new pollen
2102 record from the Sea of Marmara, *Clim. Past*, 8(5), 1941–1956, doi:10.5194/cp-8-1941-2012,
2103 2012.
2104
2105 Vandenberghe, J., French, H. M., Gorbunov, A., Marchenko, S., Velichko, A. A., Jin, H.,
2106 Cui, Z., Zhang, T. and Wan, X.: The Last Permafrost Maximum (LPM) map of the Northern

2107 Hemisphere: Permafrost extent and mean annual air temperatures, 25-17ka BP, *Boreas*,
2108 43(3), 652–666, doi:10.1111/bor.12070, 2014.

2109

2110 Varsányi, I., Palcsu, L. and Kovács, L. Ó.: Groundwater flow system as an archive of
2111 palaeotemperature: Noble gas, radiocarbon, stable isotope and geochemical study in the
2112 Pannonian Basin, Hungary, *Appl. Geochemistry*, 26(1), 91–104,
2113 doi:10.1016/j.apgeochem.2010.11.006, 2011.

2114

2115 Vegas-Vilarrúbia, T., González-Sampériz, P., Morellón, M., Gil-Romera, G., Pérez-Sanz, A.
2116 and Valero-Garcés, B.: Diatom and vegetation responses to late glacial and early holocene
2117 climate changes at lake estanya (southern pyrenees, NE Spain), *Palaeogeogr. Palaeoclimatol.*
2118 *Palaeoecol.*, 392, 335–349, doi:10.1016/j.palaeo.2013.09.011, 2013.

2119

2120 Vegas, J., Ruiz-Zapata, B., Ortiz, J. E., Galán, L., Torres, T., García-Cortés, Á., Gil-García,
2121 M. J., Pérez-González, A. and Gallardo-Millán, J. L.: Identification of arid phases during the
2122 last 50 cal. ka BP from the Fuentillejo maar-lacustrine record (Campo de Calatrava Volcanic
2123 Field, Spain), *J. Quat. Sci.*, 25(7), 1051–1062, doi:10.1002/jqs.1262, 2010.

2124

2125 Velasquez, P., Kaplan, J. O., Messmer, M., Ludwig, P. and Raible, C. C.: The role of land
2126 cover in the climate of glacial Europe, *Clim. Past*, 17(3), 1161–1180, doi:10.5194/cp-17-
2127 1161-2021, 2021.

2128

2129 Vicente-Serrano, S. M., Trigo, R. M., López-Moreno, J. I., Liberato, M. L. R., Lorenzo-
2130 Lacruz, J., Beguería, S., Morán-Tejeda, E. and El Kenawy, A.: Extreme winter precipitation
2131 in the Iberian Peninsula in 2010: Anomalies, driving mechanisms and future projections,
2132 *Clim. Res.*, 46(1), 51–65, doi:10.3354/cr00977, 2011.

2133

2134 Williams, J.W., Grimm, E.G., Blois, J., Charles, D.F., Davis, E., Goring, S.J., Graham, R.,
2135 Smith, A.J., Anderson, M., Arroyo-Cabrales, J., Ashworth, A.C., Betancourt, J.L., Bills,
2136 B.W., Booth, R.K., Buckland, P., Curry, B., Giesecke, T., Hausmann, S., Jackson, S.T.,
2137 Latorre, C., Nichols, J., Purdum, T., Roth, R.E., Stryker, M., Takahara, H. :The Neotoma
2138 Paleocology Database: A multi-proxy, international community-curated data resource. *Quat.*
2139 *Res.* 89, 156-177, doi:10.1017/qua.2017.105, 2018.

2140

2141 Williams, J. W. and Jackson, S. T.: Palynological and AVHRR observations of modern
2142 vegetational gradients in eastern North America, , 4, 485–497, 2003.

2143

2144 Williams, J. W., Webb, T., Shurman, B. N. and Bartlein, P. J.: Do Low CO₂ Concentrations
2145 Affect Pollen-Based Reconstructions of LGM Climates? A Response to “Physiological
2146 Significance of Low Atmospheric CO₂ for Plant–Climate Interactions” by Cowling and
2147 Sykes, *Quat. Res.*, 53(3), 402–404, doi:10.1006/qres.2000.2131, 2000.

2148

2149 Willis, K. J. and Van Andel, T. H.: Trees or no trees? The environments of central and
2150 eastern Europe during the Last Glaciation, *Quat. Sci. Rev.*, 23(23–24), 2369–2387,
2151 doi:10.1016/j.quascirev.2004.06.002, 2004.

2152

2153 Wu, H., Guiot, J., Brewer, S. and Guo, Z.: Climatic changes in Eurasia and Africa at the last
2154 glacial maximum and mid-Holocene: Reconstruction from pollen data using inverse
2155 vegetation modelling, *Clim. Dyn.*, 29(2–3), 211–229, doi:10.1007/s00382-007-0231-3, 2007.

2156

2157 Wu, H., Li, Q., Yu, Y., Sun, A., Lin, Y., Jiang, W. & Luo, Y. Quantitative climatic reconstruction of
2158 the Last Glacial Maximum in China. *Sci. China Earth Sci.* 62, 1269–1278 (2019).
2159 Doi:10.1007/s11430-018-9338-3, 2019.
2160
2161 Yu, G. and Harrison, S. P.: Lake status records from Europe: data base documentation,
2162 NOAA Paleoclimatology Publications Series, Boulder, Colorado., 1995.
2163
2164 Zaarur, S., Affek, H. P. and Stein, M.: Last glacial-Holocene temperatures and hydrology of
2165 the Sea of Galilee and Hula Valley from clumped isotopes in *Melanopsis* shells, *Geochim.*
2166 *Cosmochim. Acta*, 179, 142–155, doi:10.1016/j.gca.2015.12.034, 2016.
2167
2168 Zanon, M., Davis, B. A. S., Marquer, L., Brewer, S. and Kaplan, J. O.: European forest cover
2169 during the past 12,000 years: A palynological reconstruction based on modern analogs and
2170 remote sensing, *Front. Plant Sci.*, 9, doi:10.3389/fpls.2018.00253, 2018.
2171
2172 Zech, M., Buggle, B., Leiber, K., Marković, S., Glaser, B., Hambach, U., Huwe, B., Stevens,
2173 T., Sümegei, P., Wiesenberg, G. and Zöller, L.: Reconstructing Quaternary vegetation history
2174 in the Carpathian Basin, SE-Europe, using n-alkane biomarkers as molecular fossils:
2175 Problems and possible solutions, potential and limitations, *Quat. Sci. J.*, 58(2), 148–155,
2176 doi:10.3285/eg.58.2.03, 2010.
2177
2178

2179 **Tables**
 2180
 2181

Site	Site Name	Country/Ocean	Latitude	Longitude	Elevation	Site Type	Data Type	Samples	Source	Reference
1	MD95-2039 (M)	Atlantic	40.578333	-10.348333	-3381	Marine	Raw Count	21	EPD (E#1472)	Roucoux et al. 2005
2	SU81-18 (M)	Atlantic	37.77	-9.82	-3135	Marine	Raw Count	10	ACER	Turon et al. 2003
3	MD99-2331 (M)	Atlantic	41.15	-9.68	-2110	Marine	Raw Count	41	ACER	Naughton et al. 2006
4	Carn Morval	United Kingdom	49.926111	-6.313889	5	Lake	Digitised	1	Publication	Scourse 1991
5	Gorham Cave	Spain	36.132826	-5.347358	0	Cave	Digitised	1	Publication	Carrion et al. 2008
6	Dozmary Pool	United Kingdom	50.5347222	-4.5358333	265	Lake	Raw Count	32	Author	Kelly et al. 2010
7	Bajondillo	Spain	36.619722	-4.496389	20	Cave	Raw Count	1	EPD (E#1570)	Cortes-Sanchez et al 2011
8	Laguna del maar de Fuentillejo	Spain	38.937996	-4.0539	637	Lake	Digitised	1	Publication	Ruiz-Zapata et al. 2009
9	Padul-1	Spain	37.016338	-3.608503	785	Peat Bog	Digitised	13	Publication	Pons & Reille 1988
10	Padul-2	Spain	37.010833	-3.603889	726	Peat Bog	Digitised	1	Publication	Camuera et al. 2019
11	Cova di Carihuela	Spain	37.4489	-3.4297	1020	Cave	Digitised	1	Publication	Carrion 1992
12	Ifri El Baroud	Morocco	34.75	-3.3	539	Cave	Digitised	1	Publication	Poti et al. 2019
13	MD95-2043 (M)	Mediterranean	36.14	-2.621	-1841	Marine	Raw Count	7	ACER	Fletcher et al. 2008
14	San Rafael	Spain	36.773611	-2.601389	0	Peat Bog	Raw Count	2	EPD (E#574)	Pantalón-Cano 1997
15	Siles	Spain	38.24	-2.3	1320	Lake	Digitised	1	Publication	Carrion 2002
16	Torreçilla de Valmadrid	Spain	41.4469444	-0.895	570	Colluvium	Digitised	1	Publication	Valero-Garcés et al. 2004
17	Navarrés-1	Spain	39.1	-0.683333	225	Peat Bog	Raw Count	1	EPD (E#469)	Carrion & Dupré-Olivier 1996
18	Navarrés-2	Spain	39.1	-0.683333	225	Peat Bog	Raw Count	1	EPD (E#470)	Carrion & Dupré-Olivier 1996
19	Tourbiere de l'Estarrès	France	43.0933	-0.3792	356	Lake	Digitised	1	Publication	Jalut et al. 1988
20	Cova de les Malladetes	Spain	39.058	-0.321	20	Cave	Digitised	1	Publication	Dupré-Olivier 1988
21	Lourdes	France	43.033333	-0.075	430	Lake	Digitised	15	Publication	Reille & Andrieu 1995
22	Lake Estanya	Spain	42.0333333	0.53333333	670	Lake	Digitised	1	Publication	Vegas-Villarubia et al. 2013
23	Freychinède	France	42.7833	1.4333	1350	Lake	Digitised	1	Publication	Jalut et al. 1992
24	Banyoles	Spain	42.133333	2.75	173	Lake	Raw Count	13	EPD (E#931)	Pérez-Obiol & Julia 1994
25	Lac du Bouchet B5	France	44.916667	3.783333	1200	Lake	Digitised	14	Publication	Reille & de Beaulieu 1988
26	MD99-2348 (103) (M)	Mediterranean	42.692778	3.841667	-296	Marine	Raw Count	41	EPD (E#1474)	Beaudouin et al. 2007
27	Les Echets G	France	45.9	4.93	267	Peat Bog	Digitised	136	ACER	de Beaulieu & Reille 1984
28	La Grotte Walou	Belgium	50.585278	5.536389	252	Cave	Digitised	1	Publication	Damblon 2011
29	Bergsee	Germany	47.5722222	7.93638889	382	Lake	Digitised	1	Publication	Duprat-Oualid et al. 2017
30	Garaat El-Ouez	Algeria	36.818333	8.33333	45	Peat Bog	Raw Count	6	EPD (E#1501)	Benslama et al 2010
31	Pian del Lago	Italy	44.321561	9.485682	833	Lake	Digitised	1	Publication	Guido et al. 2020
32	Pilsensee	Germany	48.0267	11.1883	534	Lake	Digitised	1	Publication	Küster 1995
33	Orgiano	Italy	45.29	11.43	19	Peat Bog	Digitised	1	Publication	Paganelli 1996
34	Lago della Costa	Italy	45.2702778	11.7430556	7	Lake	Digitised	8	Publication	Kaltenrieder et al. 2009
35	Lagaccione	Italy	42.566667	11.85	355	Lake	Raw Count	7	ACER	Magri 1999
36	Lago Vico	Italy	42.3166667	12.1666667	510	Lake	Digitised	15	Publication	Magri & Sadori 1999
37	Stracciaccia	Italy	42.13	12.32	220	Lake	Raw Count	2	ACER	Giardini 2007
38	Lago di Monterosi	Italy	42.2166667	12.4333333	237	Lake	Raw Count	1	Publication	Bonatti 1970
39	Venice	Italy	45.629523	12.654086	0	Peat Bog	Digitised	1	Publication	Miola et al. 2006
40	Azzano Decimo	Italy	45.8833	12.7165	10	Alluvial Fan	Raw Count	6	ACER	Pini et al. 2009
41	Valle di Castiglione	Italy	41.89	12.75	44	Lake	Raw Count	2	ACER	Follieri et al. 1989
42	Travesio	Italy	46.2	12.87	220	Lake	Digitised	1	Publication	Monegato et al. 2007
43	Orvenco	Italy	46.252088	13.169771	380	Alluvial Fan	Digitised	1	Publication	Monegato et al. 2007
44	Rio Doidis	Italy	46.12	13.19	152	Lake	Digitised	1	Publication	Monegato et al. 2007
45	Billerio	Italy	46.22	13.21	300	Lake	Digitised	1	Publication	Monegato et al. 2007
46	Kersdorf-Briesen	Germany	52.333704	14.269142	44	Lake	Digitised	1	Publication	Strahl 2005
47	Lago Grande di Monticchio	Italy	40.944444	15.6	1326	Lake	Raw Count	6	EPD (E#932)	Watts et al. 1996
48	Nagymohos	Hungary	48.326944	20.436389	297	Peat Bog	Raw Count	14	Publication	Magyari et al 1999
49	Safarka	Slovakia	48.8819444	20.575	600	Peat Bog	Digitised	1	Publication	Jankovska 2008
50	Feher Lake	Hungary	46.45	20.65	86	Lake	Raw Count	10	Publication	Magyari et al. 2014
51	Ioannina	Greece	39.75	20.85	470	Peat Bog	Raw Count	20	ACER	Tzedakis et al. 2004
52	Kokad	Hungary	47.4027778	21.9286111	112	Peat Bog	Raw Count	2	Publication	Magyari et al. 2019
53	Lake Xinias	Greece	39.05	22.27	500	Lake	Raw Count	5	EPD (E#976)	Bottema 1979
54	Mickunai	Lithuania	54.722114	25.532218	143	Lake	Digitised	1	Publication	Satkunas & Grigiene 2012
55	Lake Sfanta Anna	Romania	46.1263889	25.8880556	946	Lake	Digitised	1	Publication	Magyari et al. 2014
56	Megali Limni	Greece	39.1	26.3	323	Lake	Digitised	1	Publication	Margari et al. 2009
57	Straldzha	Bulgaria	42.630278	26.77	138	Peat Bog	Raw Count	3	Publication	Connor et l. 2013
58	MD01-2430 (M)	Turkey	40.796833	27.725166	-580	Marine	Digitised	1	Publication	Valsecchi et al. 2012
59	Lake Iznik	Turkey	40.433889	29.533056	88	Lake	Raw Count	7	EPD (E#714)	Miebach et al 2016
60	M72/5 628-1 (M)	Black Sea	42.1035	36.62383	-418	Marine	Raw Count	6	Pangaea (833387)	Shumilovskikh et al. 2014
61	Dziguta	Georgia	42.99	41.07	35	Peat Bog	Digitised	1	Publication	Arslanov et al. 2007
62	Lake Van LG	Turkey	38.667	42.669	1649	Lake	Raw Count	10	Pangaea (853779)	Pickarski et al. 2015
63	Lake Zeribar	Iran	35.533333	46.116667	1286	Lake	Raw Count	17	EPD (E#714)	van Zeist & Bottema 1977

2182
 2183
 2184 **Table 1. List of selected sites**
 2185
 2186
 2187

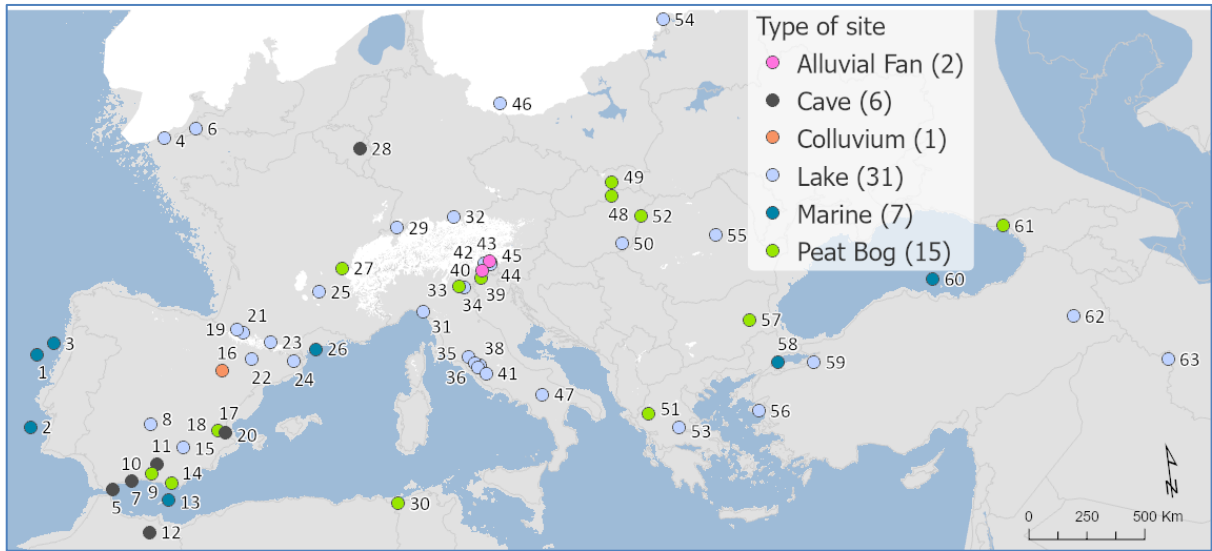
2188
2189
2190
2191
2192

	RMSE	R2
TANN	2.28	0.9
TDJF	3.35	0.91
TJJA	2.21	0.81
PANN	224.94	0.69
PDJF	78.51	0.69
PJJA	52.49	0.75
Tree Cover	21.03	0.52

2193
2194
2195
2196
2197
2198
2199
2200
2201
2202

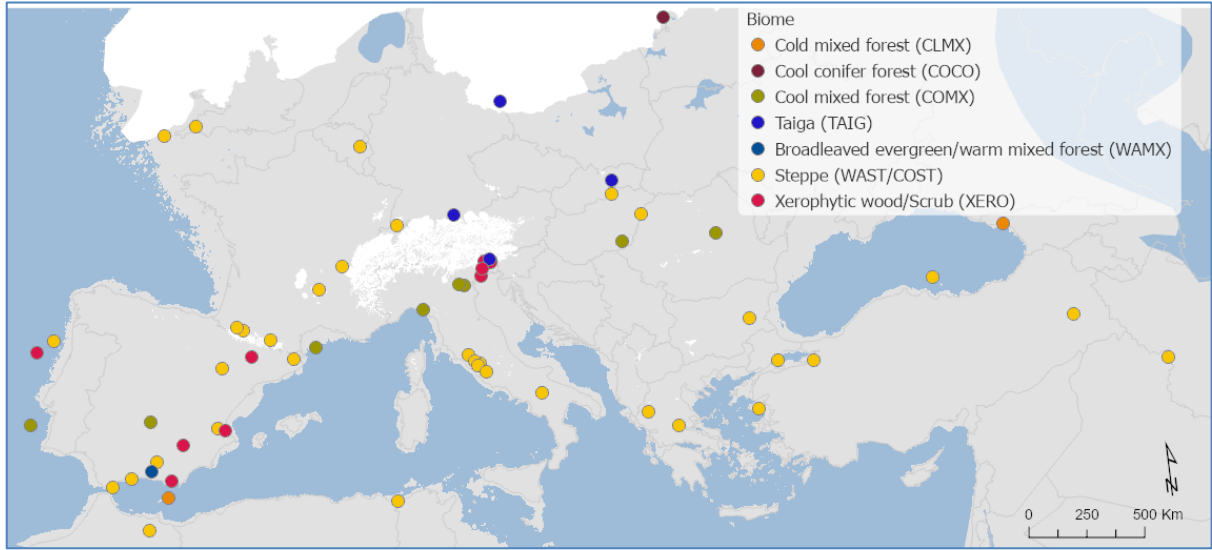
Table 2. MAT performance statistics based on the modern pollen sample training set. This includes Mean Annual Temperature and Precipitation (TANN and PANN), Mean Winter Temperature and Precipitation (TDJF and PDJF) and Mean Summer Temperature and Precipitation (TJJA and PJJA).

2203 **Figures**
2204
2205
2206



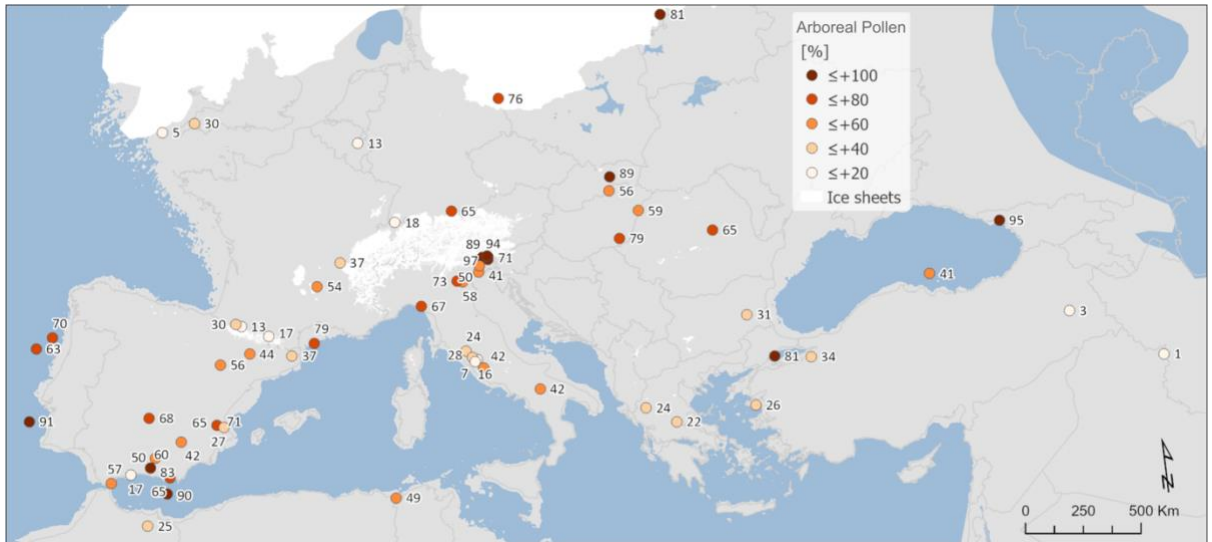
2207
2208
2209 **Figure 1. Site locations and archives (Site numbers are as shown in Table 1)**
2210
2211
2212

2213



2214
2215
2216
2217

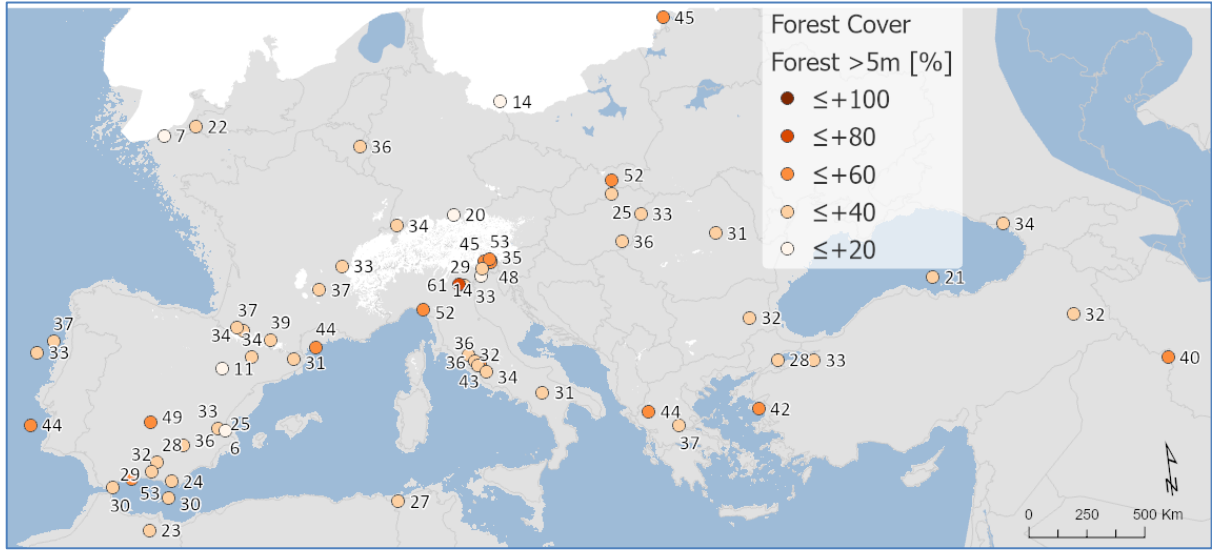
Figure 2. Pollen biomes



2218
2219
2220
2221

Figure 3. Arboreal Pollen (AP) % forest cover

2222



2223

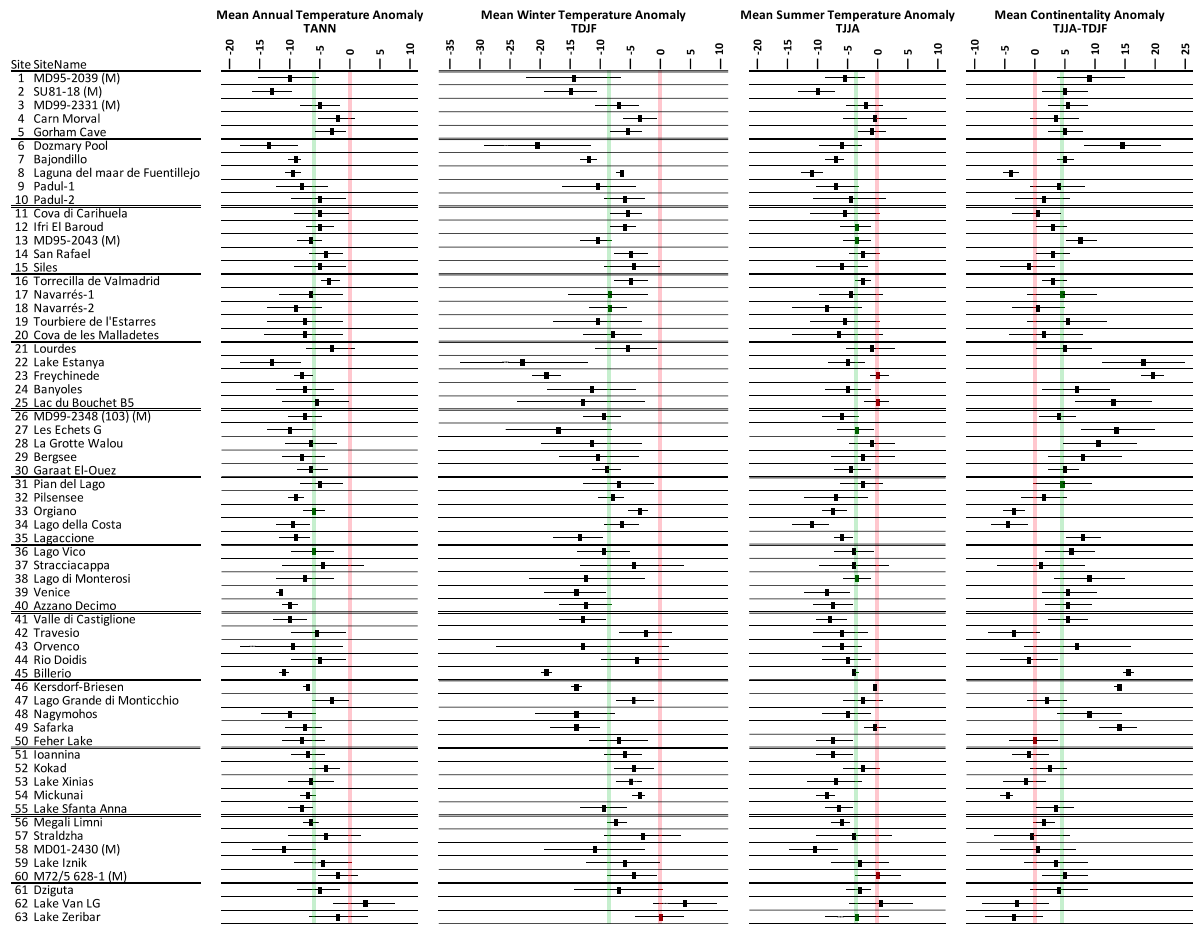
2224

2225

2226

2227

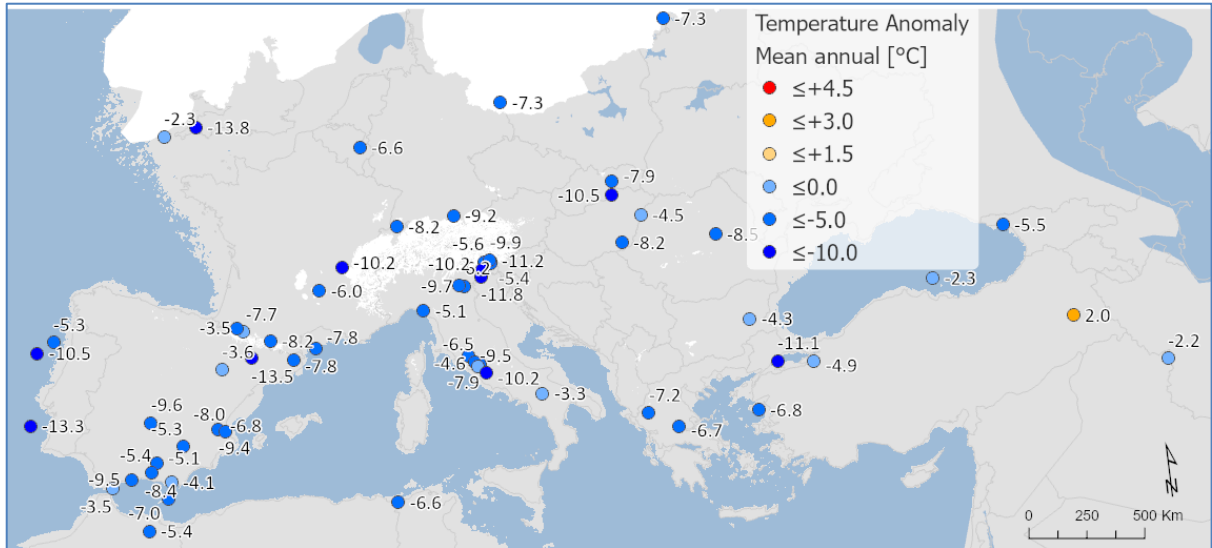
Figure 4. Modern Analogue Technique (MAT) % forest cover



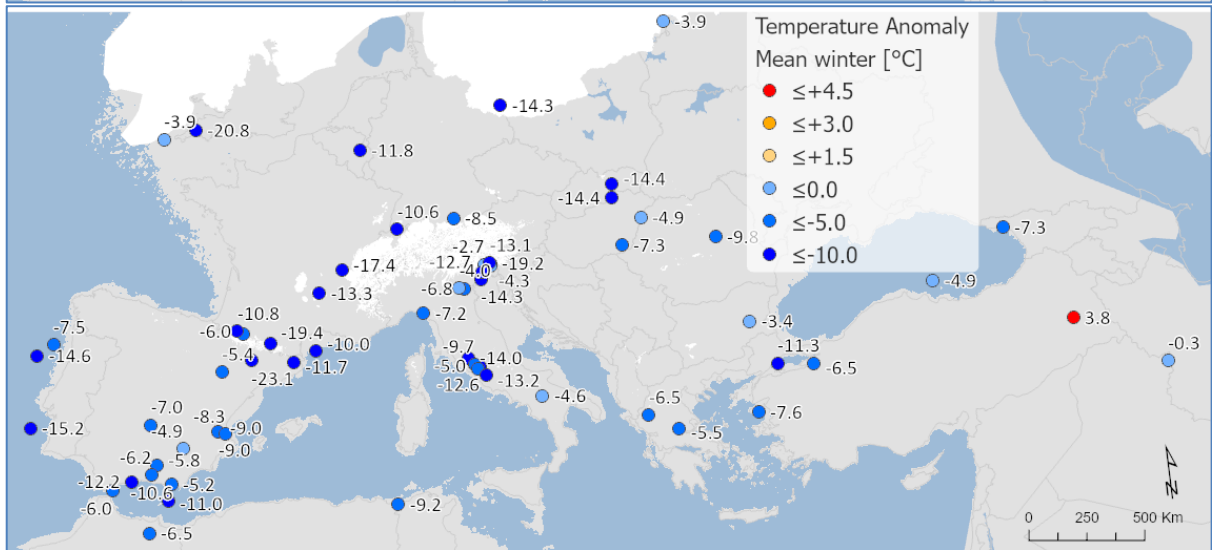
2228
2229
2230
2231
2232
2233
2234
2235
2236
2237
2238
2239

Figure 5. Pollen-based MAT reconstructions for LGM annual, winter and summer temperature anomalies (uncertainties represent one standard deviation). Continentality represents the difference in temperature between summer and winter, with positive anomalies indicating an increase in the temperature difference between summer and winter. All values are expressed as anomalies compared with the present day. The green line indicates the mean for all the sites.

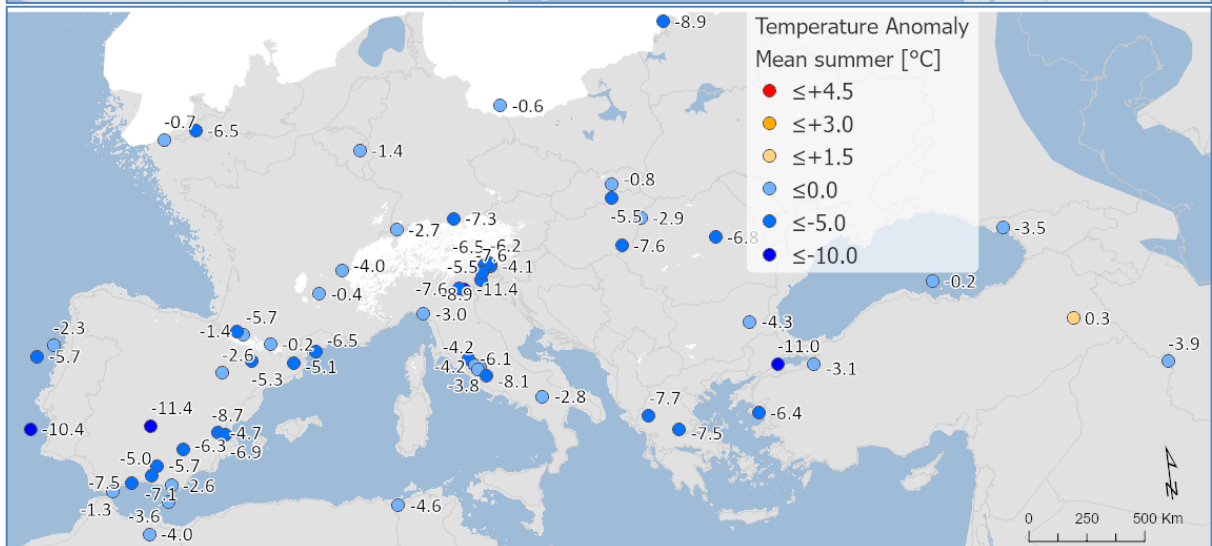
2240

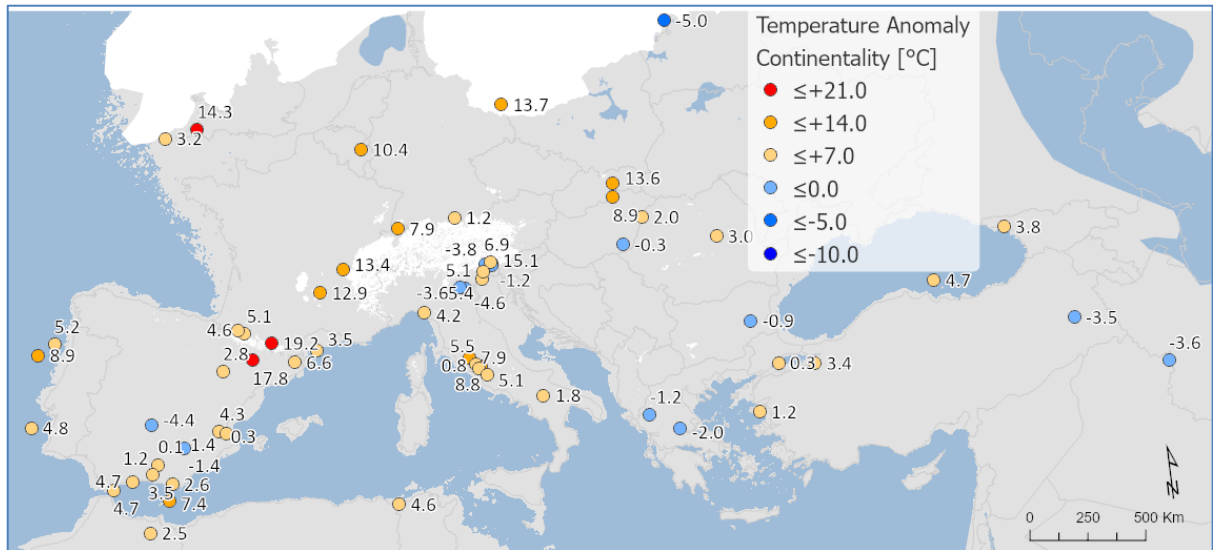


2241



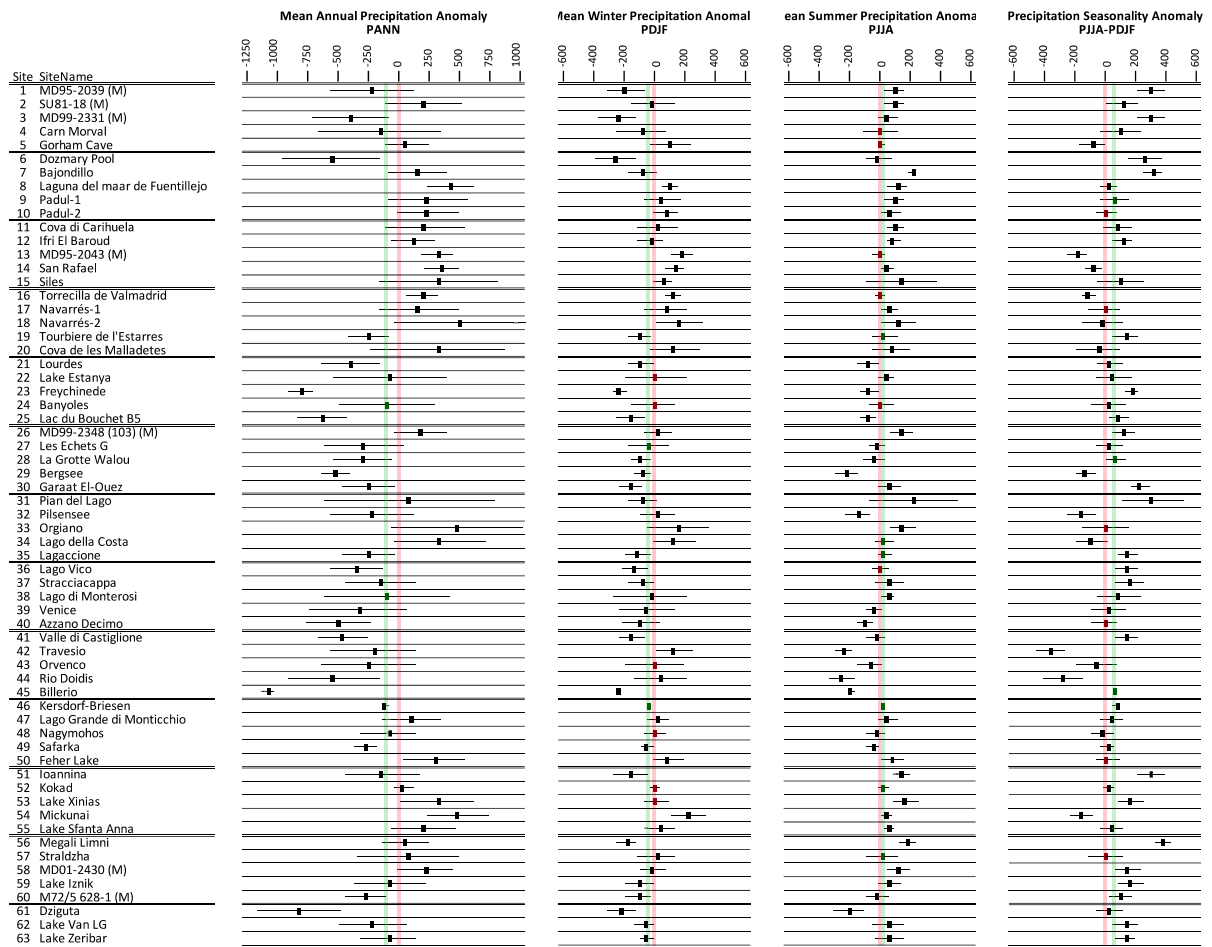
2242





2243
 2244
 2245
 2246
 2247
 2248
 2249
 2250

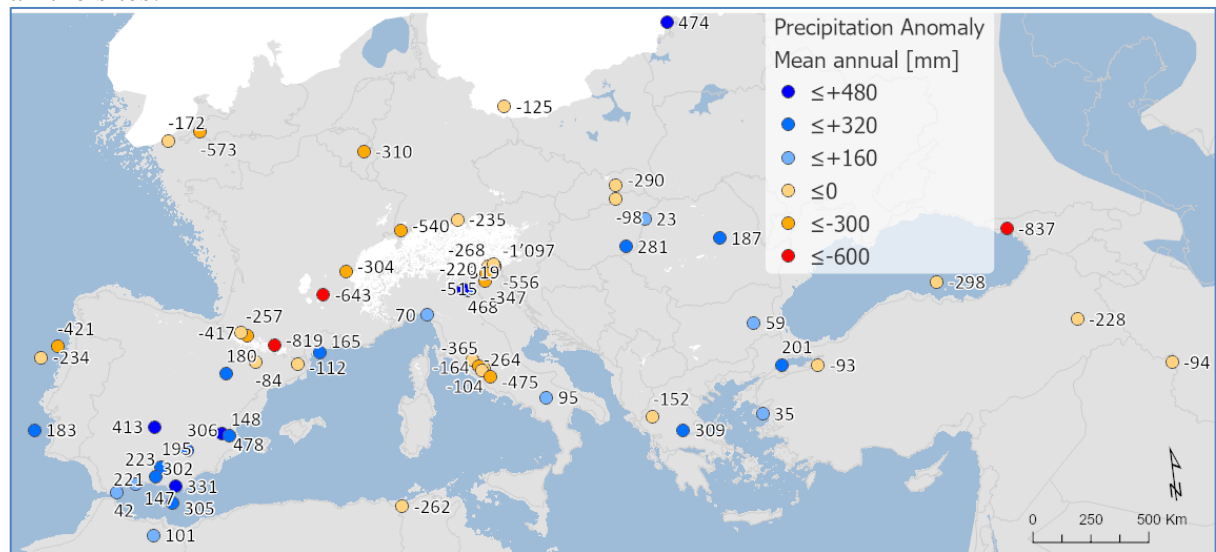
Figure 6. Maps of pollen-based MAT reconstructions for LGM annual, winter and summer temperature anomalies (as shown in figure 9). Continentality represents the difference in temperature between summer and winter, with positive anomalies indicating an increase in the temperature difference between summer and winter. All values are expressed as anomalies compared with the present day.



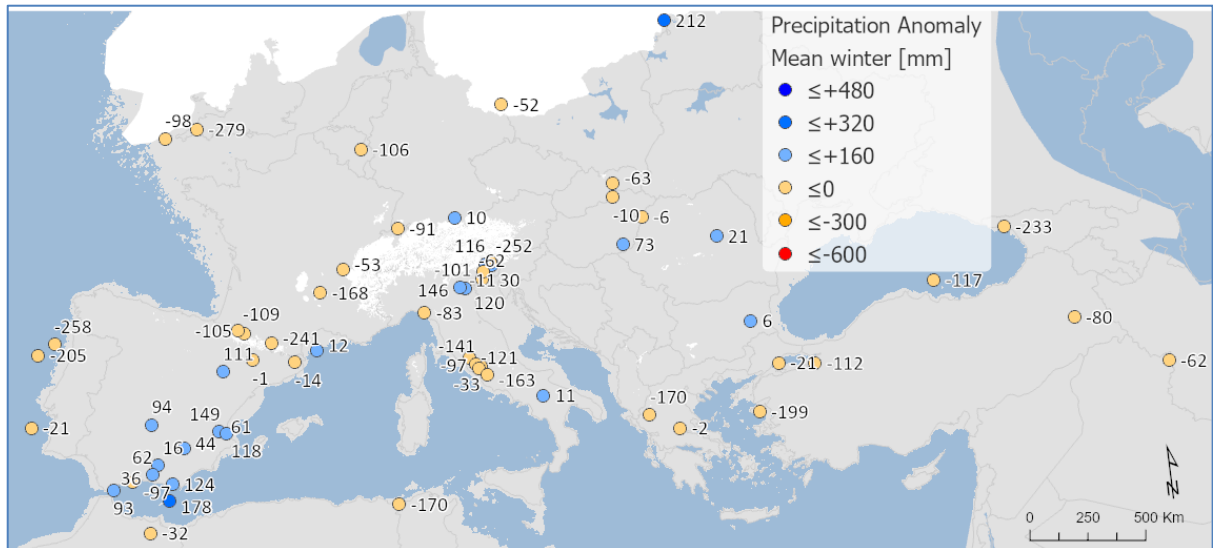
2251
2252
2253
2254
2255
2256
2257
2258
2259

Figure 7. Pollen-based MAT reconstructions for LGM annual, winter and summer precipitation anomalies (uncertainties represent one standard deviation). Seasonality represents the difference in precipitation between summer and winter, with positive anomalies indicating an increase in summer precipitation compared to winter. All values are expressed as anomalies compared with the present day. The green line indicates the mean for all the sites.

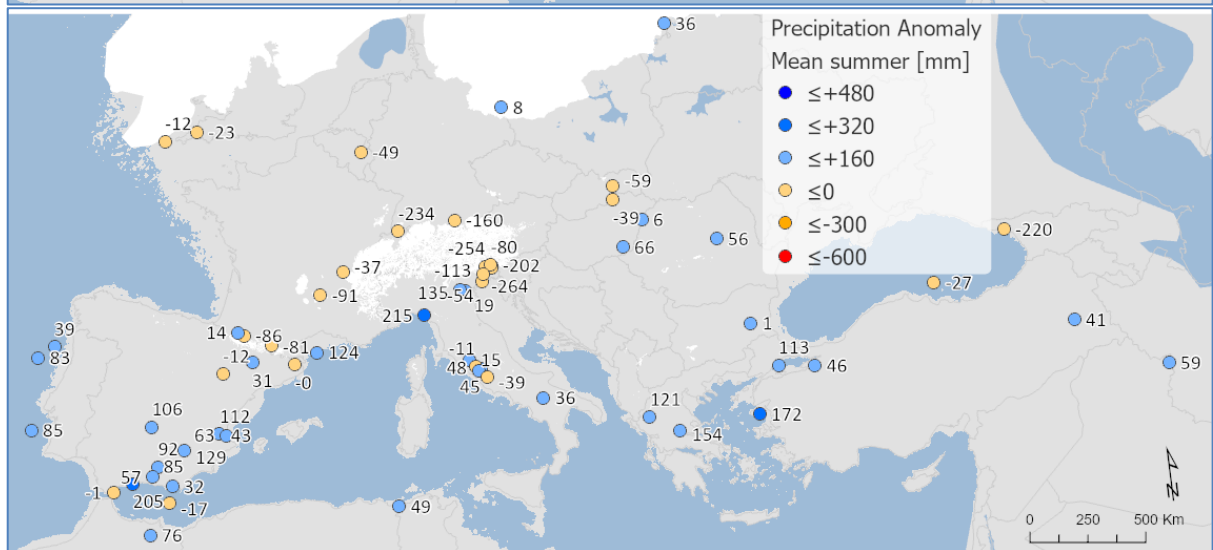
2260



2261



2262



2263

2264

2265

2266

2267

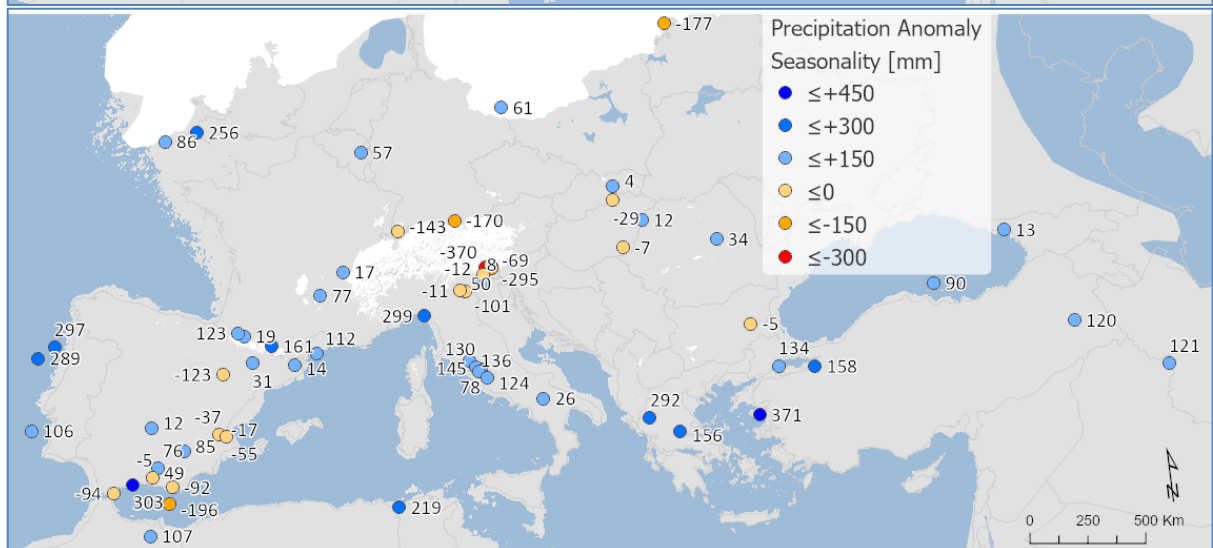
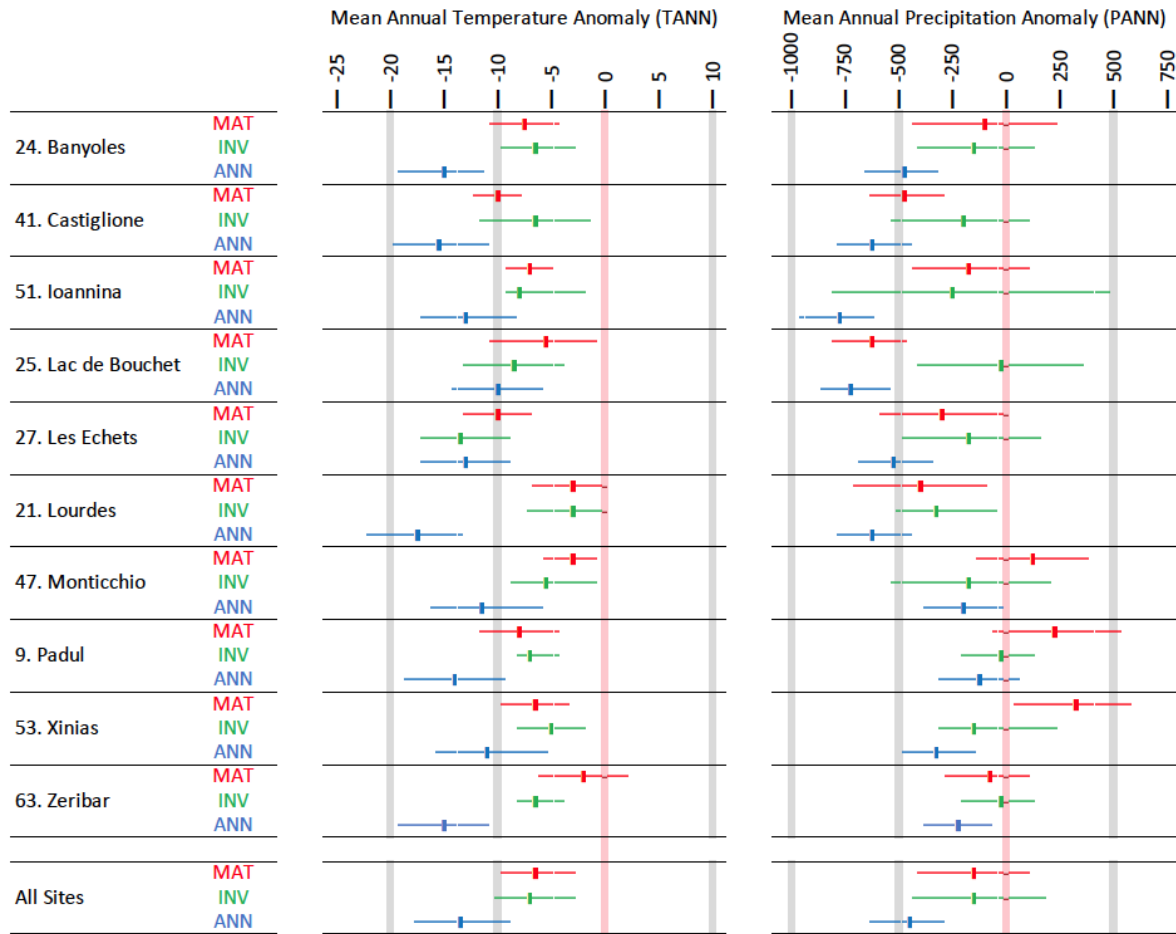


Figure 8. Maps of pollen-based MAT reconstructions for LGM annual, winter and summer precipitation anomalies (as shown in figure 11). Seasonality represents the difference in precipitation between summer and winter, with positive anomalies indicating an increase in

2268 summer precipitation compared to winter. All values are expressed as anomalies compared
2269 with the present day.
2270
2271

2272



2273

2274

2275

2276

2277

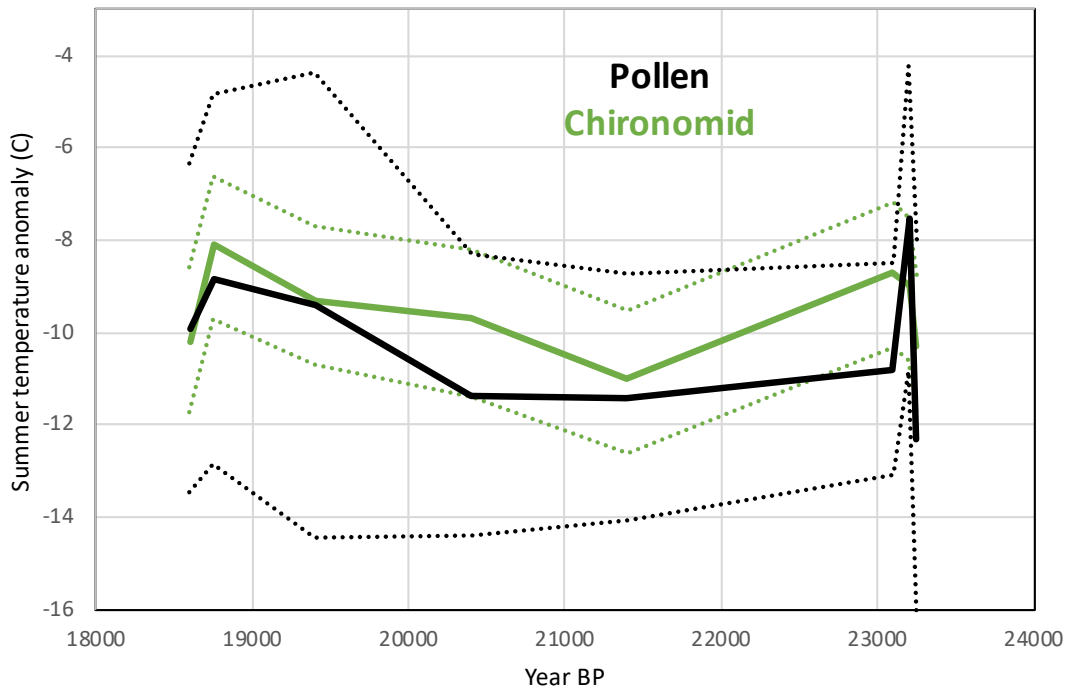
2278

2279

2280

Figure 9. A site-by-site comparison between LGM pollen-climate reconstructions based on Modern Analogue Technique MAT (this study), neural-networks ANN (Peyron et al., 1998), and Inverse Modelling INV (Wu et al., 2007). The results show that MAT and INV give similar climate reconstructions, but ANN is significantly cooler/drier.

2281
2282
2283



2284
2285
2286
2287
2288
2289
2290

Figure 10. Comparison between LGM pollen-climate MAT and chironomid summer temperature reconstructions at Lago della Costa, Italy (chironomid reconstruction and pollen data from Samartin et al., 2016). Dash lines show uncertainties.

2291
2292
2293

Appendix

Site	Site Name	COHMAP Quality	COHMAP													Upper 14C	Upper Cal. BP	Lower 14C	Lower Cal. BP
			< 17k	18k	19k	20k	21k	22k	23k	24k	25k >								
1	MD95-2039 (M)	3C													14830±80	18166±269	19950±210	23883±374	
2	SU81-18 (M)	2C													17510±270	20952±404	21250±280	25420±441	
3	MD99-2331 (M)	2C													16170±130	19325±303	19770±170	23682±336	
4	Carn Morval	4C														18600±3700	21500±890/800	25867±1127	
5	Gorham Cave	4D															18440±160	22055±341	
6	Dozmary Pool	2C													14568±129	17569±523	18325±216	21769±602	
7	Bajondillo	1C														18701±2154			
8	Laguna del maar de Fuentillejo	5D													16540±90	19847±308			
9	Padul-1	3D													18300±300	21821±412	19100±160	22922±308	
10	Padul-2	1D															17450±539	21082±539	
11	Cova di Carihuela	2C													15700±220	18958±280	21430±130	25659±226	
12	Ifri El Baroud	2D													17296±87	20761±293			
13	MD95-2043 (M)	2C													15440±90	18533±294	18260±120	21951±335	
14	San Rafael	3D													9980±60	11464±133	16860±120	20083±292	
15	Siles	2D													17030±80	20345±351			
16	Torreçilla de Valmadrid	2D													17100±85	20456±366			
17	Navarrés-1	4D													18360±195	22001±353	20700±295	24664±411	
18	Navarrés-2	5D													5150±50	5881±85	16000±	19144±	
19	Tourbiere de l'Estarres	1C													17150±250	20522±470	18970±160	22847±317	
20	Cova de les Malladetes	5D													16300±1500	19686±1723			
21	Lourdes	4D													18510±130	22112±130	20025±175	23952±355	
22	Lake Estanya	5D														9498±50		19184±251	
23	Freychinede	3C													14800±800	17912±856	21300±760	25615±1030	
24	Banyoles	2C													19878±100			27862±3000	
25	Lac du Bouchet B5	4C													15350±350	18513±435	19200±300	23006±384	
26	MD99-2348 (103) (M)	1D													17660±60	21065±310	19350±90	23111±271	
27	Les Echets G	1C													17530±270	20970±407	18030±250	21704±473	
28	La Grotte Walou	1D																21200±700	
29	Bergsee	2D															17780±90	21244±306	
30	Garaat El-Ouez	2C													16010±320	19200±801			
31	Pian del Lago	2D																21260±320	
32	Pilsensee	6D													15860±250	19073±290			
33	Orgiano	2D													17760±160	21221±373	19290±520	23141±621	
34	Lago della Costa	2C													15400±150	18484±330	19285±160	23052±302	
35	Lagacione	2C													16080±450	19369±527	20615±940	24746±1201	
36	Lago Vico	3C													14385±140	17541±272	20500±230	24430±376	
37	Stracciaccappa	4C													12060±130	14093±281	19745±820	22675±955	
38	Lago di Monterosi	2D													17040±350	20398±544			
39	Venice	5D															18640±100	22277±336	
40	Azzano Decimo	2D													18000±300	21637±529	21025±245	25179±449	
41	Valle di Castiglione	3C													14220±145	17443±270	20300±700	24266±842	
42	Travesio	5D															18780±200	22483±406	
43	Orvenco	2D													17760±160	21221±373	19290±520	23141±621	
44	Rio Doidis	5D															18860±190	22390±373	
45	Billerio	3D															18165±200	21872±382	
46	Kersdorf-Briesen	1D															17622±94	21183±356	
47	Lago Grande di Monticchio	2C														20204±		24014±	
48	Nagymohos	2C													14246±144	17361±425	18159±247	21735±622	
49	Safarka	3D															18287±1512	21912±1781	
50	Feher Lake	1D													17715±250	21190±463	19911±81	23841±313	
51	Ioannina	3C													15330±140	18420±312	20760±230	24748±330	
52	Kokad	5D													14326±63	17433±443	16280±90	19685±538	
53	Lake Xinias	6C													11150±130	13049±160	21390±430	25671±648	
54	Mickunai	1D														21000±2200			
55	Lake Sfanta Anna	1D													17626±96	20955±432			
56	Megali Limni	6D													19072±237	22906±340			
57	Straldzha	6C													14696±65	18022±364	23653±114	28580±390	
58	MD01-2430 (M)	4C													12050±75	14904±324	18310±380	21746±968	
59	Lake Iznik	7D													16910±100	19515±115			
60	M72/5 628-1 (M)	2C													16835±85	18490±	19495±90	21280±	
61	Dziguta	4C													12990±160	15839±483	20560±880	24666±1126	
62	Lake Van LG	2C														18590±62		23290±596	
63	Lake Zeribar	4C													13650±160	16610±399	22000±500	26462±880	

COHMAP chronological quality classification:
 1C: Bracketing dates within 2000 14C (2360 Cal.) yr interval about the time being assessed
 2C: Bracketing dates, one within 2000 14C (2360 Cal.) yr and the second within 4000 14C (4682 Cal.) yr of the time being assessed
 3C: Bracketing dates within 4000 14C (4682 Cal.) yr interval about the time being assessed
 4C: Bracketing dates, one being within 4000 14C (4682 Cal.) yr and the second being within 6000 14C (7490 Cal.) yr of the time being assessed
 5C: Bracketing dates within 6000 14C (7490 Cal.) yr interval about the time being assessed
 6C: Bracketing dates, one within 6000 14C (7490 Cal.) yr and the second within 8000 14C (9681 Cal.) yr of the time being assessed
 7C: Poorly dated
 1D: Date within 250 14C (206 Cal.) yr of the time being assessed
 2D: Date within 500 14C (684 Cal.) yr of the time being assessed
 3D: Date within 750 14C (975 Cal.) yr of the time being assessed
 4D: Date within 1000 14C (1123 Cal.) yr of the time being assessed
 5D: Date within 1500 14C (1881 Cal.) yr of the time being assessed
 6D: Date within 2000 14C (2360 Cal.) yr of the time being assessed
 7D: Poorly dated

2294
2295
2296
2297
2298
2299
2300
2301
2302
2303
2304
2305
2306
2307
2308
2309
2310
2311
2312
2313

Table A1. Chronological control

2314
2315

Site Number	Site Name	Site Type	TANN	TDJF	TJJA	PANN	PDJF	PJJA
1	MD95-2039 (M)	Marine	15.7	10.7	20.8	1047	427	70
2	SU81-18 (M)	Marine	20.8	15.3	26.5	629	282	25
3	MD99-2331 (M)	Marine	14.6	9.8	19.4	1239	507	88
4	Carn Morval	Lake	12.5	8.7	16.9	1183	392	206
5	Gorham Cave	Cave	18.3	13.4	23.7	740	336	25
6	Dozmary Pool	Lake	10.3	6.0	15.2	1271	422	236
7	Bajondillo	Cave	16.6	10.5	23.4	542	223	27
8	Laguna del maar de Fuentillejo	Lake	16.1	8.1	25.4	474	156	47
9	Padul-1	Peat Bog	16.6	9.6	24.9	417	157	23
10	Padul-2	Peat Bog	16.6	9.6	24.9	417	157	23
11	Cova di Carihuela	Cave	15.7	8.1	25.1	551	187	57
12	Ifri El Baroud	Cave	16.9	10.7	24.0	457	184	22
13	MD95-2043 (M)	Marine	17.9	12.4	24.0	214.2	37	72
14	San Rafael	Peat Bog	18.1	11.9	24.9	243	87	14
15	Siles	Lake	14.4	6.8	23.4	658	195	92
16	Torrecilla de Valmadrid	Colluvium	14.2	6.6	22.5	390	75	82
17	Navarrés-1	Peat Bog	17.0	10.9	23.8	421	96	51
18	Navarrés-2	Peat Bog	17.0	10.9	23.8	421	96	51
19	Tourbiere de l'Estalles	Lake	13.0	6.1	20.4	1045	272	217
20	Cova de les Malladetes	Cave	18.1	12.1	24.8	478	117	60
21	Lourdes	Lake	12.6	5.5	20.1	1002	256	212
22	Lake Estanya	Lake	12.8	5.1	21.0	641	125	152
23	Freychinede	Lake	10.8	3.9	19.0	1128	257	277
24	Banyoles	Lake	14.3	7.7	21.9	698	157	139
25	Lac du Bouchet B5	Lake	8.2	1.3	15.9	1070	251	221
26	MD99-2348 (103) (M)	Marine	14.6	8.0	21.9	618	158	95
27	Les Echets G	Peat Bog	11.4	3.6	19.6	876	175	215
28	La Grotte Walou	Cave	10.3	3.2	17.0	903	215	249
29	Bergsee	Lake	9.6	1.4	17.6	1048	189	387
30	Garaat El-Ouez	Peat Bog	17.3	11.0	24.3	830	360	33
31	Pian del Lago	Lake	12.4	5.1	20.0	995	266	149
32	Pilsensee	Lake	9.3	0.6	17.7	947	151	374
33	Orgiano	Peat Bog	13.0	3.3	22.3	907	200	228
34	Lago della Costa	Lake	12.9	3.3	22.1	888	196	224
35	Lagaccione	Lake	14.2	7.2	21.7	705	203	109
36	Lago Vico	Lake	13.7	6.4	21.5	870	258	132
37	Stracciaccappa	Lake	14.6	7.3	22.4	867	266	115
38	Lago di Monterosi	Lake	15.0	7.7	22.9	837	248	115
39	Venice	Peat Bog	13.4	4.5	22.1	1050	221	277
40	Azzano Decimo	Alluvial Fan	13.3	4.4	22.1	1170	241	311
41	Valle di Castiglione	Lake	16.3	9.1	24.0	988	294	144
42	Travesio	Lake	12.6	3.7	21.3	1415	281	375
43	Orvenco	Alluvial Fan	13.0	3.3	22.3	907	200	228
44	Rio Doidis	Lake	12.8	4.1	21.2	1529	315	392
45	Billerio	Lake	12.8	4.1	21.2	1529	315	392
46	Kersdorf-Briesen	Lake	8.8	-1.0	17.9	538	110	175
47	Lago Grande di Monticchio	Lake	11.5	4.1	19.8	518	154	76
48	Nagymohos	Peat Bog	9.5	-1.5	19.1	616	103	230
49	Safarka	Peat Bog	7.0	-3.2	16.0	755	119	280
50	Feher Lake	Lake	11.0	-0.1	20.7	546	112	185
51	Ioannina	Peat Bog	14.7	6.5	23.3	1000	364	98
52	Kokad	Peat Bog	10.2	-0.9	19.8	601	130	204
53	Lake Xiniás	Lake	15.6	7.5	24.1	563	211	47
54	Mickunai	Lake	6.0	-5.0	16.3	682	131	230
55	Lake Sfanta Anna	Lake	11.6	5.2	18.4	867	253	172
56	Megali Limni	Lake	15.5	8.2	23.4	684	357	28
57	Straldzha	Peat Bog	12.5	2.6	21.8	591	158	135
58	MD01-2430 (M)	Marine	18.0	8.7	27.5	595	219	75
59	Lake Iznik	Lake	13.9	6.1	21.8	677	250	85
60	M72/5 628-1 (M)	Marine	14.5	8.0	21.6	857	251	156
61	Dziguta	Peat Bog	14.1	6.6	21.7	1549	409	373
62	Lake Van LG	Lake	12.0	0.9	23.1	635	201	34
63	Lake Zeribar	Lake	17.1	5.0	29.0	427	167	6

2316
2317
2318
2319
2320

Table A2. Modern climate values for each site used in the calculation of anomalies (taken from WorldClim 2, Fick & Hijmans 2017)

2321
2322
2323

Biome	Change in Biome compared to the Control								
	Control	0 Pinaceae	+5% Pinaceae	+10% Pinaceae	+20% Pinaceae	+50% Pinaceae	+100% Pinaceae	+200% Pinaceae	+400% Pinaceae
CLDE	25	454	0	0	0	-1	-1	-4	-4
TAIG	1489	-1430	16	38	74	192	337	554	914
CLMX	70	108	1	2	3	-6	-4	4	6
COCO	388	-388	0	-1	3	6	25	50	74
TEDE	33	16	1	1	1	-1	-2	-8	-5
COMX	2952	-761	1	8	14	-4	-42	-101	-284
WAMX	418	-28	-1	0	-1	-6	-11	-29	-62
XERO	699	-323	3	4	12	45	68	113	180
DESE	0	0	0	0	0	0	0	0	0
STEP	1752	1388	-14	-39	-83	-173	-296	-468	-663
TUND	387	964	-7	-13	-23	-52	-74	-111	-156
Total	8213	5860	44	106	214	486	860	1442	2348

2324
2325

2326

2327

2328

2329

2330

2331

2332

2333

2334

2335

2336

2337

2338

2339

2340

2341

2342

2343

2344

Table A3. This shows the results of experiment to test the sensitivity of pollen Biomes to changes in the amount of Pinaceae in the pollen assemblage using 8213 modern pollen samples from the EMPD2. Pinaceae can be over-represented in marine samples, and it has been proposed that removing all Pinaceae from these samples is better than leaving the Pinaceae in the pollen assemblage. The 'Control' column on the left shows the number of samples that were classified for each Biome without changing the amount of Pinaceae (ie using the original pollen assemblage). The other 8 columns to the right show the number of samples where the Biome changed relative to the number shown in the control column as a result of either removal of all Pinaceae ('0 Pinaceae'), or by artificially increasing the amount of Pinaceae respectively from 5 to 400% of the original count ('+5% Pinaceae' to '+400% Pinaceae'). For instance, for the CLDE (Cold Deciduous) Biome, 25 pollen samples were classified as CLDE without any change in Pinaceae ('Control'), but 454 more samples were classified as CLDE when all Pinaceae was removed ('0 Pinaceae') compared to 4 fewer samples that were classified as CLDE when Pinaceae was increased by as much as 400% ('+400% Pinaceae'). The totals along the bottom show that out of the 8213 pollen samples included in the experiment, 5860 biomes changed when all Pinaceae was removed, compared to up to 2348 when Pinaceae was artificially increased by up to 400%.

2345

Temperature Anomlay

Site Name	Site Number	TANN delta		TDJF delta		TJJA delta		PANN delta		PDJF delta		PJJA delta	
		Pinaceae	No Pinaceae	Pinaceae	No Pinaceae	Pinaceae	No Pinaceae	Pinaceae	No Pinaceae	Pinaceae	No Pinaceae	Pinaceae	No Pinaceae
MD95-2039 (M)	1	-10.5	-12.3	-14.6	-17.9	-5.7	-5.9	-234.3	-236.3	-205.4	-196.4	83.1	63.0
SU81-18 (M)	2	-13.3	-21.4	-15.2	-23.0	-10.4	-17.7	183.3	703.2	-21.1	124.4	85.1	167.7
MD99-2331 (M)	3	-5.3	-4.8	-7.5	-7.0	-2.3	-1.4	-420.6	-435.6	-257.7	-251.1	39.4	19.0
MD95-2043 (M)	13	-7.0	-6.0	-11.0	-9.9	-3.6	-2.7	304.6	332.5	178.4	201.9	-17.3	-22.9
MD99-2348 (103) (M)	26	-7.8	-8.8	-10.0	-11.5	-6.5	-7.3	164.7	218.0	12.1	7.6	124.0	179.5
MD01-2430 (M)	58	-11.1	-13.5	-11.3	-14.5	-11.0	-12.8	200.6	349.1	-20.8	31.4	113.1	127.9
M72/5 628-1 (M)	60	-2.3	-0.5	-4.9	-3.0	-0.2	1.7	-298.0	-311.1	-116.8	-100.1	-27.0	-51.7
Site Average		-8.2	-9.6	-10.6	-12.4	-5.7	-6.6	-14.2	88.5	-61.6	-26.0	57.2	68.9

Standard Deviation

Site Name	Site Number	TANN STDEV		TDJF STDEV		TJJA STDEV		PANN STDEV		PDJF STDEV		PJJA STDEV	
		Pinaceae	No Pinaceae	Pinaceae	No Pinaceae	Pinaceae	No Pinaceae	Pinaceae	No Pinaceae	Pinaceae	No Pinaceae	Pinaceae	No Pinaceae
MD95-2039 (M)	1	4.6	3.7	7.5	4.0	2.9	4.0	330.6	268.9	110.5	96.7	53.6	55.6
SU81-18 (M)	2	3.1	4.0	4.0	3.4	2.8	4.8	297.1	149.3	126.6	58.0	47.3	28.4
MD99-2331 (M)	3	2.9	4.0	3.4	3.8	2.8	5.0	302.6	368.6	103.5	134.2	57.6	64.3
MD95-2043 (M)	13	2.0	4.7	2.4	5.6	2.1	4.1	115.9	121.5	59.3	72.1	36.2	25.2
MD99-2348 (103) (M)	26	2.4	3.8	3.0	4.2	2.7	4.6	192.7	242.9	75.8	68.2	58.9	52.1
MD01-2430 (M)	58	5.1	2.3	8.1	2.0	3.9	2.8	218.7	182.8	78.9	58.3	53.4	45.0
M72/5 628-1 (M)	60	3.2	3.9	3.8	4.0	3.5	4.6	149.0	171.9	67.1	48.2	56.5	61.8
Site Average		3.3	3.8	4.6	3.9	3.0	4.3	229.5	215.1	88.8	76.5	51.9	47.5

2346
2347
2348
2349
2350
2351
2352
2353
2354
2355
2356
2357
2358
2359

Table A4. A comparison of the LGM reconstructed climate for marine sites showing the effect of excluding Pinaceae (shaded) from the pollen assemblage, compared to the results of including Pinaceae (unshaded, also presented in Figures 6-8). It has been proposed that because of the potential for over-representation of Pinaceae in marine pollen samples, it is better to exclude Pinaceae completely from marine pollen samples. Comparing the two approaches, temperatures are generally 1-2C cooler, and precipitation slightly higher when Pinaceae is excluded. The differences for both temperature and precipitation are significantly less than the standard deviation of their uncertainties.

	All surface samples		Steppe only	
	RMSE	R2	RMSE	R2
TANN	2.28	0.9	2.51	0.87
TDJF	3.35	0.91	3.26	0.88
TJJA	2.21	0.81	2.49	0.82
PANN	224.94	0.69	185.7	0.71
PDJF	78.51	0.69	66.5	0.66
PJJA	52.49	0.75	43.8	0.79

2360
2361
2362
2363
2364
2365
2366
2367
2368
2369
2370

Table A5. A comparison of MAT performance statistics based on the modern pollen sample training set using all surface samples from the EMPD2 used in the LGM reconstruction (as shown in Table 3), and a subset of 1588 samples from the EMPD2 that were classified as steppe. The results show little difference between the two different types of samples. The table includes Mean Annual Temperature and Precipitation (TANN and PANN), Mean Winter Temperature and Precipitation (TDJF and PDJF) and Mean Summer Temperature and Precipitation (TJJA and PJJA).

Site Name	Site#	Pollen Biome	Modern Analogue Biome	Modern Analogue Ecoregion
MD95-2039	1	XERO	Mediterranean Forests, woodlands and scrubs	Iberian conifer forests
SU81-18	2	COMX	Mediterranean Forests, woodlands and scrubs	Iberian conifer forests
MD99-2331	3	STEP	Mediterranean Forests, woodlands and scrubs	Alps conifer and mixed forests
Carn Morval	4	STEP	Temperate broadleaf and mixed forests	North Atlantic moist mixed forests
Gorham Cave	5	STEP	Mediterranean Forests, woodlands and scrubs	Cyprus Mediterranean forests
Dozmary Pool	6	STEP	Temperate Coniferous Forest	Alps conifer and mixed forests
Bajondillo	7	STEP	Temperate broadleaf and mixed forests	Central European mixed forests
Laguna del maar de Fuentillejo	8	COMX	Mediterranean Forests, woodlands and scrubs	Northwest Iberian montane forests
Padul	9	STEP	Mediterranean Forests, woodlands and scrubs	Central Anatolian steppe
Padul-15-05	10	WAMX	Mediterranean Forests, woodlands and scrubs	Iberian sclerophyllous and semi-deciduous forests
Cova di Carhuela	11	STEP	Deserts and xeric shrublands	Azerbaijan shrub desert and steppe
Ifri El Baroud	12	STEP	Mediterranean Forests, woodlands and scrubs	Iberian sclerophyllous and semi-deciduous forests
MD95-2043	13	CLMX	Mediterranean Forests, woodlands and scrubs	Southern Anatolian montane conifer and deciduous forests
San Rafael	14	XERO	Mediterranean Forests, woodlands and scrubs	Tyrrhenian-Adriatic Sclerophyllous and mixed forests
Siles	15	XERO	Mediterranean Forests, woodlands and scrubs	Northwest Iberian montane forests
Torreçilla de Valmadrid	16	STEP	Mediterranean Forests, woodlands and scrubs	Southern Anatolian montane conifer and deciduous forests
Navarres	17	XERO	Mediterranean Forests, woodlands and scrubs	Iberian sclerophyllous and semi-deciduous forests
Navarres	18	STEP	Temperate broadleaf and mixed forests	Pyrenees conifer and mixed forests
Tourbiere de IEstarres	19	STEP	Temperate grasslands, savannas and shrublands	Eastern Anatolian montane steppe
Cova de les Malladetes	20	XERO	Mediterranean Forests, woodlands and scrubs	Pyrenees conifer and mixed forests
Lourdes	21	STEP	Temperate broadleaf and mixed forests	Gissaro-Alai open woodlands
Estanya	22	XERO	Temperate broadleaf and mixed forests	Western Siberian hemiboreal forests
Freychinede	23	STEP	Temperate grasslands, savannas and shrublands	Mongolian-Manchurian grassland
Lake Banyoles	24	STEP	Temperate grasslands, savannas and shrublands	Gissaro-Alai open woodlands
Lac du Bouchet B5	25	STEP	Temperate grasslands, savannas and shrublands	Gissaro-Alai open woodlands
MD99-2348-103	26	COMX	Temperate broadleaf and mixed forests	Rodope montane mixed forests
Les Echets G - DIGI	27	STEP	Temperate broadleaf and mixed forests	Western Siberian hemiboreal forests
La Grotte Walou	28	STEP	Temperate broadleaf and mixed forests	Kazakh forest steppe
Bergsee	29	STEP	Temperate broadleaf and mixed forests	Kazakh forest steppe
Garaat El-Ouez	30	STEP	Mediterranean Forests, woodlands and scrubs	Anatolian conifer and deciduous mixed forests
Pian del Lago	31	COMX	Temperate broadleaf and mixed forests	Western European broadleaf forests
Pilsensee	32	TAIG	Tundra	Kola Peninsula tundra
Orgiano	33	COMX	Temperate broadleaf and mixed forests	Western European broadleaf forests
Lago della Costa	34	COMX	Temperate Coniferous Forest	Alps conifer and mixed forests
Lagaccione	35	STEP	Temperate grasslands, savannas and shrublands	Gissaro-Alai open woodlands
Lago Vico	36	STEP	Temperate grasslands, savannas and shrublands	Gissaro-Alai open woodlands
Stracciaccappa	37	STEP	Mediterranean Forests, woodlands and scrubs	Western European broadleaf forests
Lago di Monterosi	38	STEP	Temperate grasslands, savannas and shrublands	Northwest Iberian montane forests
Venice	39	XERO	Tundra	Scandinavian Montane Birch forest and grasslands
Azzano Decimo	40	XERO	Temperate broadleaf and mixed forests	Scandinavian Montane Birch forest and grasslands
Valle di Castiglione	41	STEP	Temperate broadleaf and mixed forests	Tian Shan montane steppe and meadows
Travesio	42	XERO	Mediterranean Forests, woodlands and scrubs	Iberian conifer forests
Orvenco	43	TAIG	Temperate broadleaf and mixed forests	Western Siberian hemiboreal forests
Rio Doidis	44	XERO	Mediterranean Forests, woodlands and scrubs	Cyprus Mediterranean forests
Billerio	45	TAIG	Temperate broadleaf and mixed forests	Western Siberian hemiboreal forests
Kersdorf-Briesen	46	TAIG	Temperate broadleaf and mixed forests	Western Siberian hemiboreal forests
Lago Grande di Monticchio	47	STEP	Temperate broadleaf and mixed forests	Tian Shan montane steppe and meadows
Nagymohos Pleistocene	48	STEP	Tundra	Sarmatic mixed forests
Safarka	49	TAIG	Boreal forests / Taiga	Ural montane forests and tundra
Fehertó	50	COMX	Temperate Coniferous Forest	Alps conifer and mixed forests
Ioannina	51	STEP	Temperate broadleaf and mixed forests	Central European mixed forests
Kokad	52	STEP	Temperate broadleaf and mixed forests	East European forest steppe
Lake Xiniás	53	STEP	Temperate broadleaf and mixed forests	Western European broadleaf forests
Mickunai	54	COCO	Tundra	Scandinavian Montane Birch forest and grasslands
Lake Sfanta Anna	55	COMX	Temperate Coniferous Forest	Alps conifer and mixed forests
Lesvos ML01 Megali Limni	56	STEP	Temperate broadleaf and mixed forests	Rodope montane mixed forests
Straldzha	57	STEP	Temperate broadleaf and mixed forests	Aegean and Western Turkey sclerophyllous and mixed forests
MD01-2430	58	STEP	Temperate broadleaf and mixed forests	Euxine-Colchic broadleaf forests
Lake Iznik	59	STEP	Temperate broadleaf and mixed forests	Tian Shan montane steppe and meadows
M72/5 628-1	60	STEP	Deserts and xeric shrublands	Azerbaijan shrub desert and steppe
Dziguta Core 1	61	CLMX	Temperate broadleaf and mixed forests	Northeastern Spain and Southern France Mediterranean forests
Lake Van LG	62	STEP	Mediterranean Forests, woodlands and scrubs	Aegean and Western Turkey sclerophyllous and mixed forests
Lake Zeribar	63	STEP	Temperate grasslands, savannas and shrublands	Pontic steppe

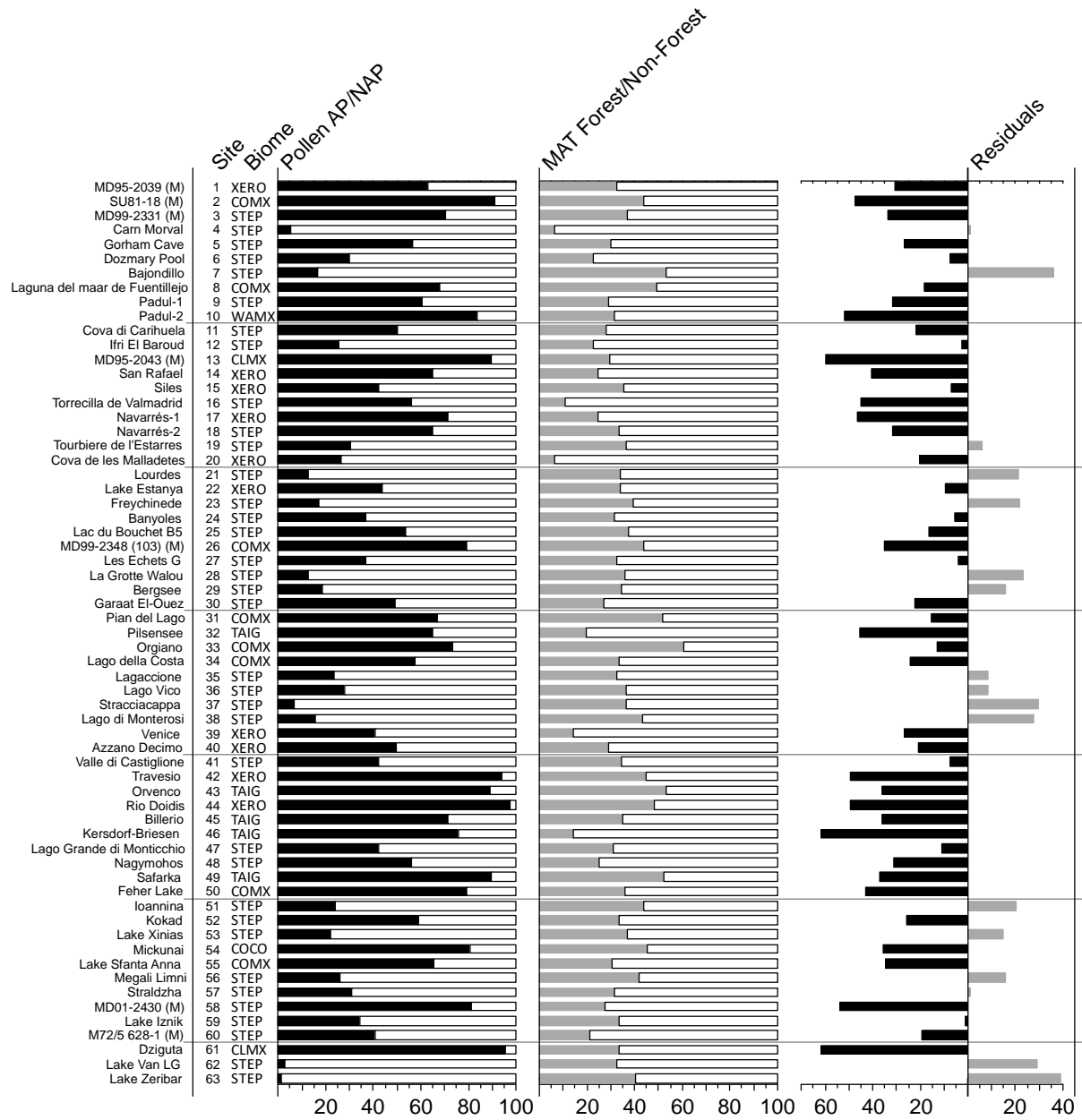
Notes: Modern analogue Biomes and Ecoregions were calculated as the most commonly occurring amongst all 6 best modern analogue pollen samples in all LGM samples for each pollen site/record. These are taken from the EMPD2 (Davis et al 2020), using the classification of Olsen et al 2001.

2371
2372
2373
2374
2375
2376
2377
2378

Table A6. The biome and ecoregion of the modern surface samples used as analogues in the pollen-climate reconstructions.

2379
 2380
 2381
 2382
 2383

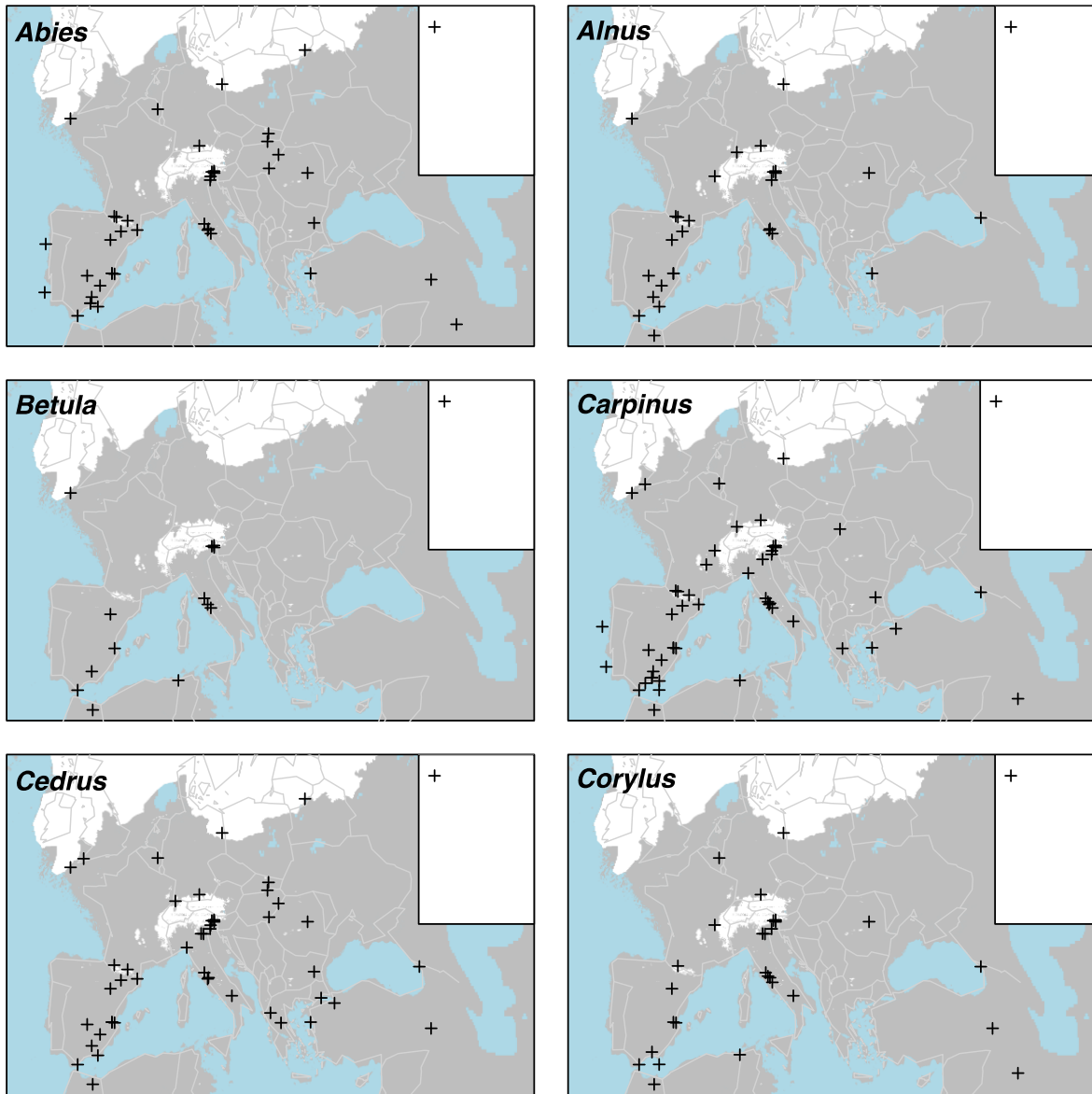
Figures



2384
 2385
 2386
 2387
 2388

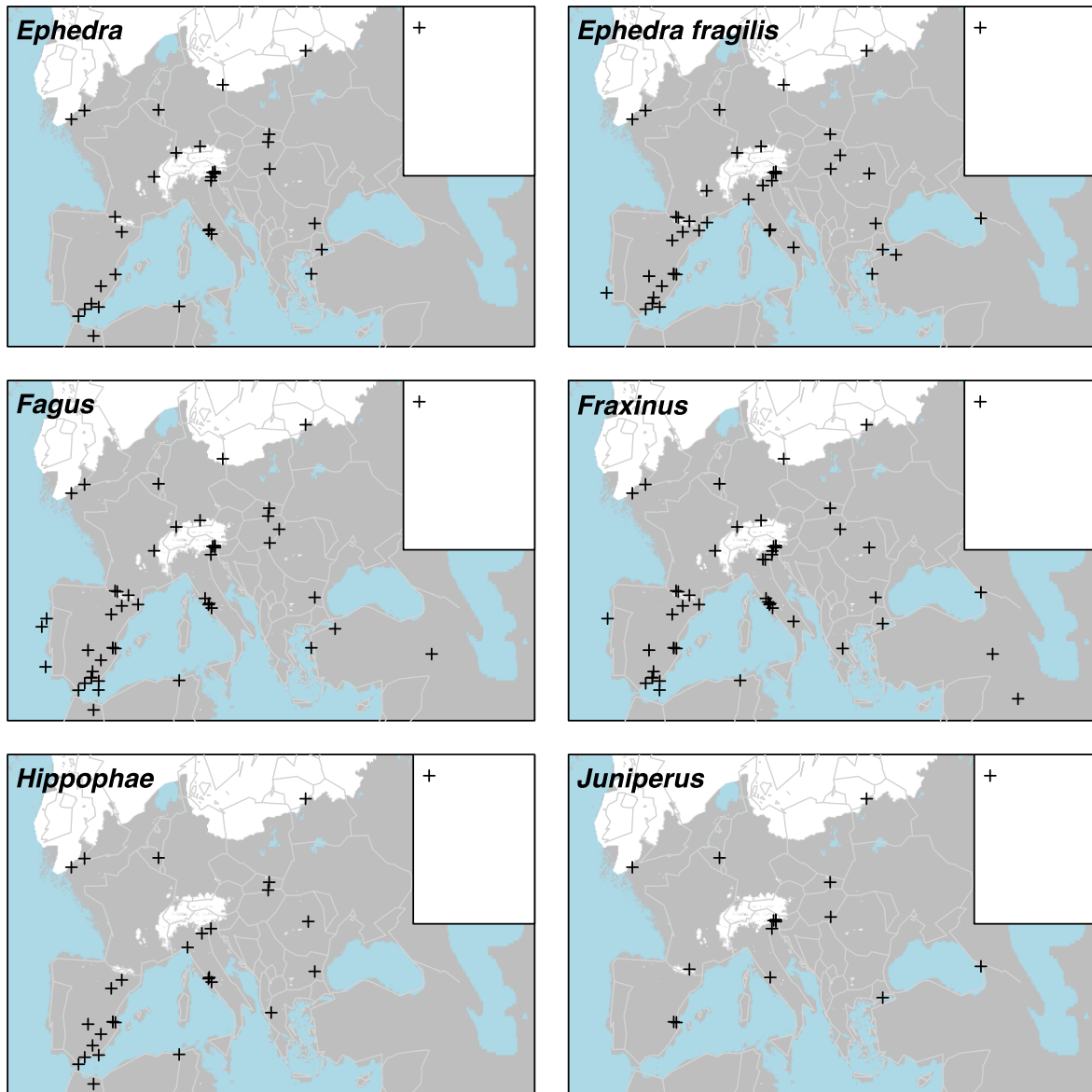
Figure A1. Pollen biomes (see figure 2 for key), Arboreal Pollen (AP) % forest cover, MAT % forest cover and residuals (AP % compared to MAT Forest %)

2391
2392
2393
2394



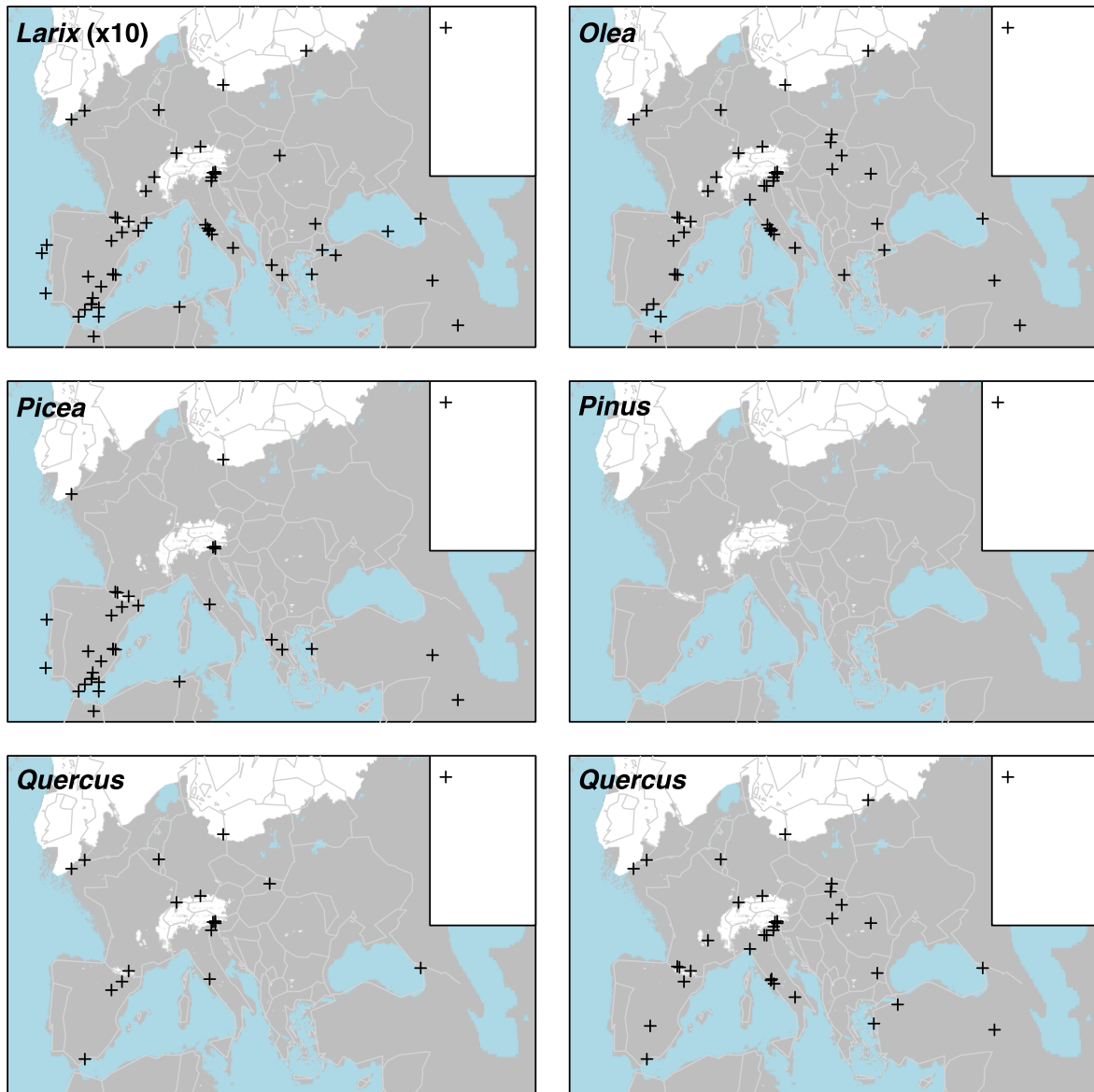
2395
2396
2397
2398

Figure A3. Percentage maps of *Abies*, *Alnus*, *Betula*, *CarPinus*, *Cedrus* and *Corylus*



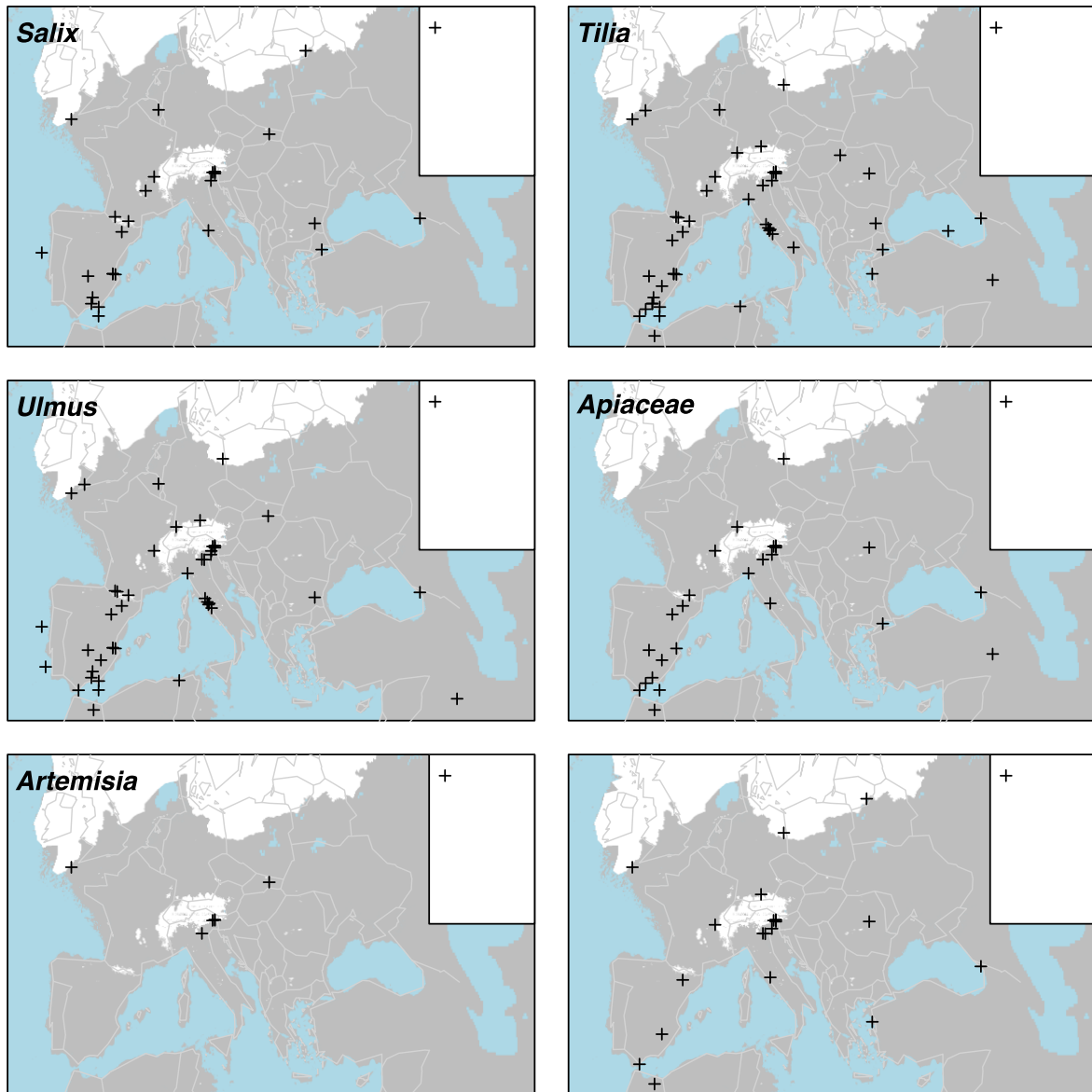
2399
 2400
 2401
 2402
 2403

Figure A4. Percentage maps of *Ephedra*, *Ephedra fragilis*, *Fagus*, *Fraxinus*, *Hippophae* and *Juniperus*



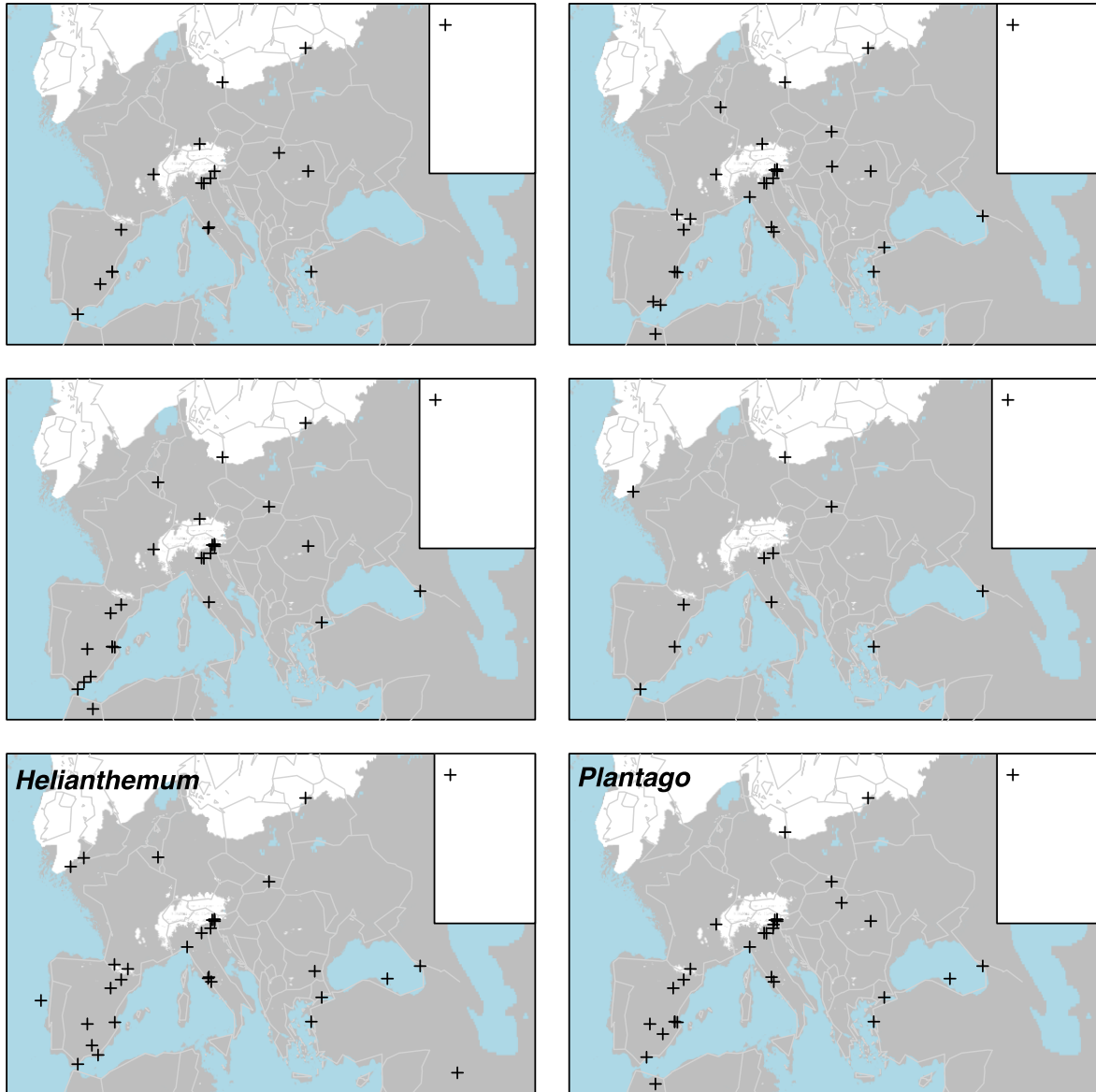
2404
 2405
 2406
 2407
 2408

Figure A5. Percentage maps of *Larix* (x10 exaggeration), *Olea*, *Picea*, *Pinus*, *Quercus* (deciduous) and *Quercus* (evergreen)



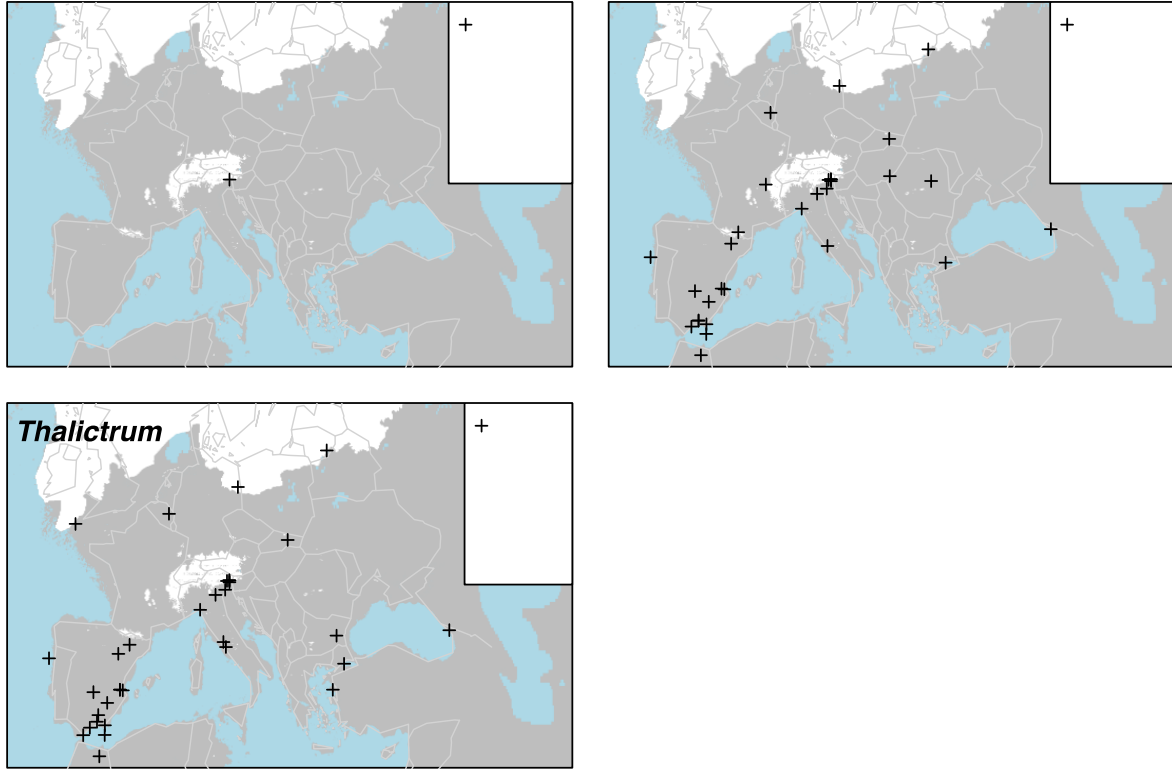
2409
 2410
 2411
 2412

Figure A6. Percentage maps of *Salix*, *Tilia*, *Ulmus*, *Apiaceae*, *Artemisia* and *Asteraceae* (Asteroideae)



2413
 2414
 2415
 2416
 2417

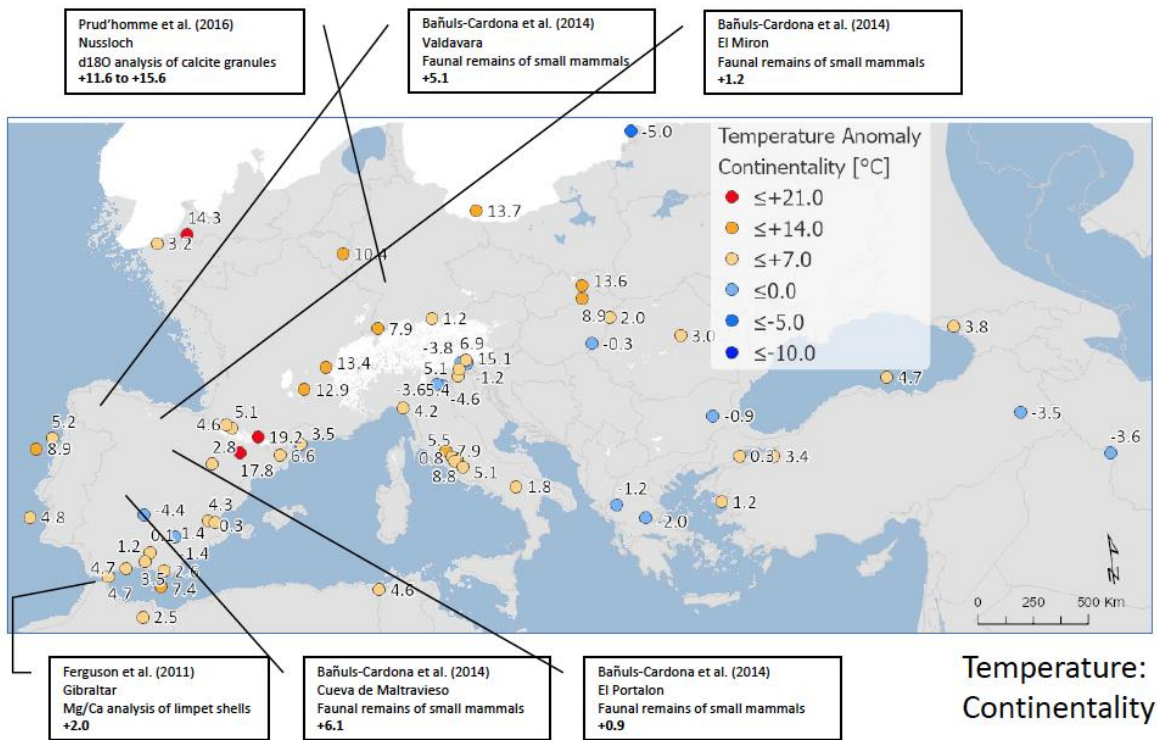
Figure A7. Percentage maps of Asteraceae (Cichorioideae), Brassicaceae, Caryophyllaceae, Chenopodiaceae, *Helianthemum* and *Plantago*



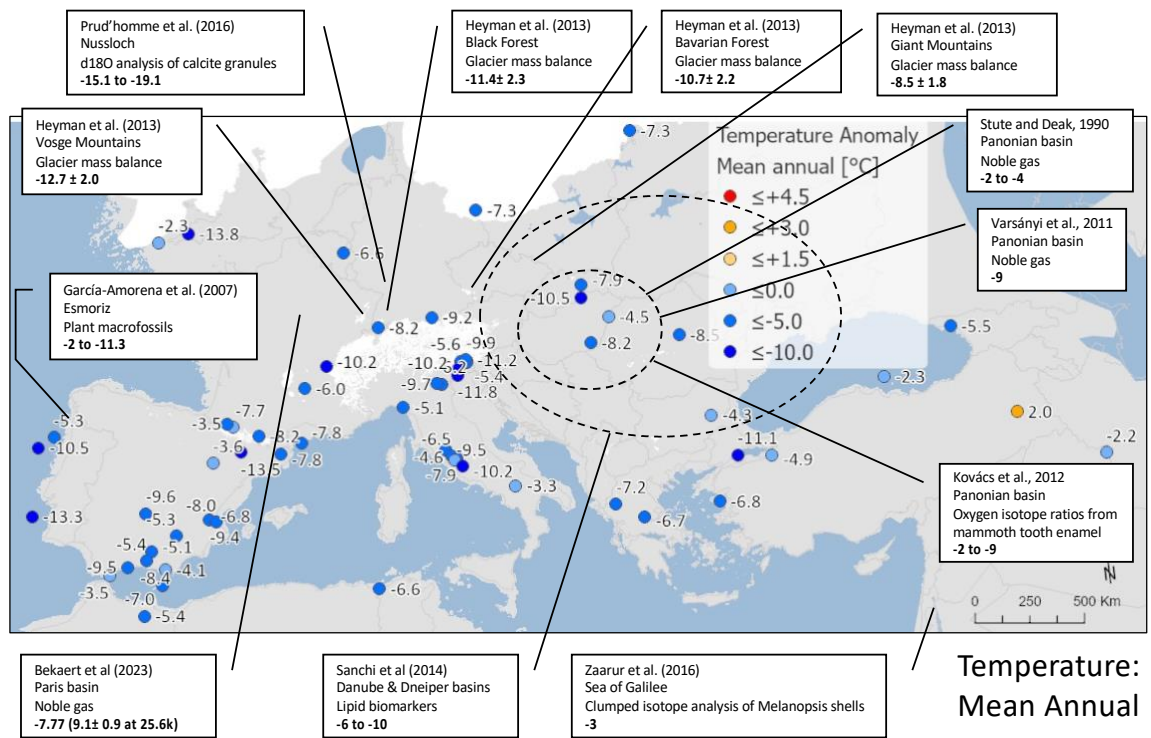
2418
 2419
 2420
 2421
 2422
 2423
 2424
 2425
 2426

Figure A8. Percentage maps of Poaceae, Rubiaceae and *Thalictrum*

2427



2428

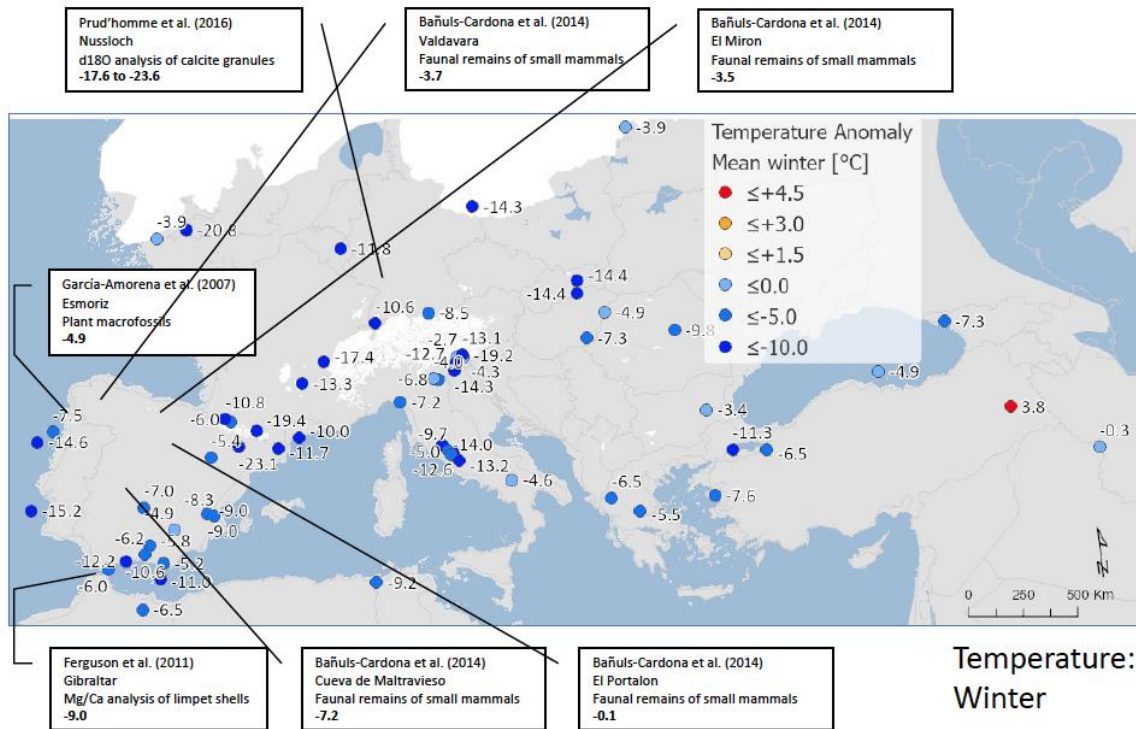


2429

2430

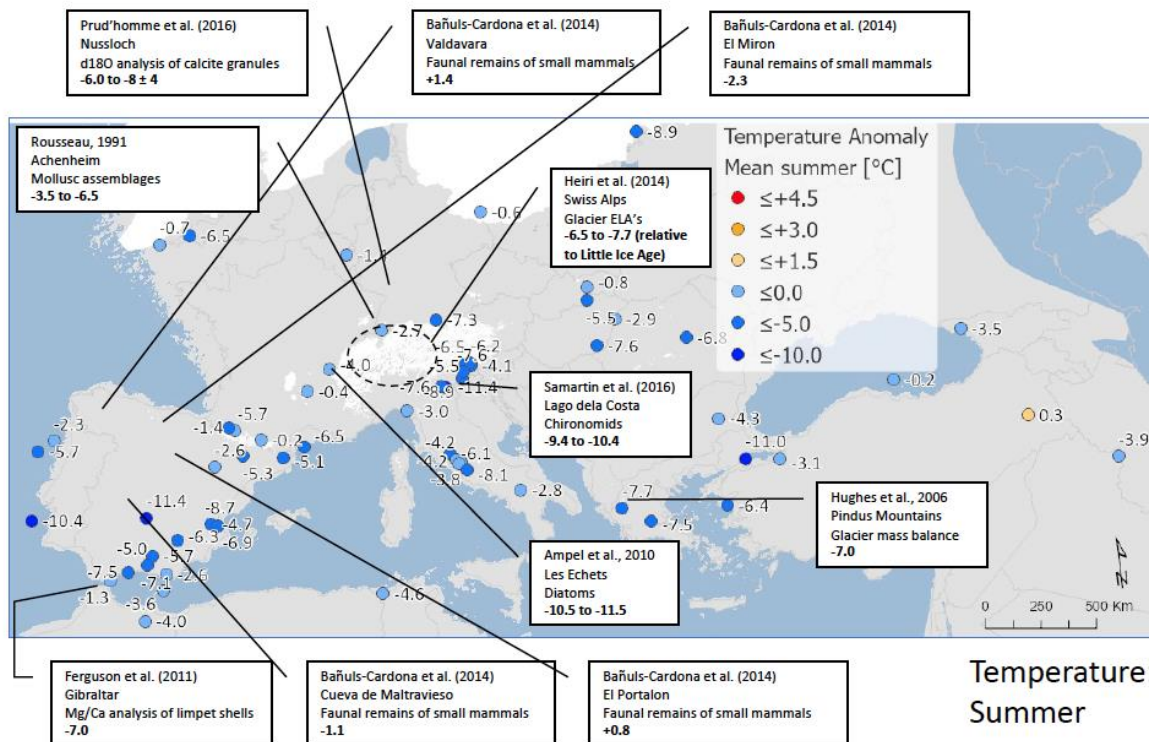
2431

2432



Temperature:
Winter

2433
2434

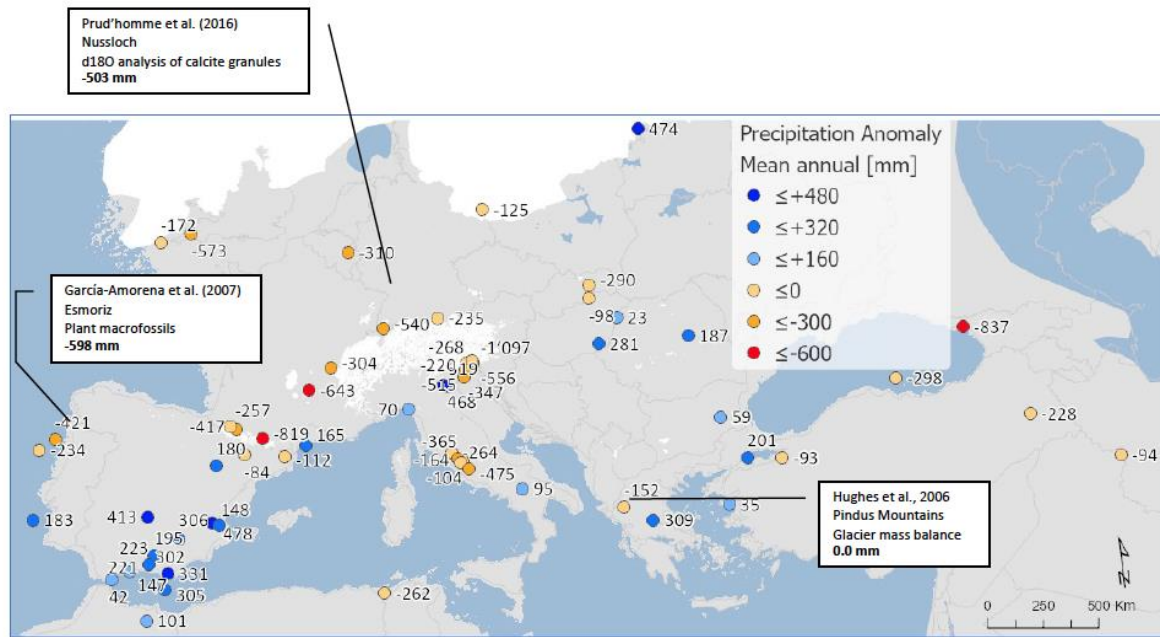


Temperature:
Summer

2435
2436

2437 Figure A9. Maps of pollen-based MAT reconstructions for LGM annual, winter and summer
2438 temperature anomalies (as shown in figure 10), shown together with the results of other
2439 published studies. Continentality represents the difference in temperature between summer
2440 and winter, with positive anomalies indicating an increase in the temperature difference
2441 between summer and winter. All values are expressed as anomalies compared with the
2442 present day unless otherwise indicated.

2443



Precipitation:
Mean Annual

2444

2445

2446 Figure A10. Maps of pollen-based MAT reconstructions for LGM annual precipitation

2447 anomalies (as shown in figure 12), shown together with the results of other published studies.

2448 All values are expressed as anomalies compared with the present day.

2449

2450

2451